GEOLOGIC UNITS	DESCRIPTION	HYDROSTRATIGRAPHIC UNIT	MODFLOW Model Layer
Glacial Drift/Recent Alluvium	mostly silt, sand, and gravel with till lenses and lake deposits	Aquifer with some local aquitard units	Typically Layers 1 & 2
Decorah Shale	glauconitic shale	Aquitard	Not in model
Platteville Formation and Glenwood Shale	massive to thinly bedded, fractured dolomite & shale	poorly transmissive aquifer to aquitard	Not in model
St. Peter Sandstone	upper 100 feet is uniform fine sandstone; lower 50 feet is shale	Aquifer	Typically Layer 2
		Aquitard	Leakance on Layer 2
Prairie du Chien Group	Shakopee Fm (upper unit) contains zones of highly fractured rock; Oneota Dol. (lower) is massive	Aquifer (Shakopee)	Typically Layer 3
		Aquitard (Oneota)	Typically Layer 4
Jordan Sandstone	medium sandstone with fractures and some cementation	Aquifer	Typically Layer 5
St. Lawrence Formation	dolomitic shale	Aquitard	Typically Layer 6
Franconia Formation	calcareous sandstone to shaley sandstone	Aquifer (upper Franconia)	Typically Layer 7
		Aquitard (lower Franconia)	Leakance on Layer 7
Ironton-Galesville Sandstones	fine to medium sandstone	Aquifer	Layer 8
Eau Claire Formation	dolomitic shale	Aquitard	Not in model
Mt. Simon and Hinckley Sandstones	sandstone	Aquifer	Not in model
Precambrian Crystaline Rocks	undifferentiated crystalline and volcanic rocks	Aquitard	Not in model

Figure 1

Hydrostratigraphic Column for Southern Washington County

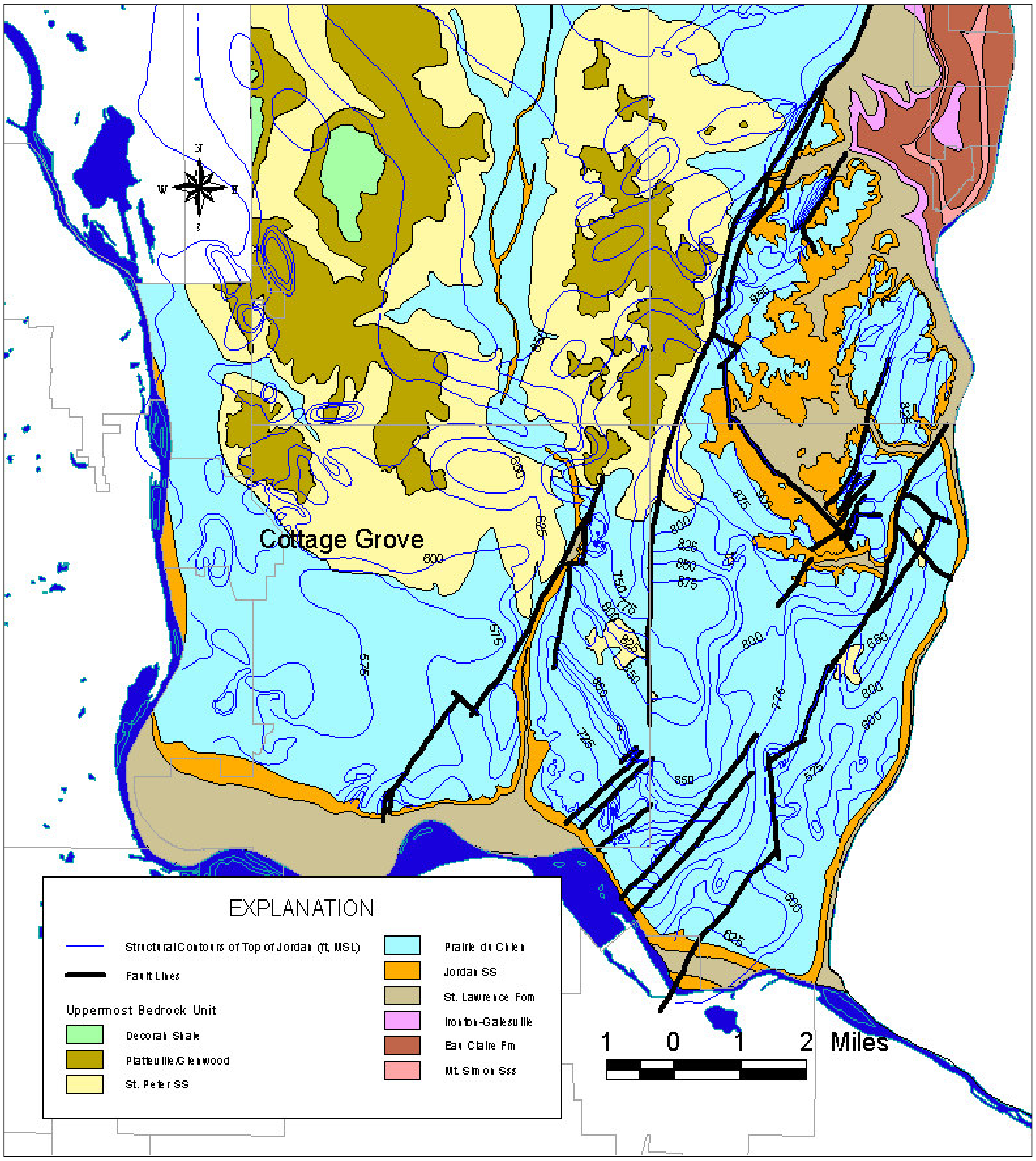

(adapted from Mossler, 2003)

Figure 2

Location of Faults in Southern Washington County

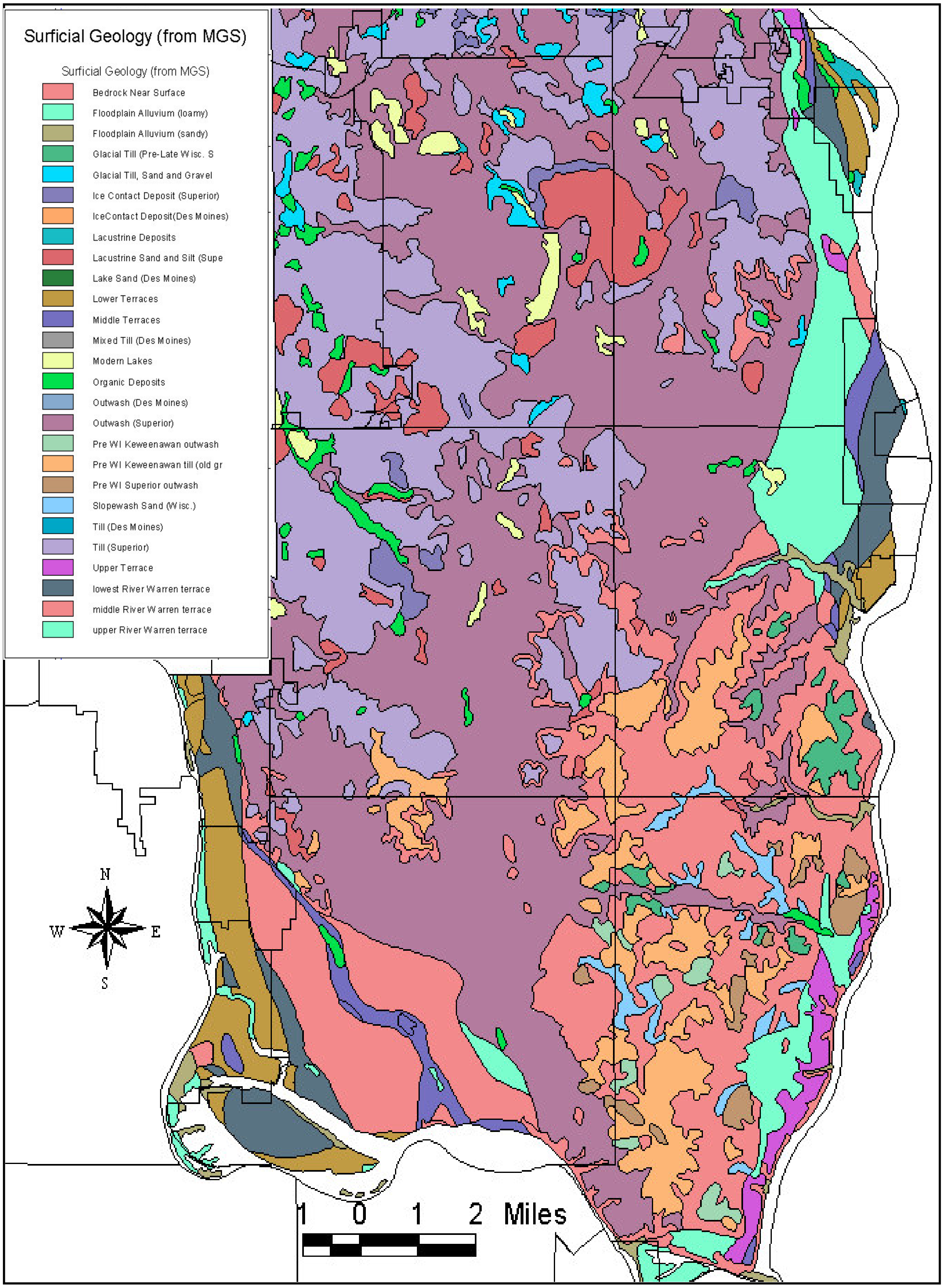

Figure 3

Surficial Geology of Southern Washington County

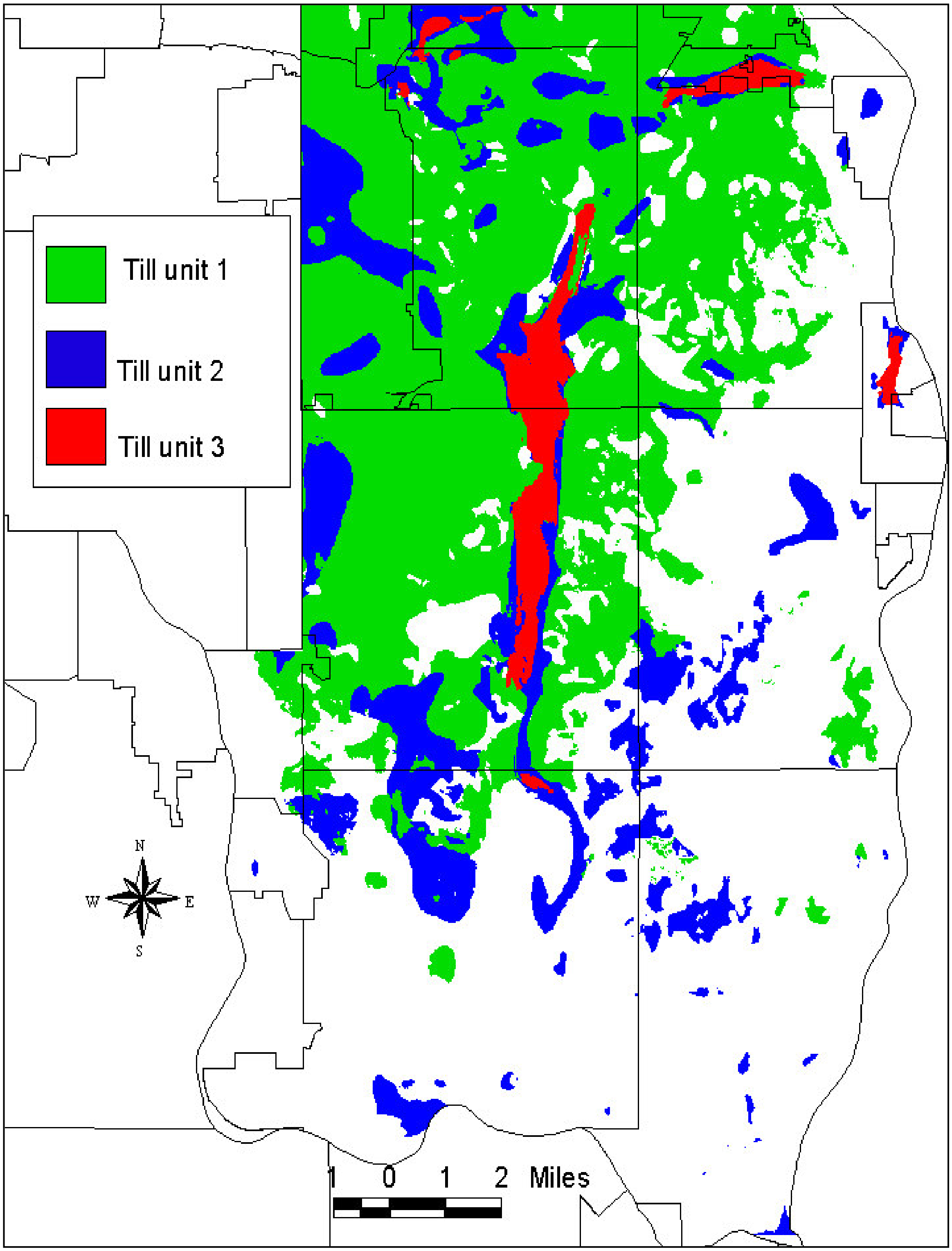

(adapted from MGS Grid Data)

Figure 4

Glacial Till Units in South Washington County

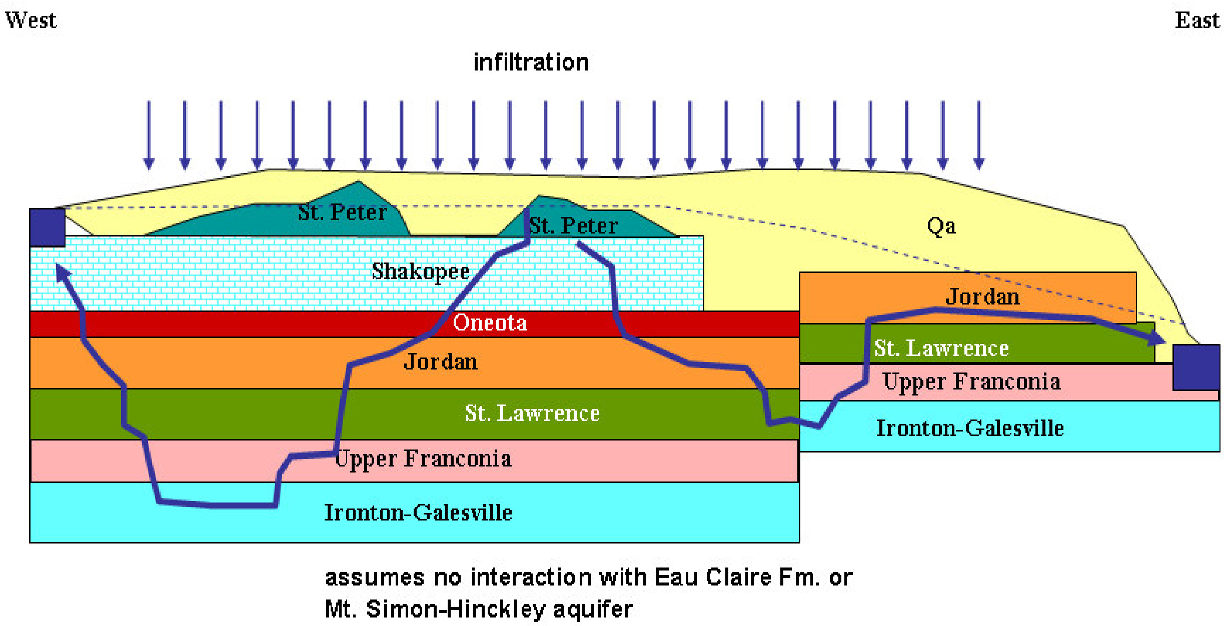

Figure 5

Conceptual Hydrogeologic Model

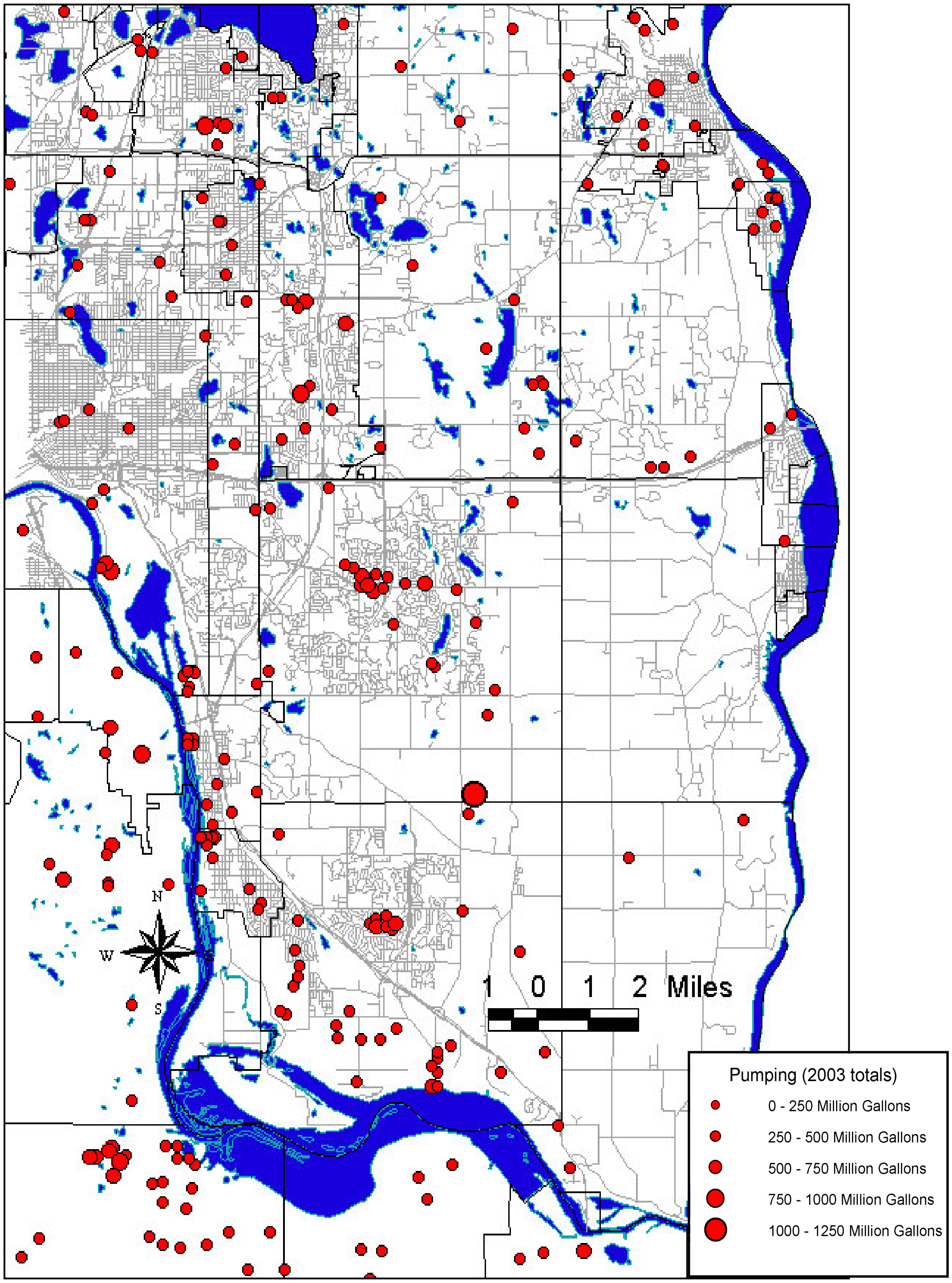

Figure 6

Pumping Rates for Appropriated Wells (2003)

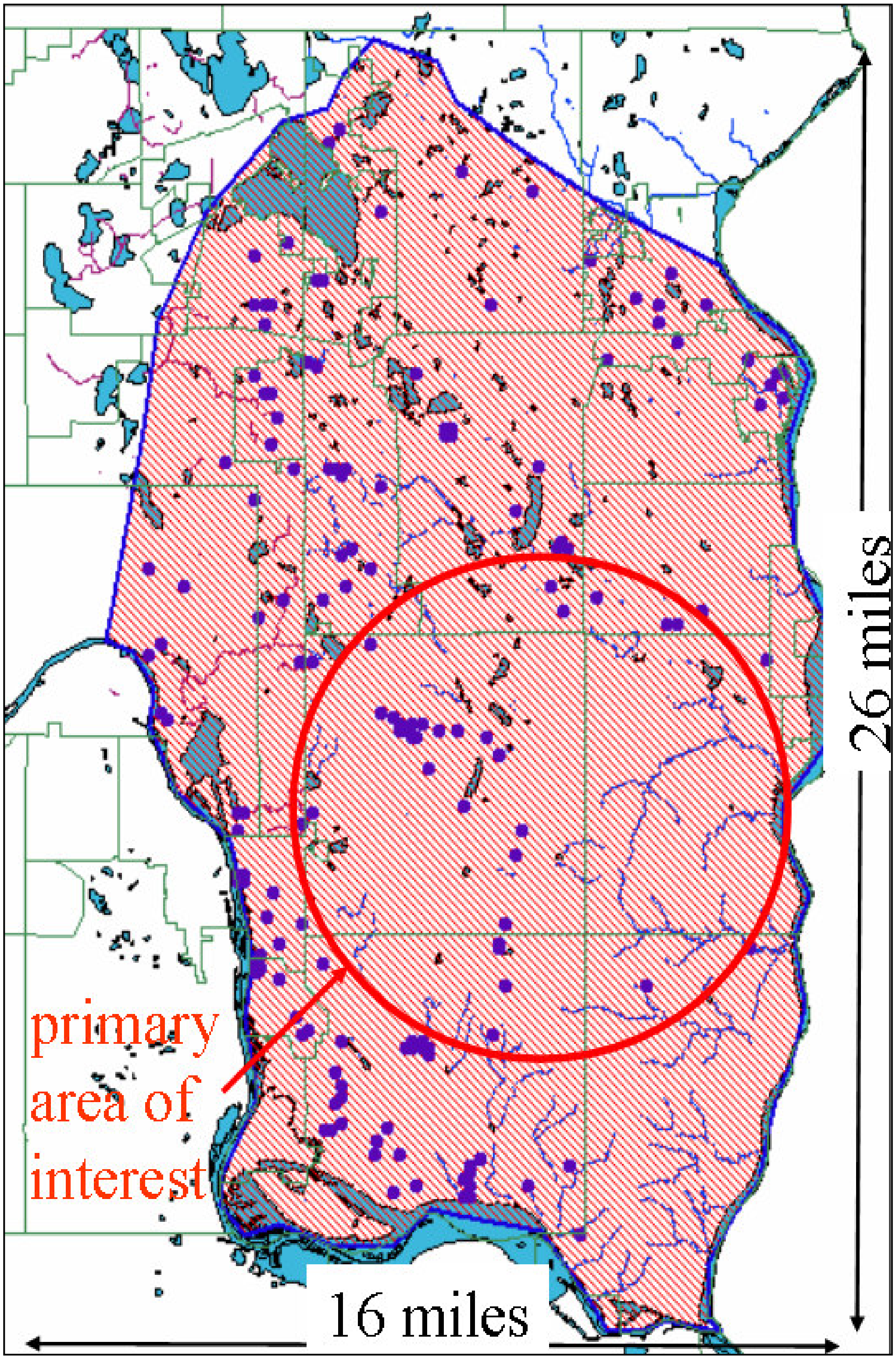

Figure 7

Model Domain and Area of Primary Interest

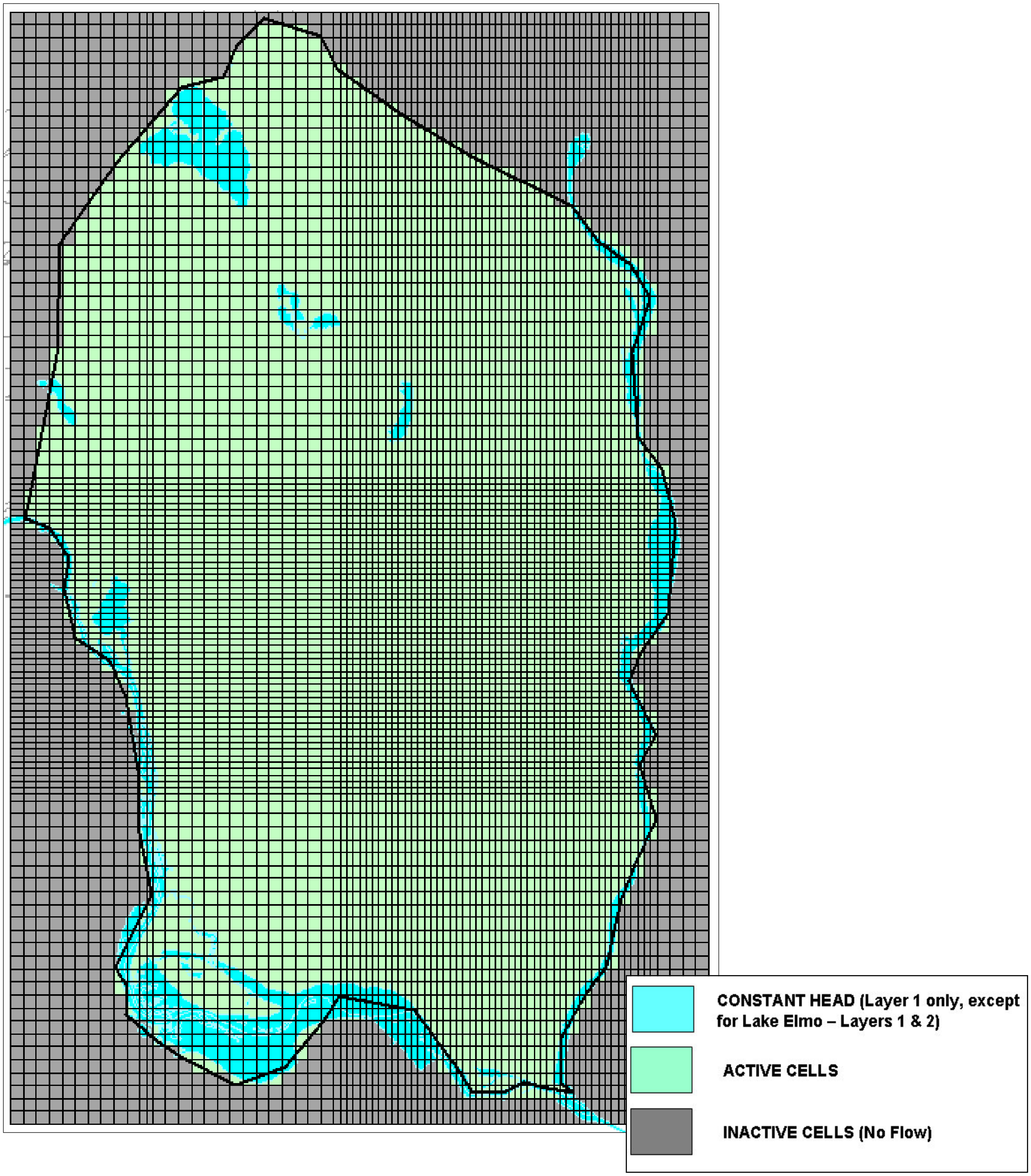

Figure 8

Finite-Difference Grid for Regional Model and Boundary Conditions

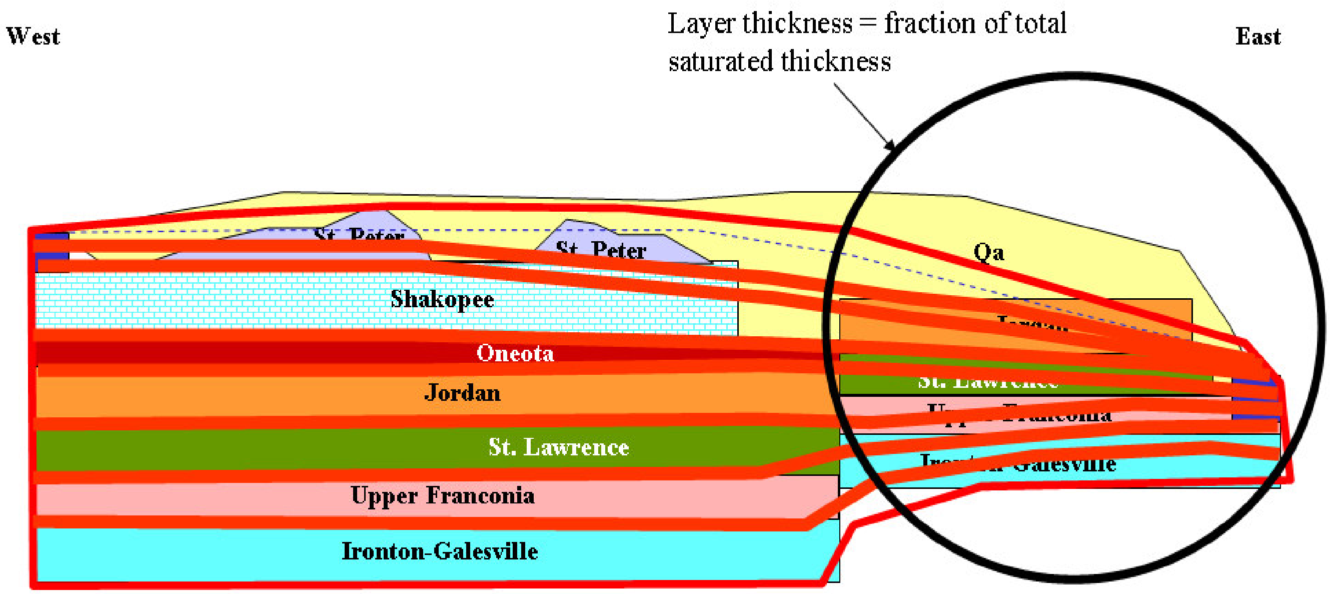

Figure 9

Schematic Illustration of Computation Layer Assignments

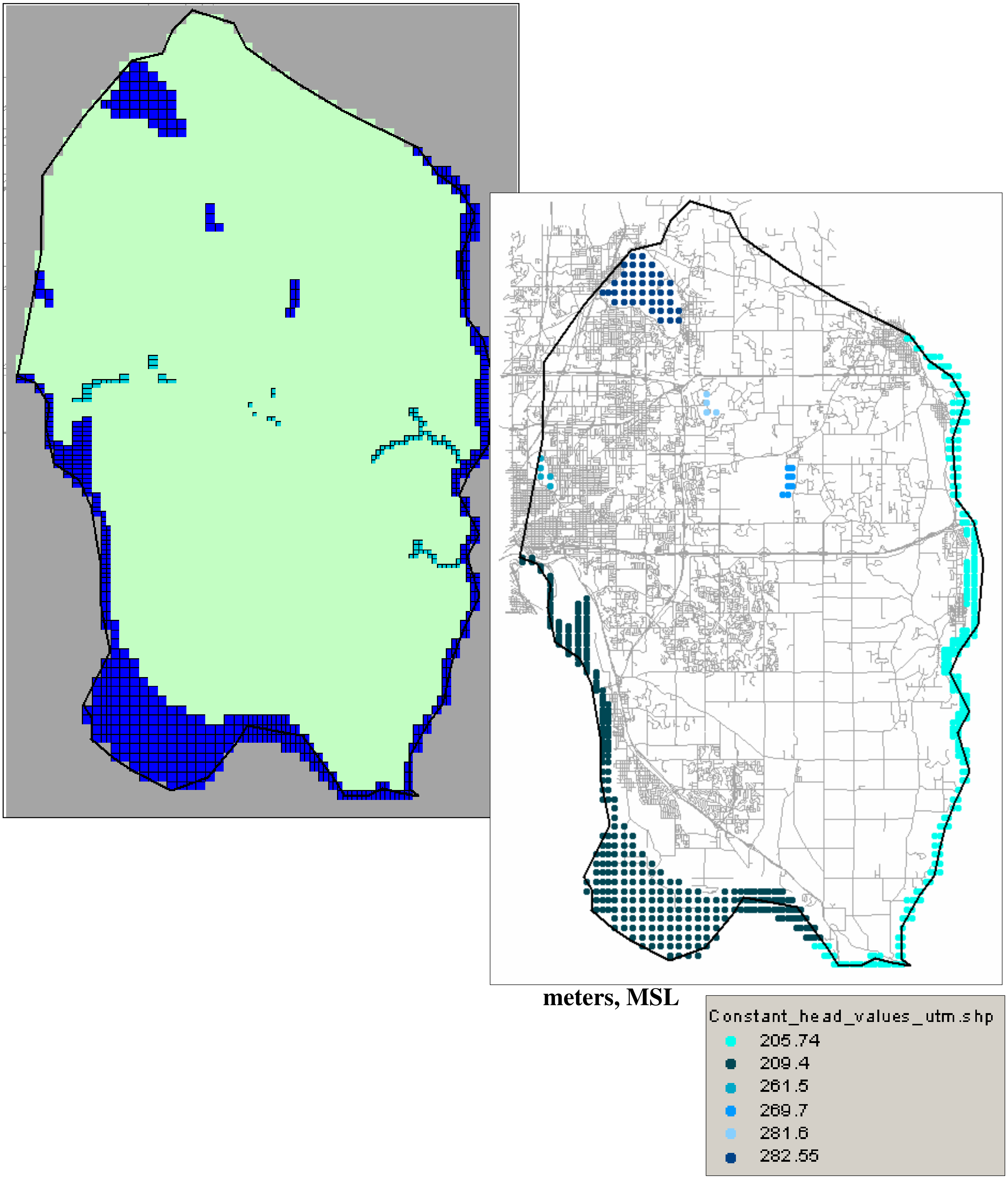

Figure 10

Constant Head Cells in Layer 1

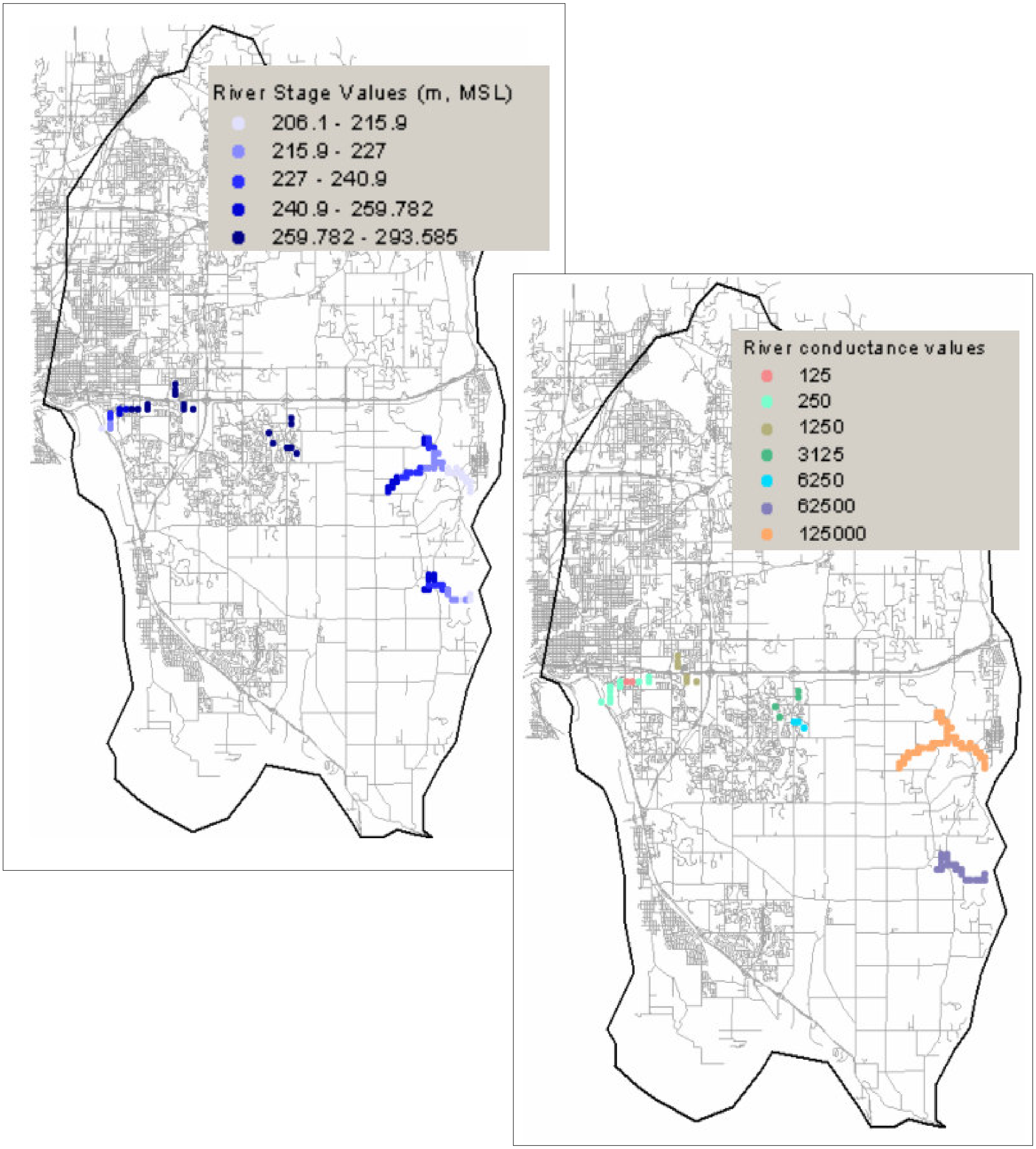

Figure 11

River and Drain Package Features in Layer 1

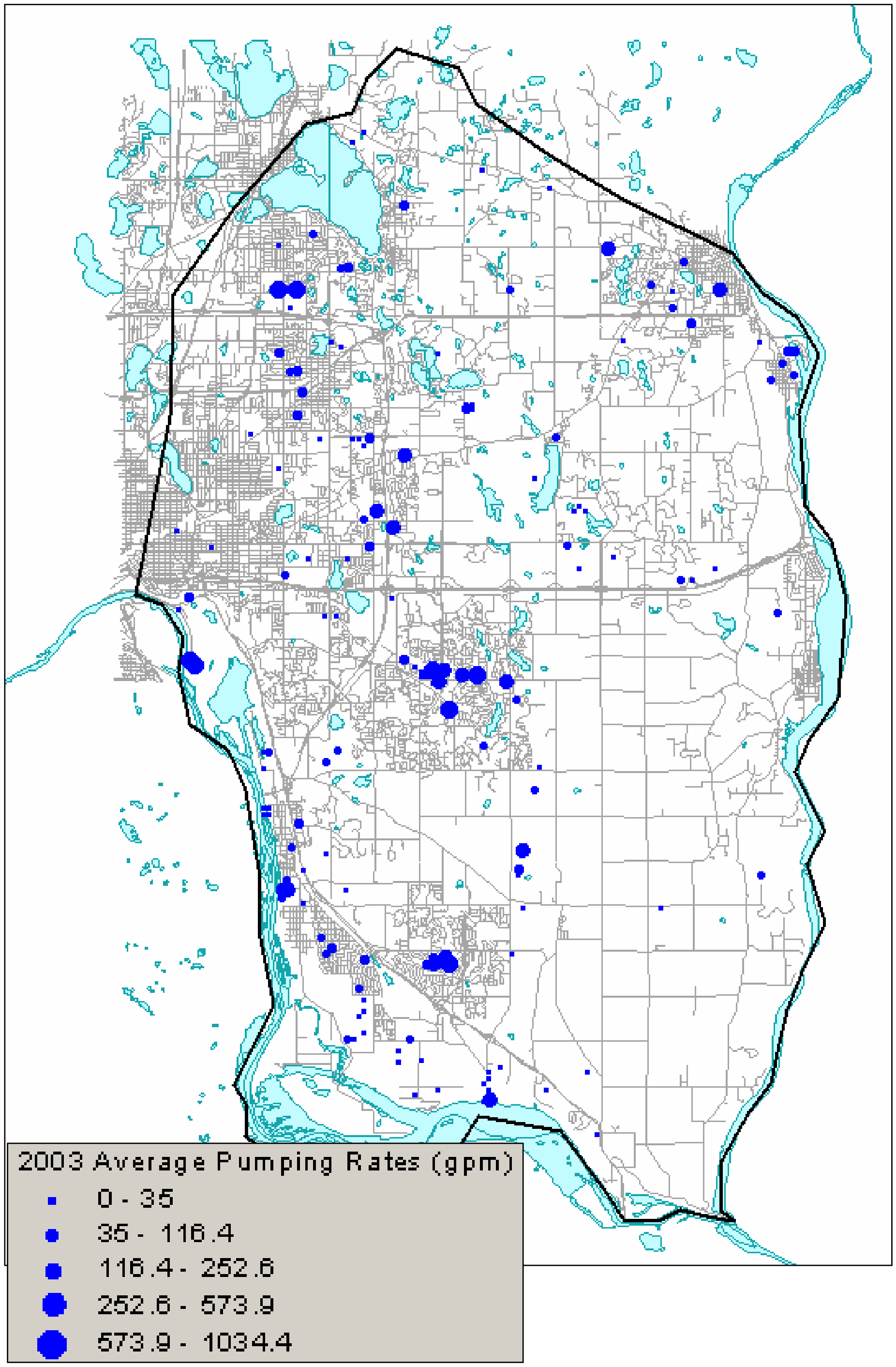

Figure 12

High Capacity Wells in Model (2003 pumping rates shown)

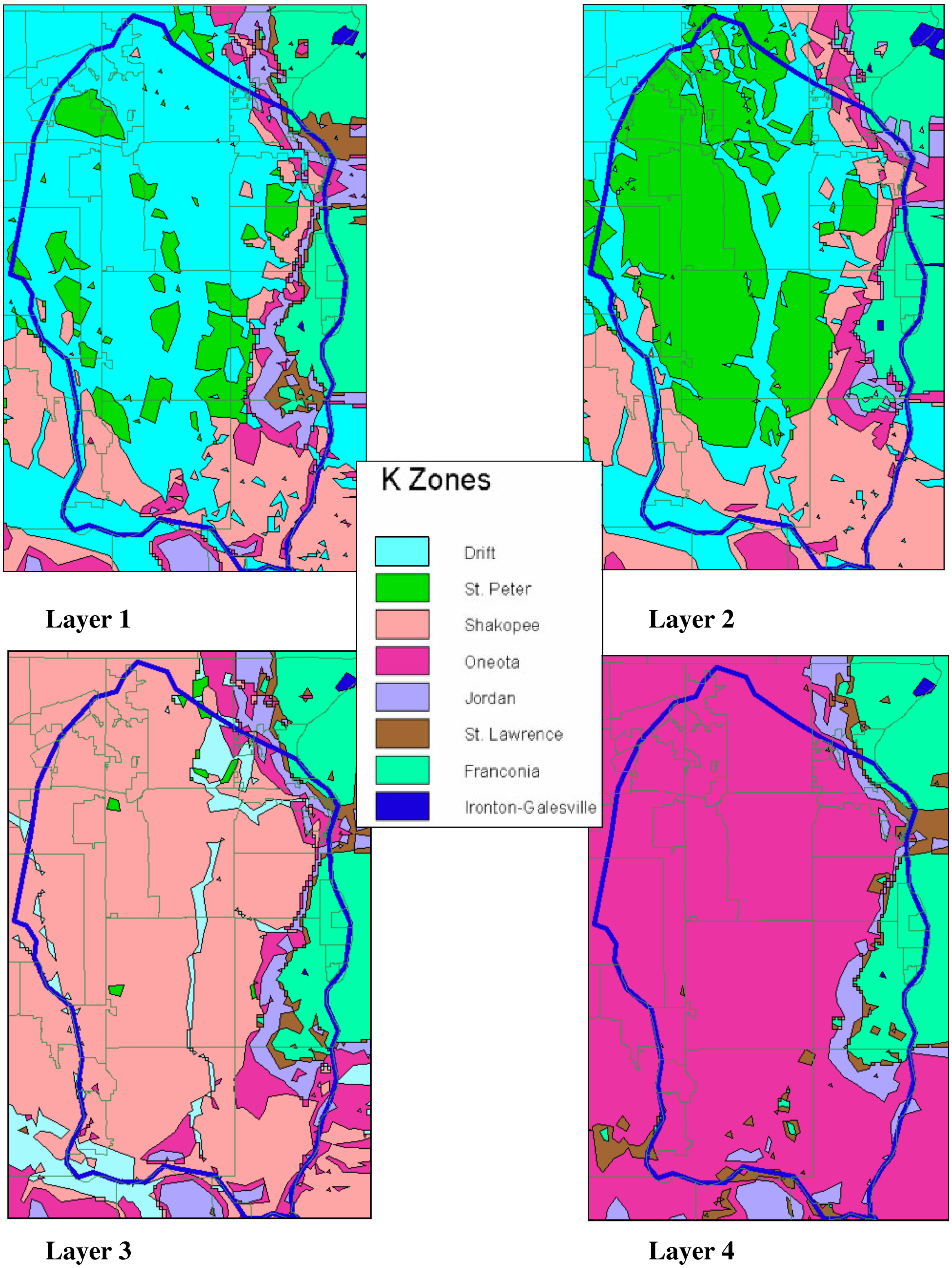

Figure 13

Geologic Representation in Computation Layers 1 to 4

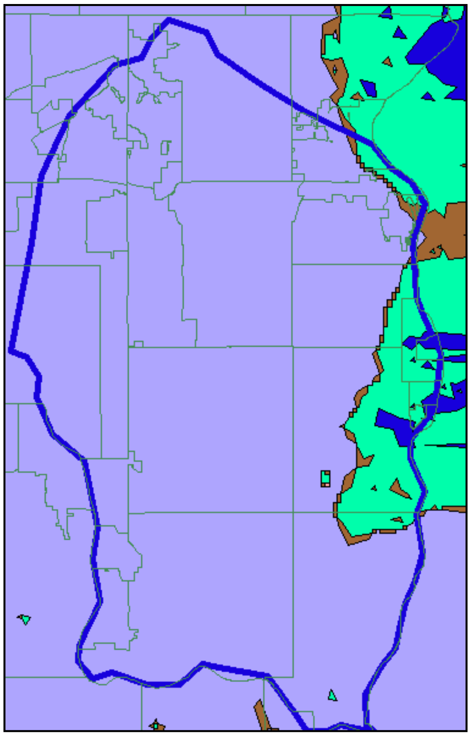

Layer 5

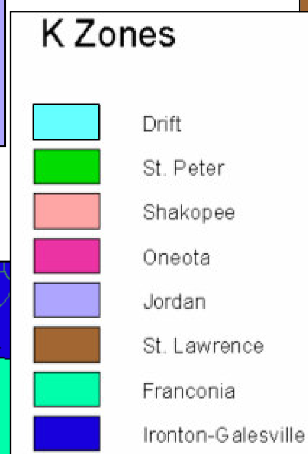

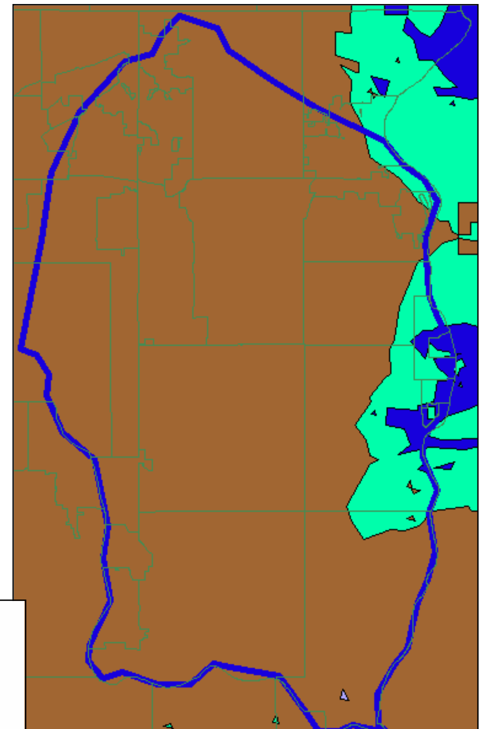

Layer 6

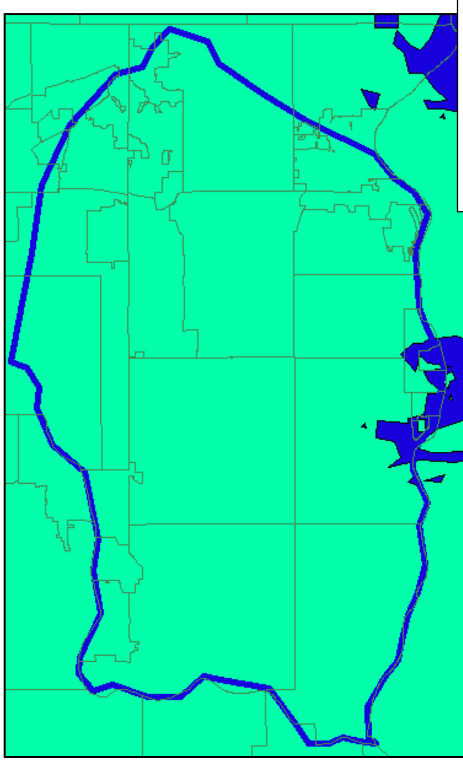

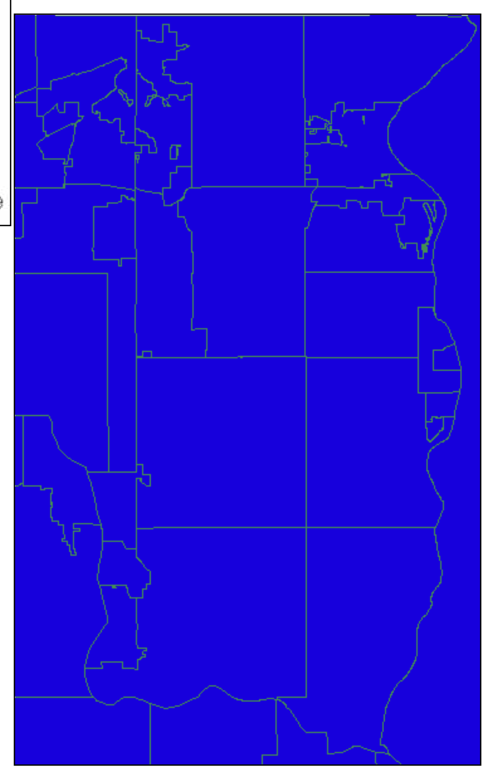

Layer 7

Layer 8

Figure 14

Geologic Representation in Computation Layers 5 to 8

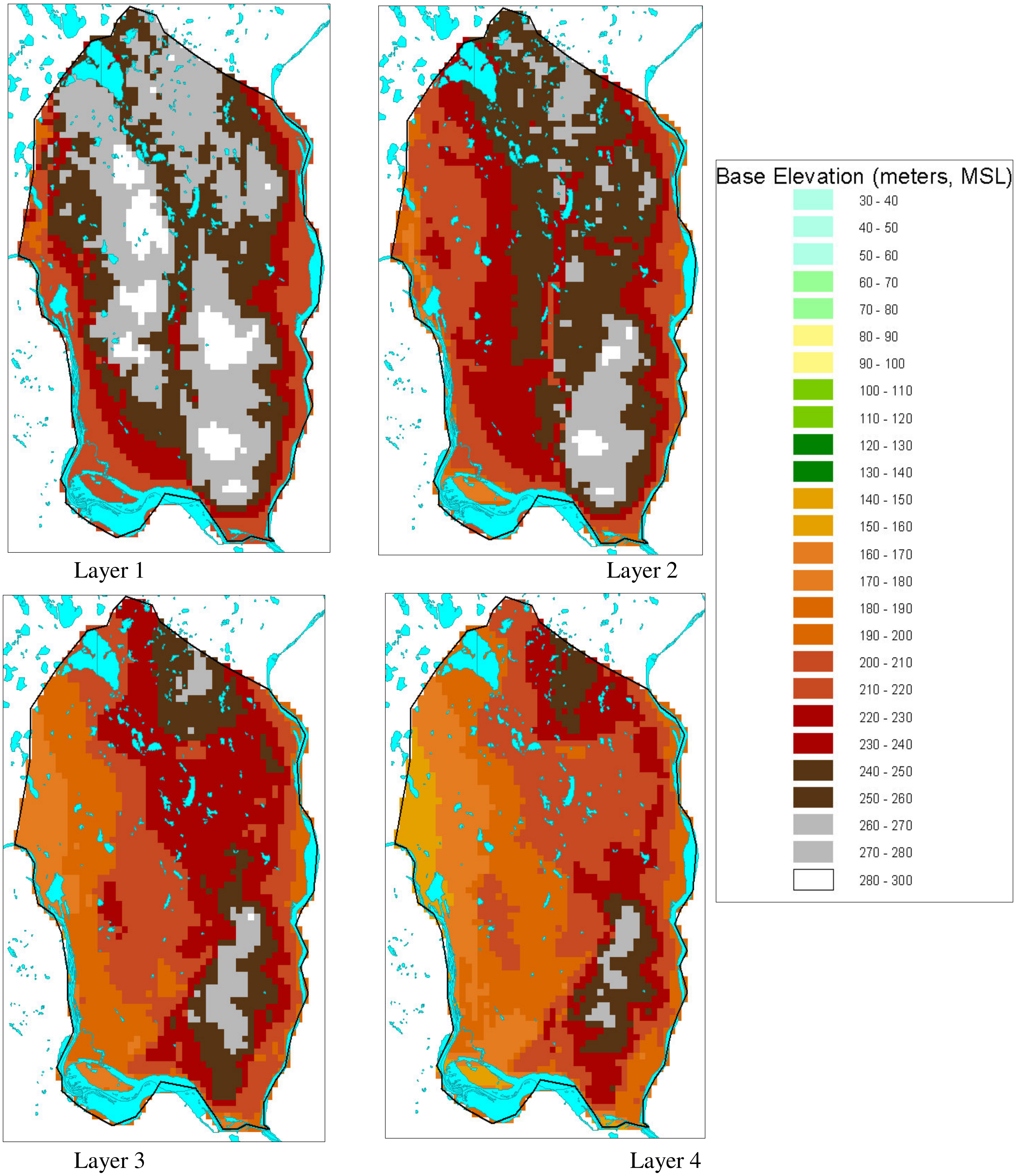

Figure 15

Base Elevations (meters, MSL) of Layers 1 to 4

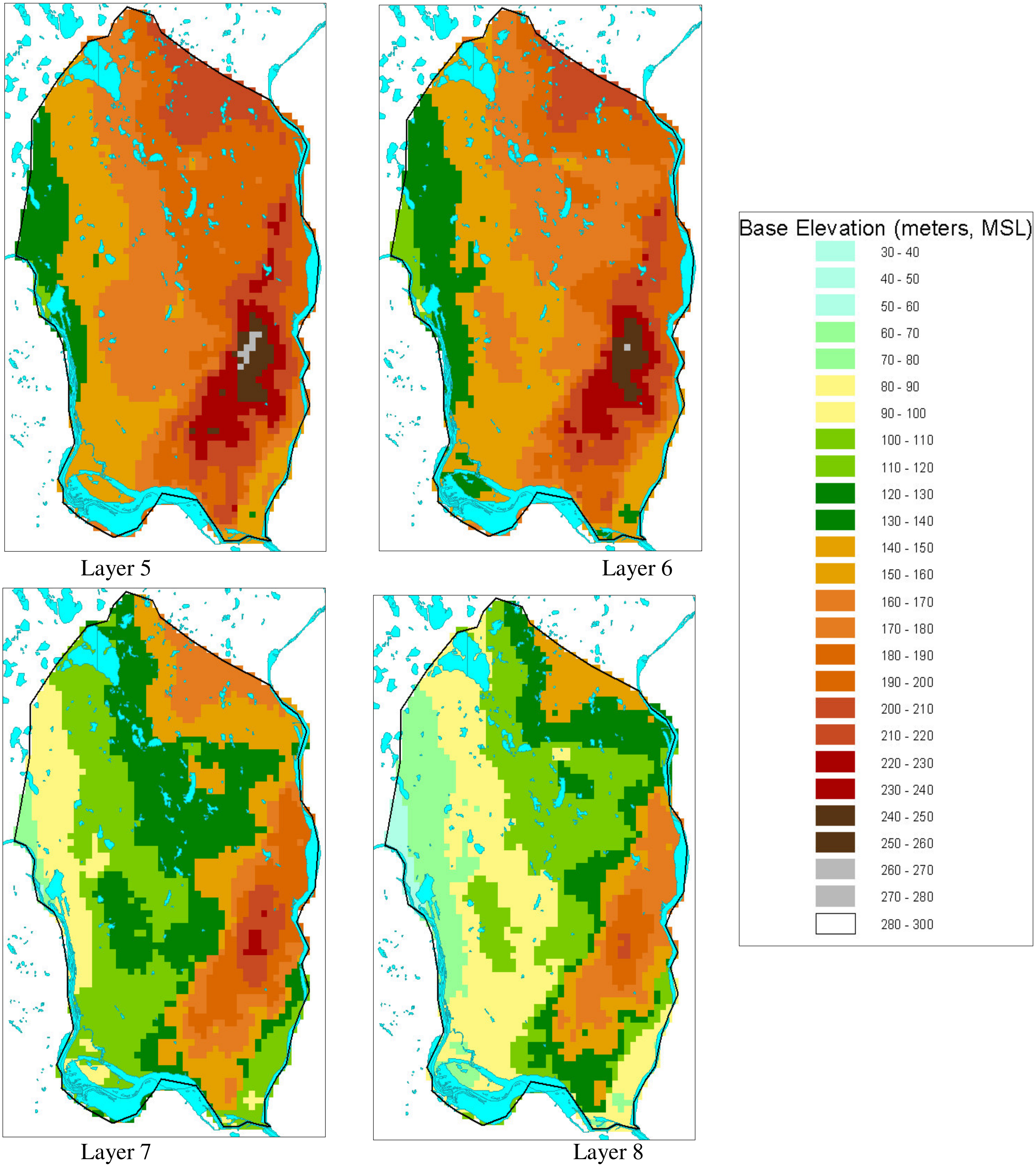

Figure 16

Base Elevations (meters, MSL) of Layers 5 to 8

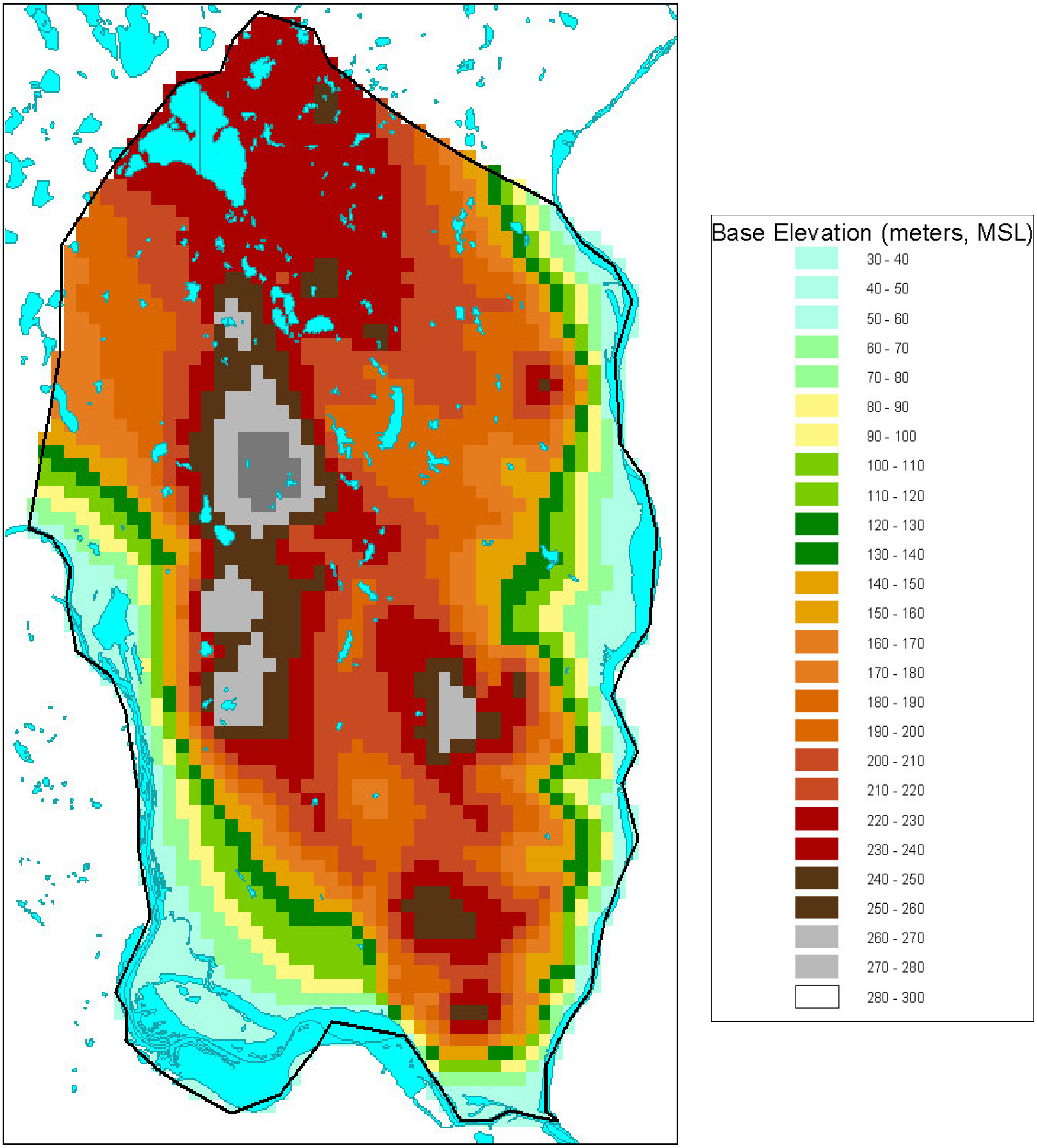

Figure 17

Elevation (meters, MSL) of Top of Layer 1

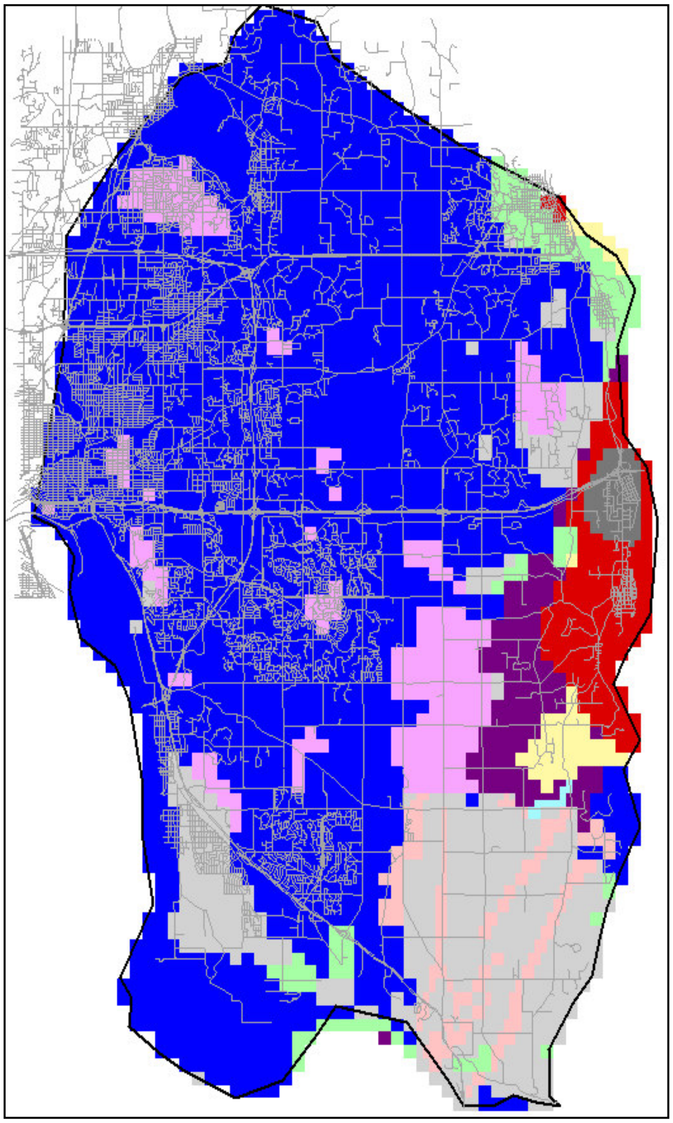

Horizontal Hydraulic Conductivity

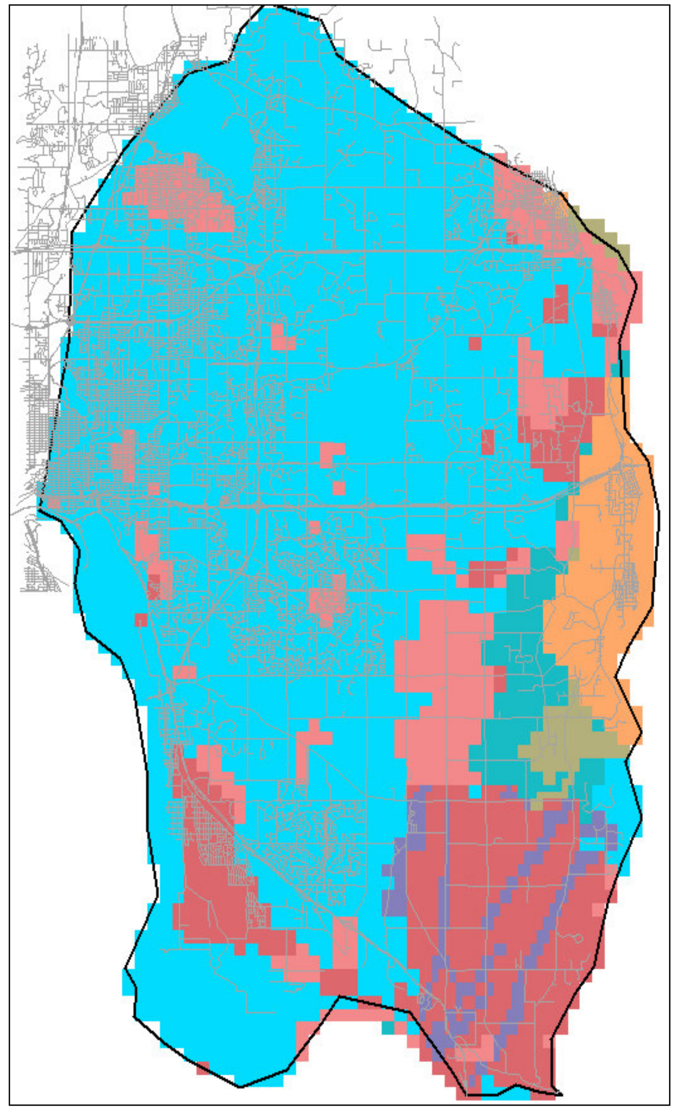

Vertical Hydraulic Conductivity

Figure 18

Optimized Horizontal and Vertical Hydraulic Conductivity Zones (Layer 1)

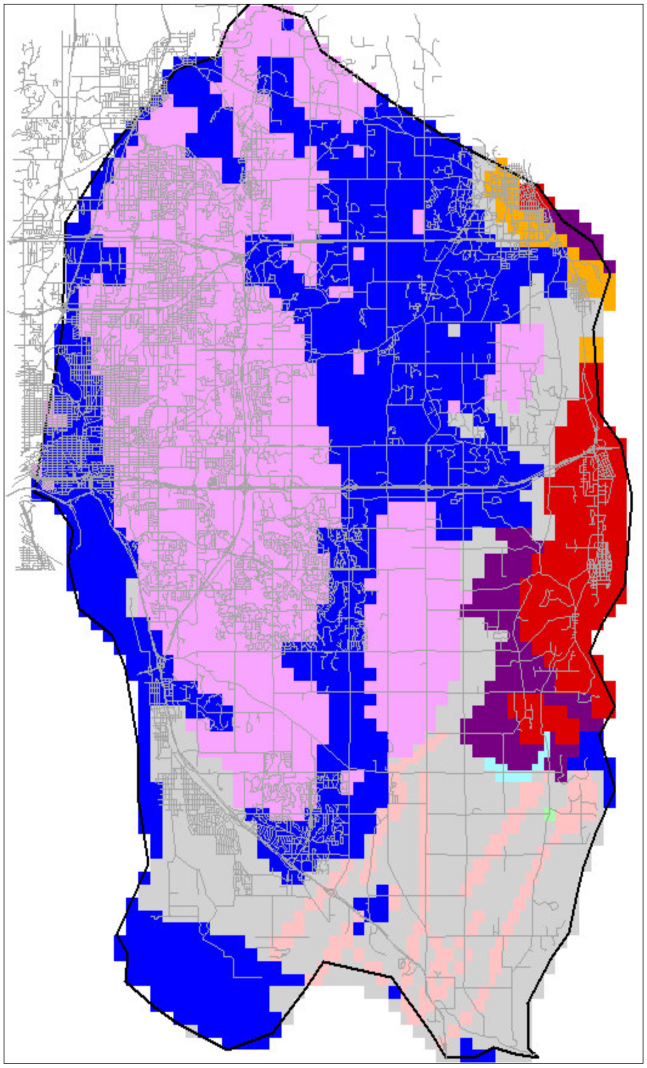

Horizontal Hydraulic Conductivity

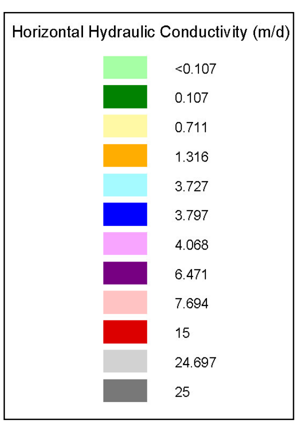

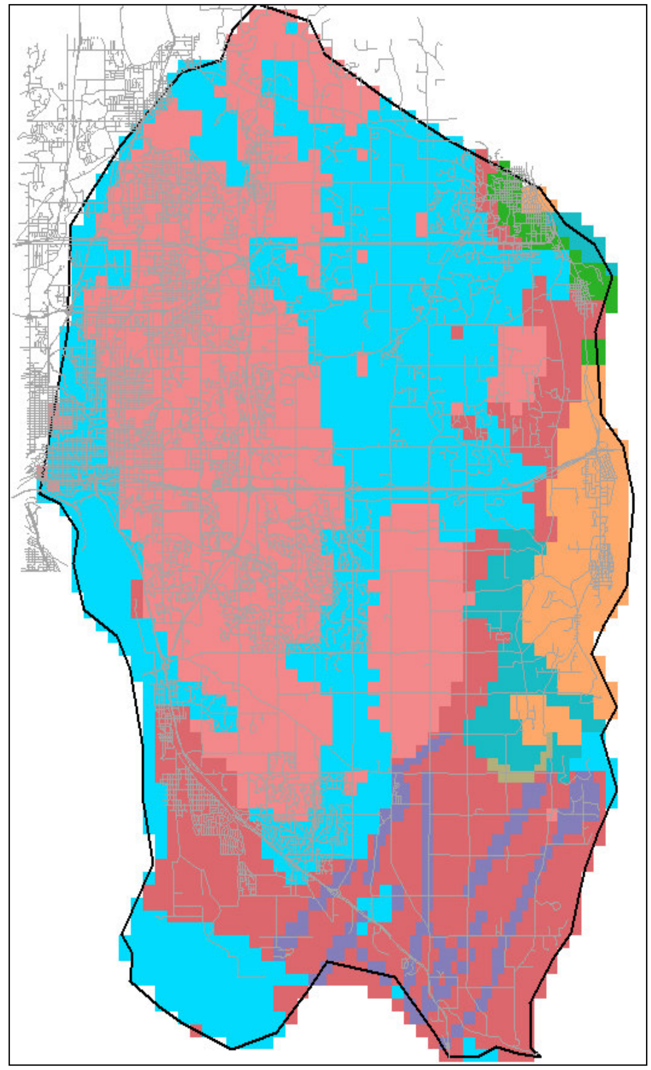

Vertical Hydraulic Conductivity

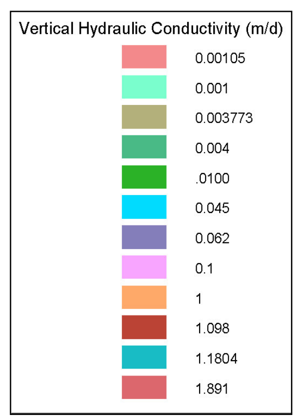

Figure 19

Optimized Horizontal and Vertical Hydraulic Conductivity Zones (Layer 2)

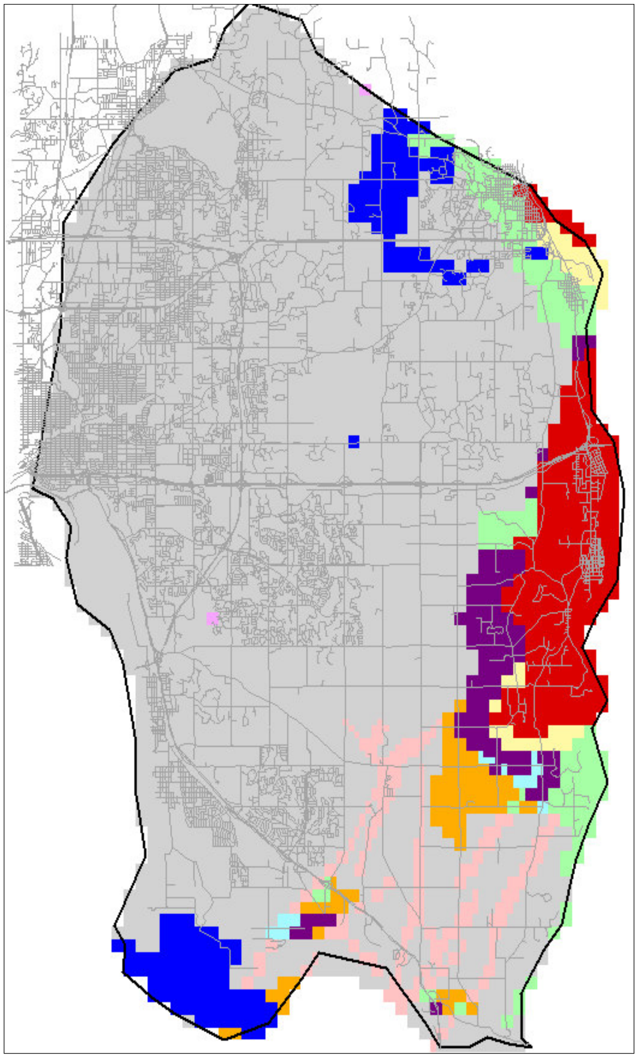

Horizontal Hydraulic Conductivity

Horizontal Hydraulic Conductivity (m/d)

<0.107
0.107
0.711
1.316
3.727
3.797
4.068
6.471
7.694
15
24.697
25

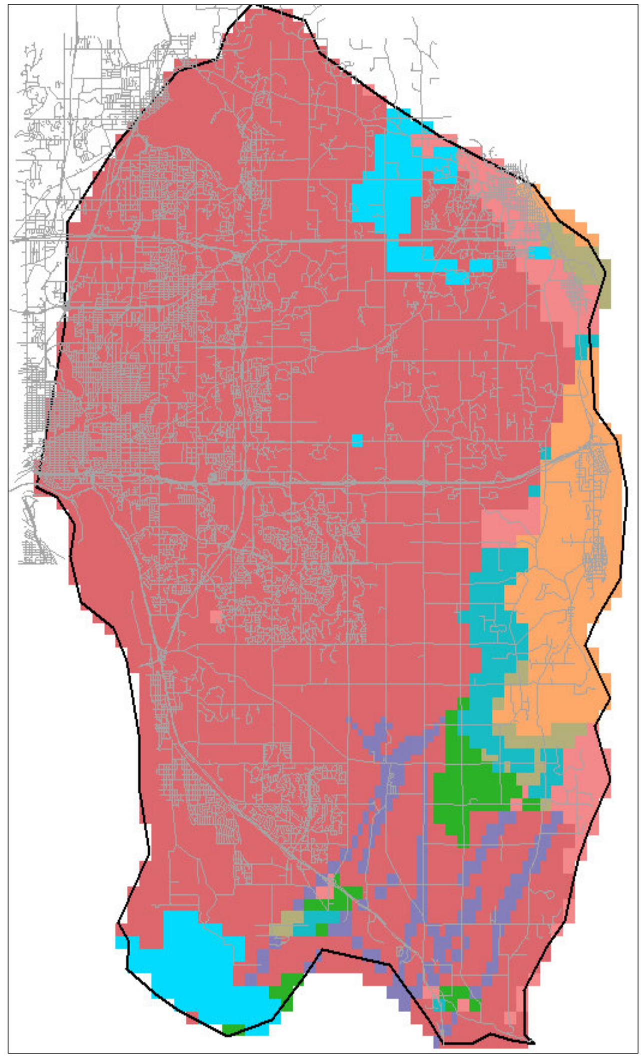

Vertical Hydraulic Conductivity

Vertical Hydraulic Conductivity (m/d)

0.00105
0.001
0.003773
0.004
.0100
0.045
0.062
0.1
1
1.098
1.1804
1.891

Figure 20

Optimized Horizontal and Vertical Hydraulic Conductivity Zones
(Layer 3)

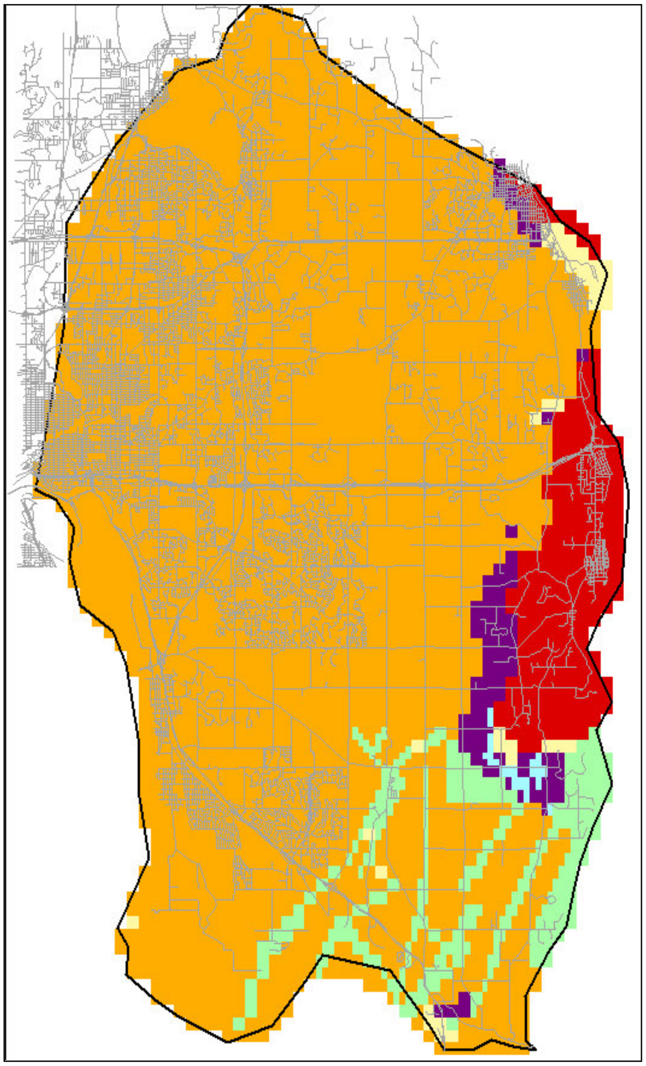

Horizontal Hydraulic Conductivity

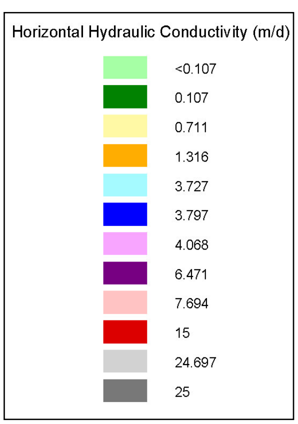

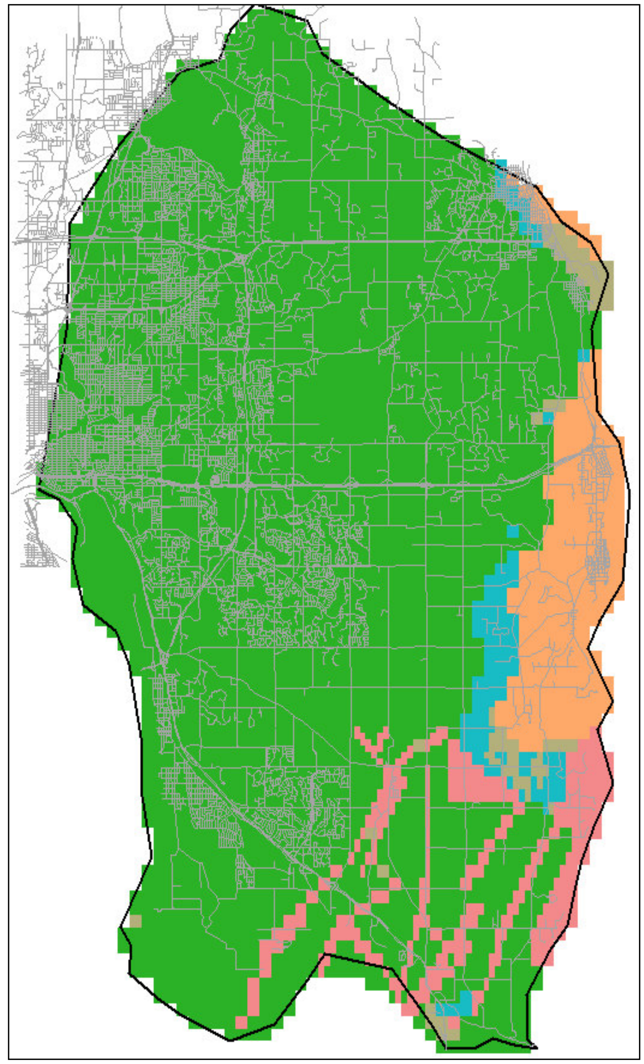

Vertical Hydraulic Conductivity

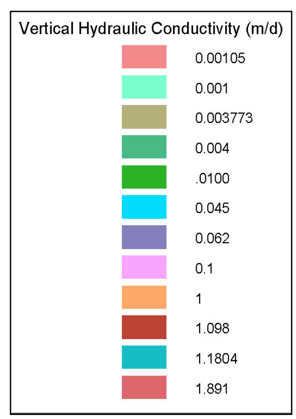

Figure 21

Optimized Horizontal and Vertical Hydraulic Conductivity Zones (Layer 4)

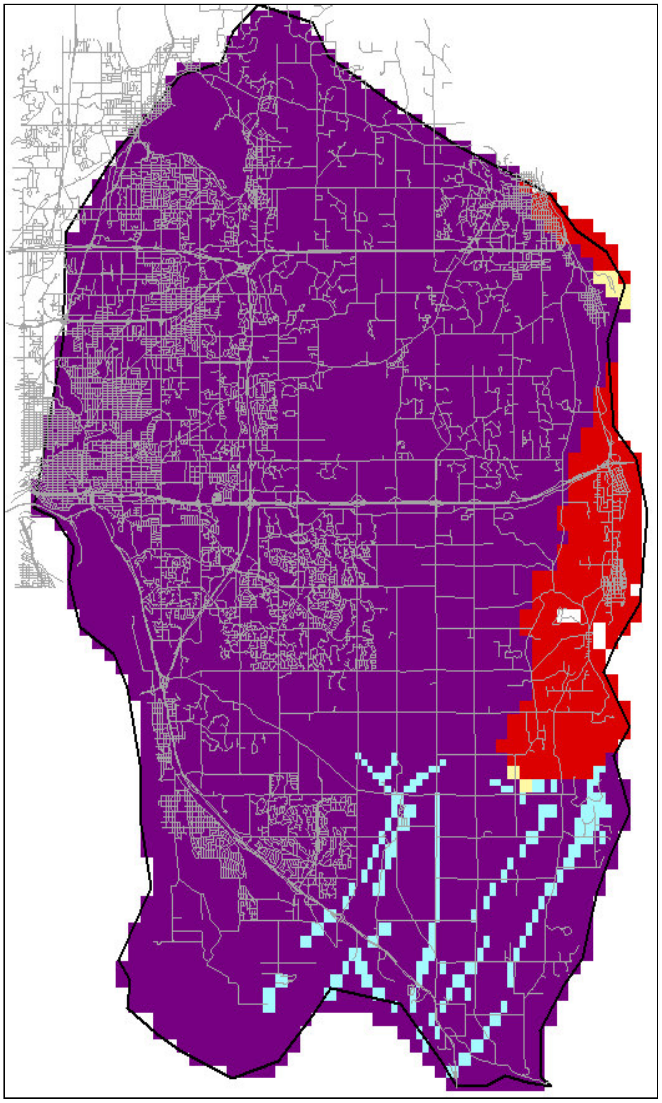

Horizontal Hydraulic Conductivity

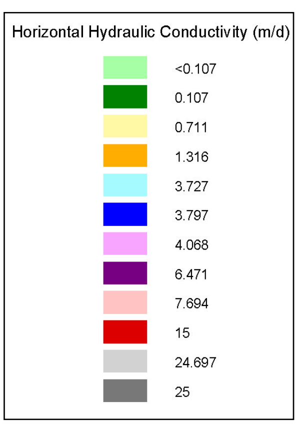

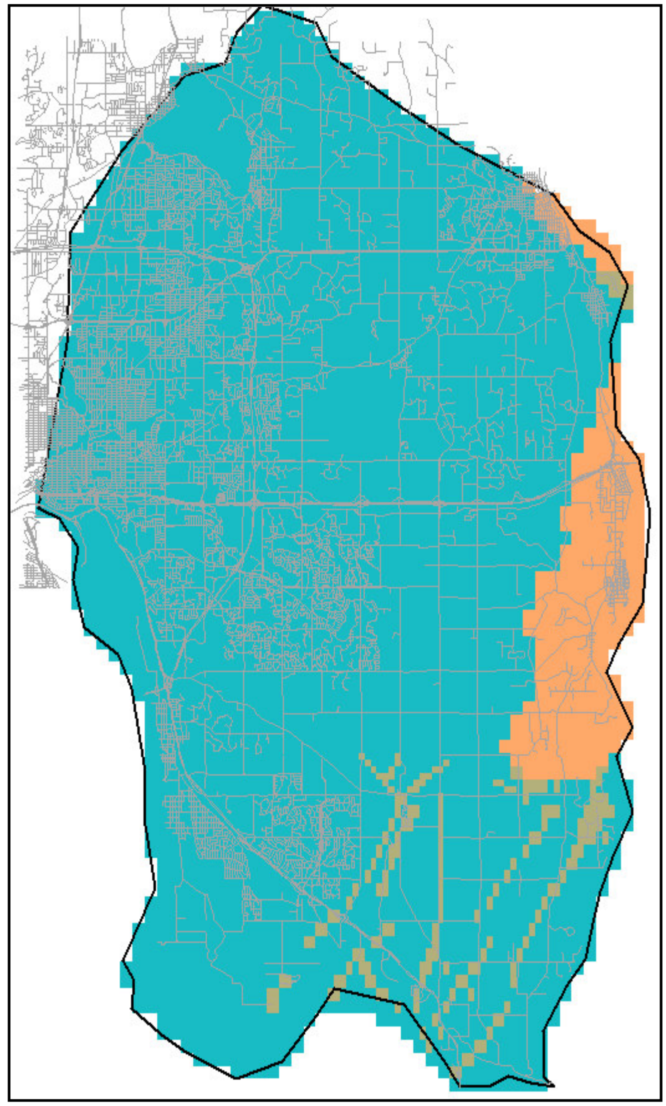

Vertical Hydraulic Conductivity

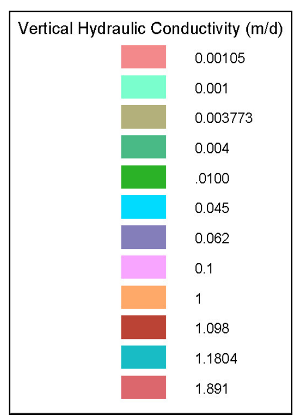

Figure 22

Optimized Horizontal and Vertical Hydraulic Conductivity Zones (Layer 5)

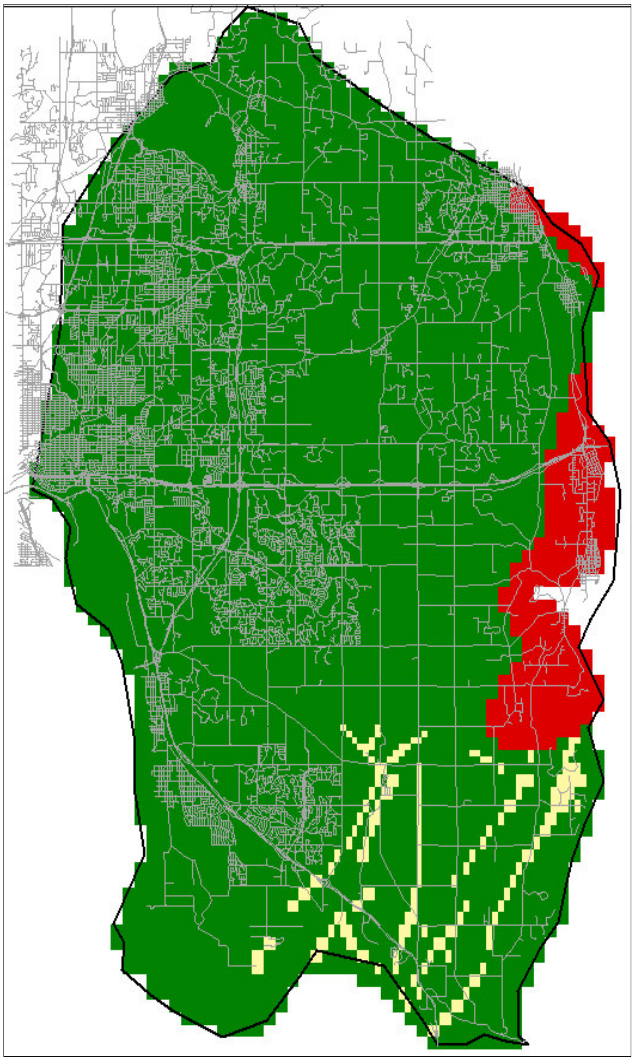

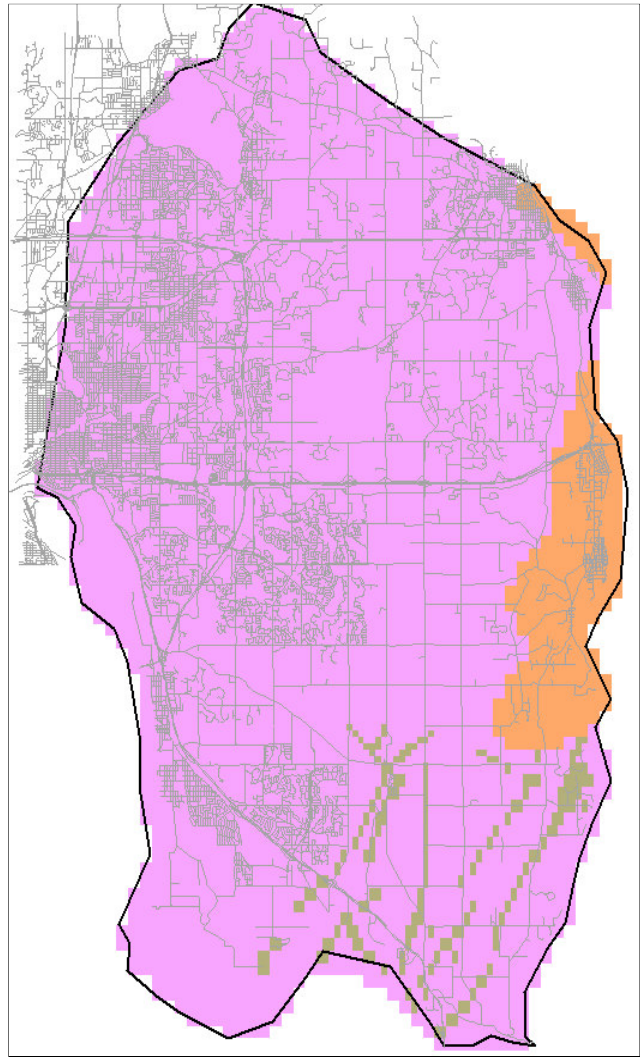

Horizontal Hydraulic Conductivity

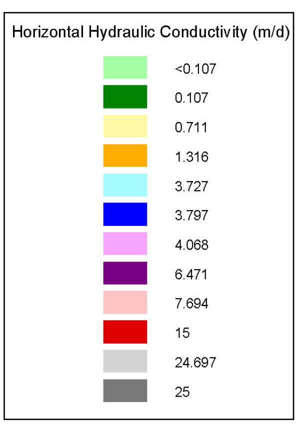

Vertical Hydraulic Conductivity

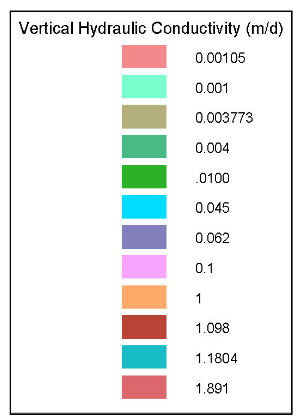

Figure 23

Optimized Horizontal and Vertical Hydraulic Conductivity Zones (Layer 6)

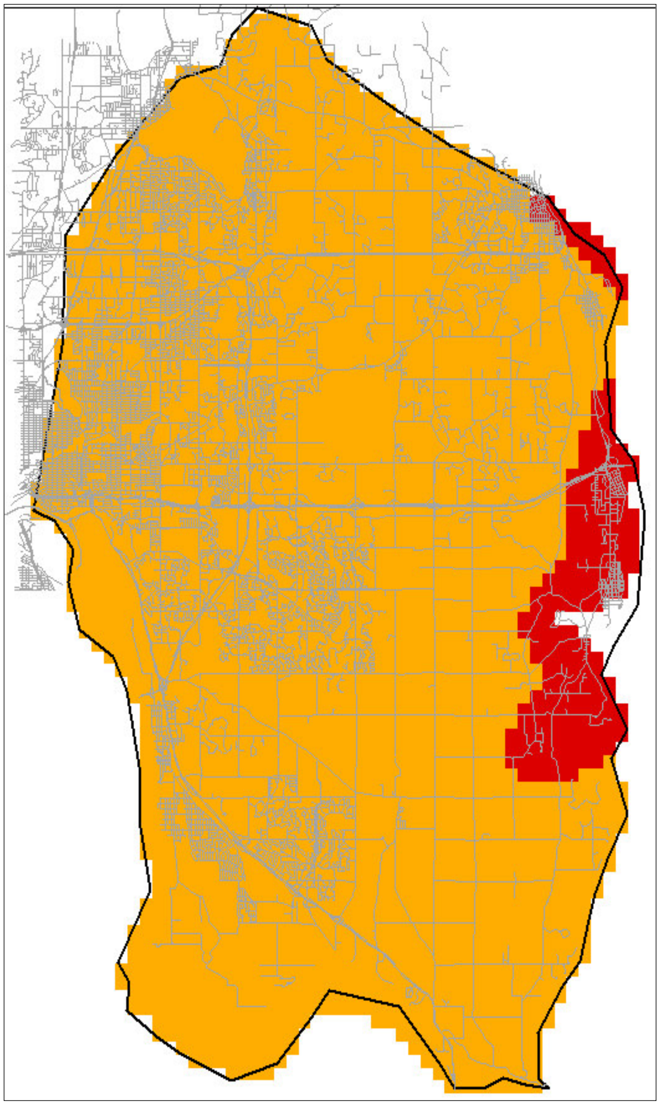

Horizontal Hydraulic Conductivity

Horizontal Hydraulic Conductivity (m/d)

- <0.107
- 0.107
- 0.711
- 1.316
- 3.727
- 3.797
- 4.068
- 6.471
- 7.694
- 15
- 24.697
- 25

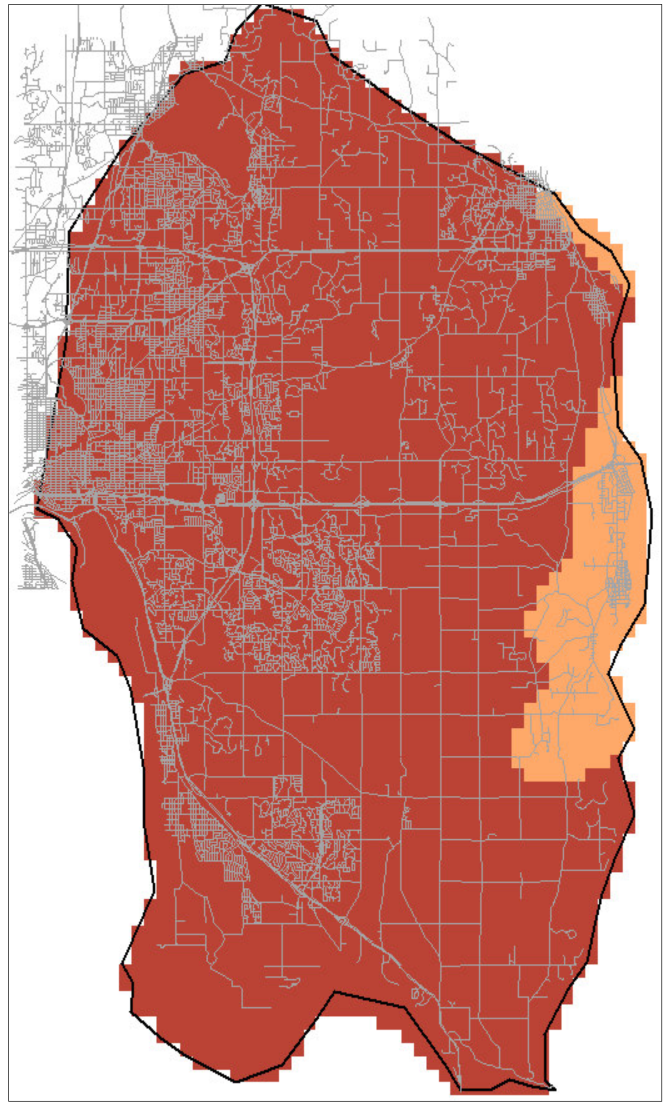

Vertical Hydraulic Conductivity

Vertical Hydraulic Conductivity (m/d)

- 0.00105
- 0.001
- 0.003773
- 0.004
- .0100
- 0.045
- 0.062
- 0.1
- 1
- 1.098
- 1.1804
- 1.891

Figure 24

Optimized Horizontal and Vertical Hydraulic Conductivity Zones
(Layer 7)

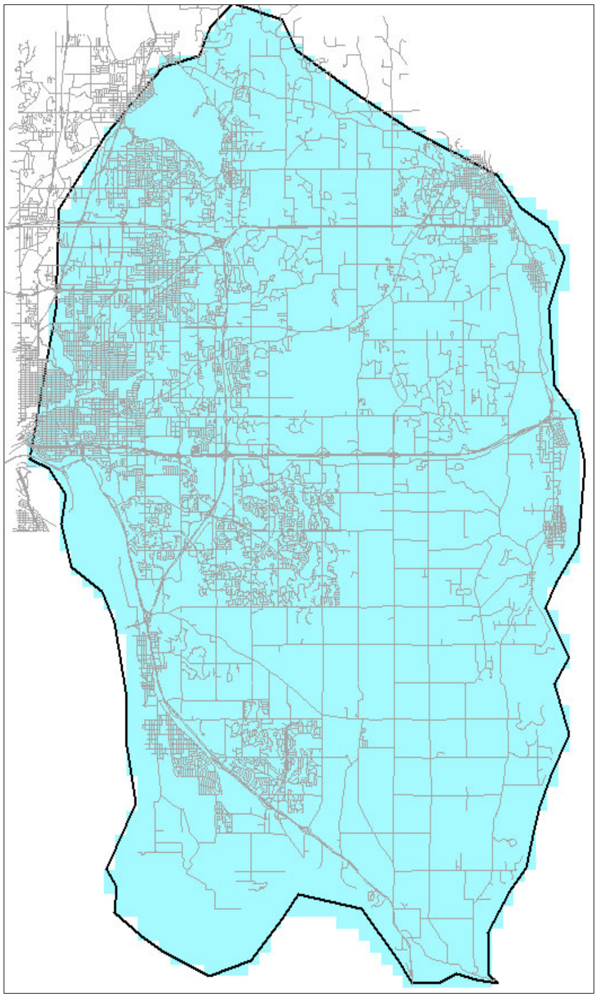

Horizontal Hydraulic Conductivity

Horizontal Hydraulic Conductivity (m/d)

- <0.107
- 0.107
- 0.711
- 1.316
- 3.727
- 3.797
- 4.068
- 6.471
- 7.694
- 15
- 24.697
- 25

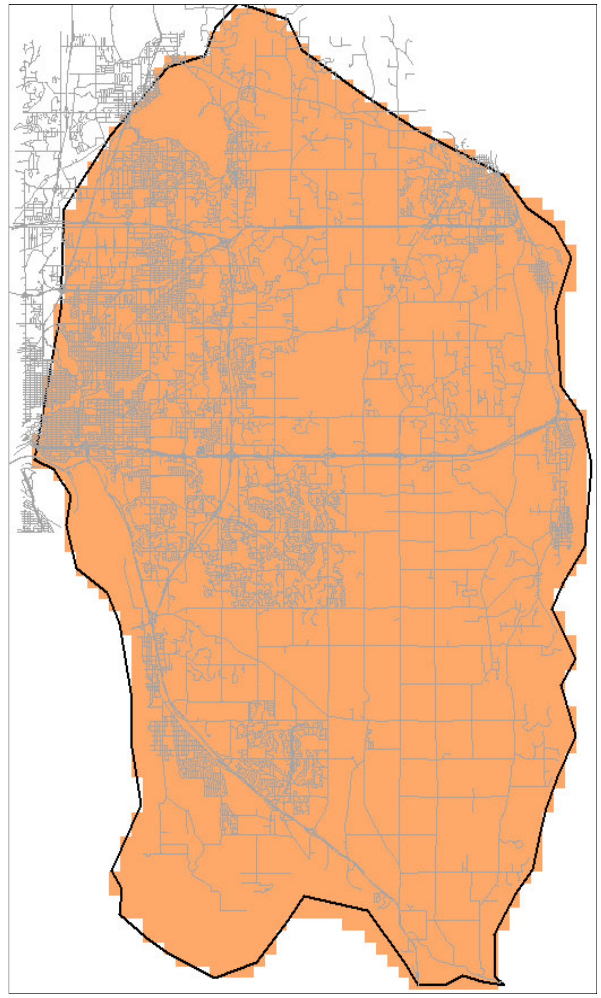

Vertical Hydraulic Conductivity

Vertical Hydraulic Conductivity (m/d)

- 0.00105
- 0.001
- 0.003773
- 0.004
- .0100
- 0.045
- 0.062
- 0.1
- 1
- 1.098
- 1.1804
- 1.891

Figure 25

Optimized Horizontal and Vertical Hydraulic Conductivity Zones (Layer 8)

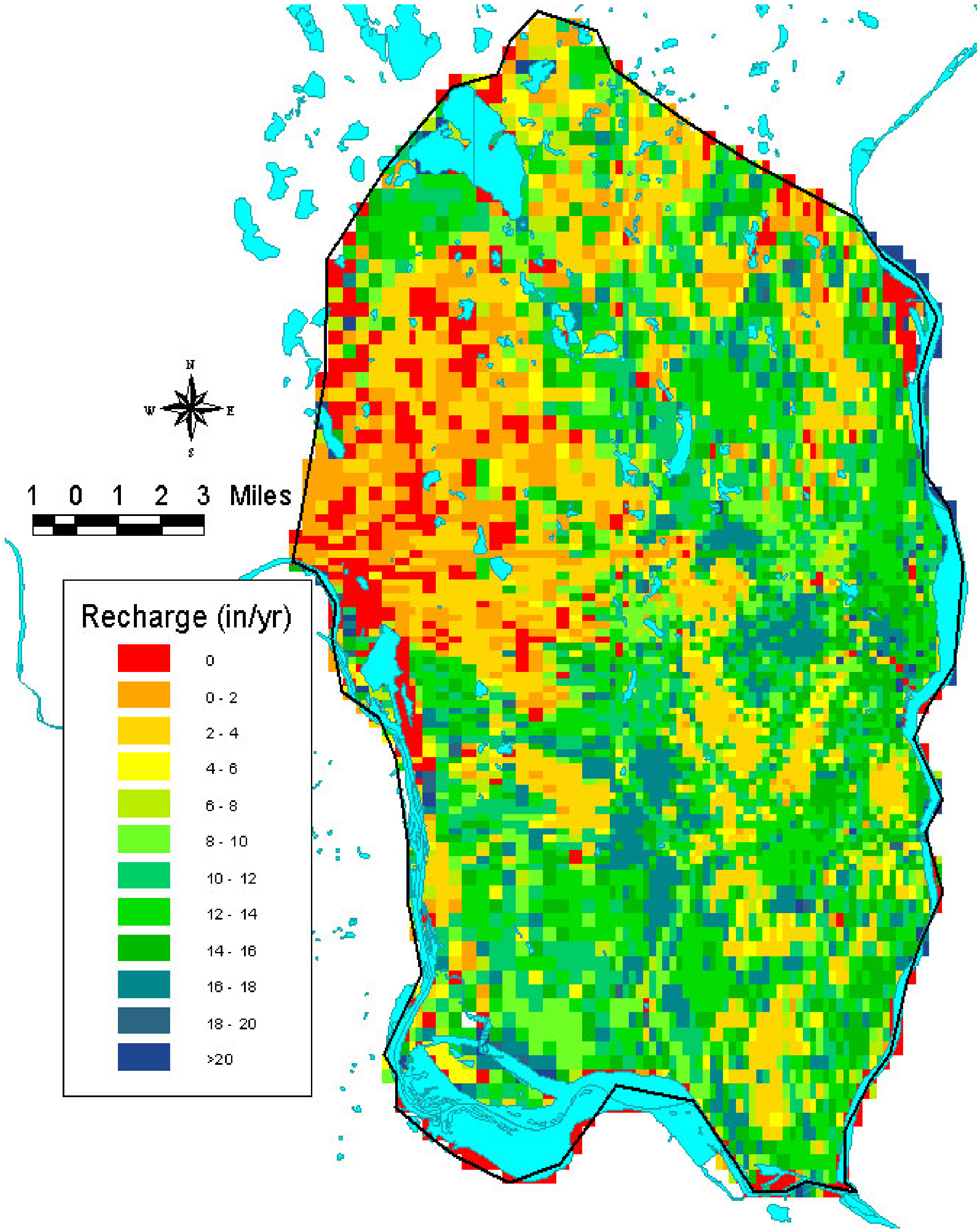

Figure 26

"Typical Year" Annualized Recharge (in/yr) – Derived from MIKE SHE MODEL for Input as Recharge in MODFLOW

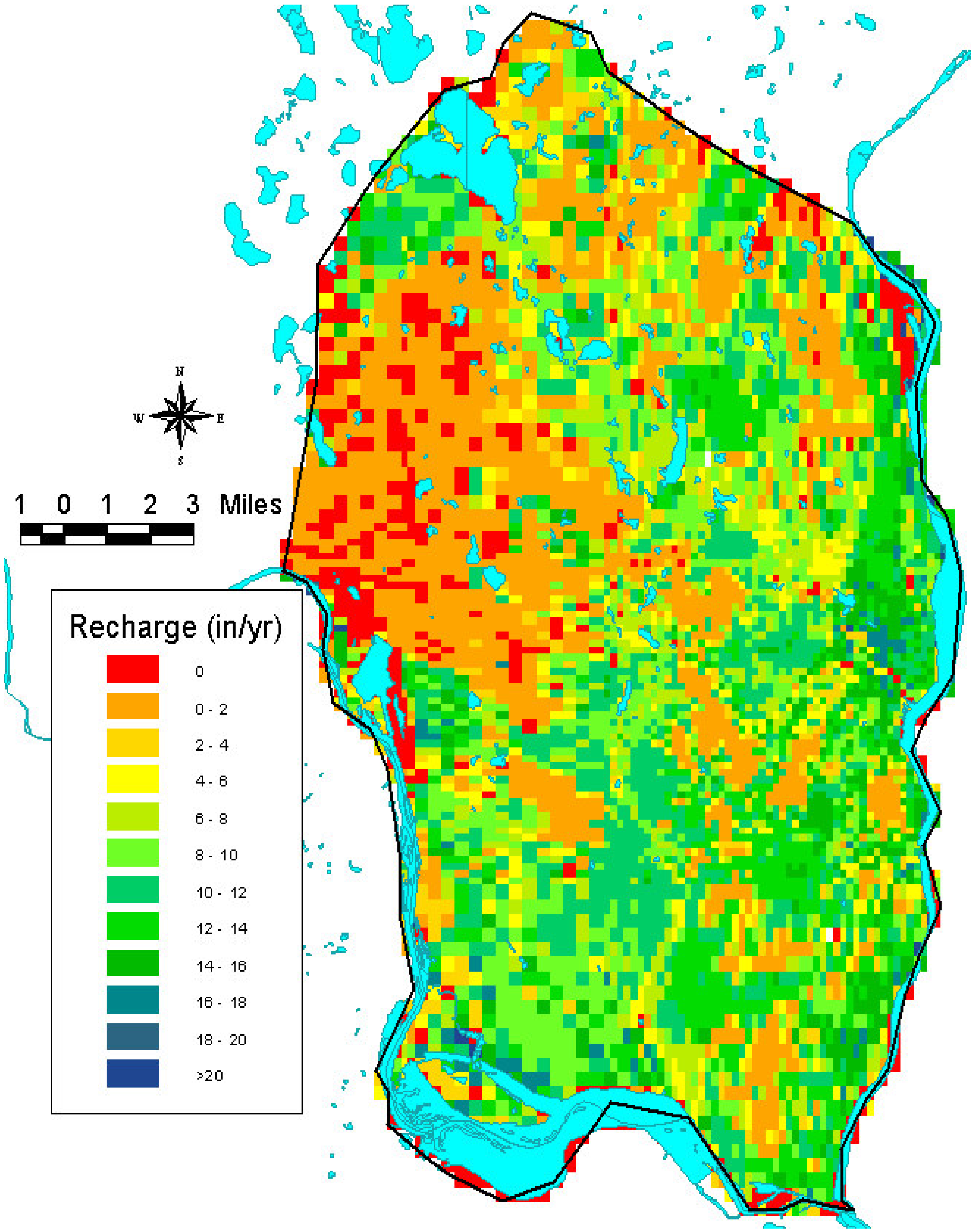

Figure 27

"Dry Year" (1988) Annualized Recharge (in/yr) – Derived from MIKE SHE MODEL for Input as Recharge in MODFLOW

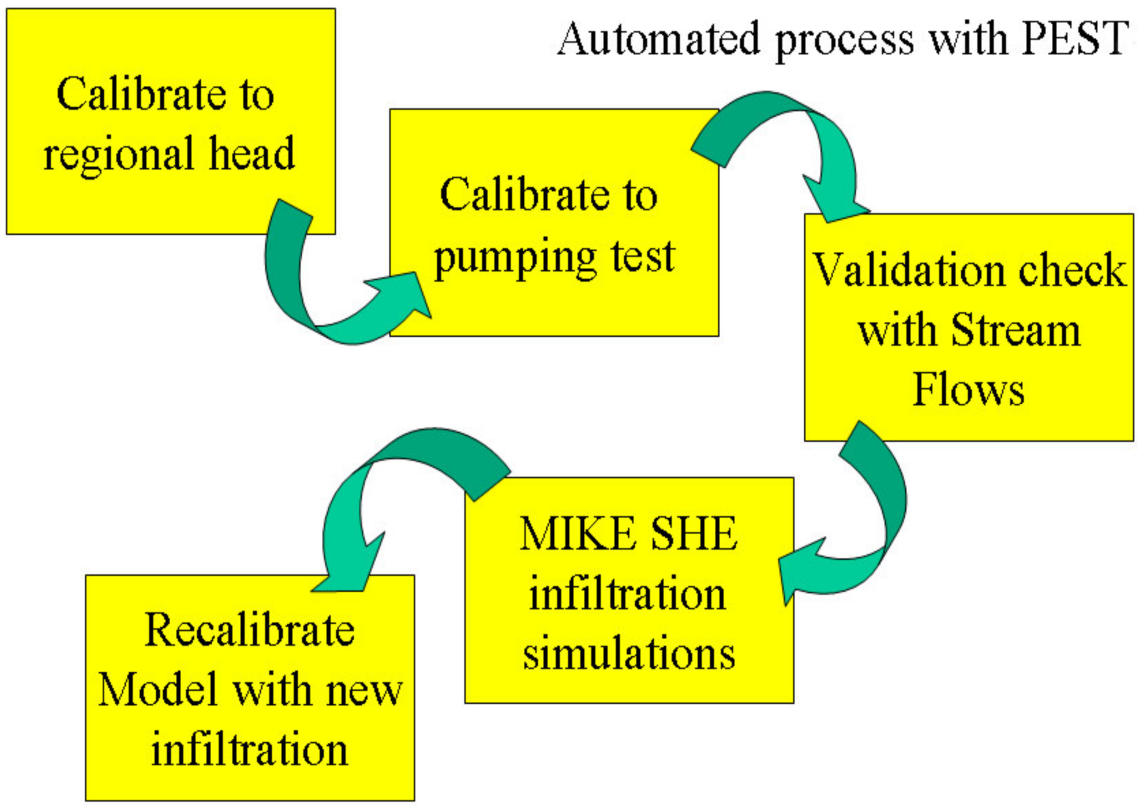

Figure 28

Flow Chart of the Calibration/Optimization Processes

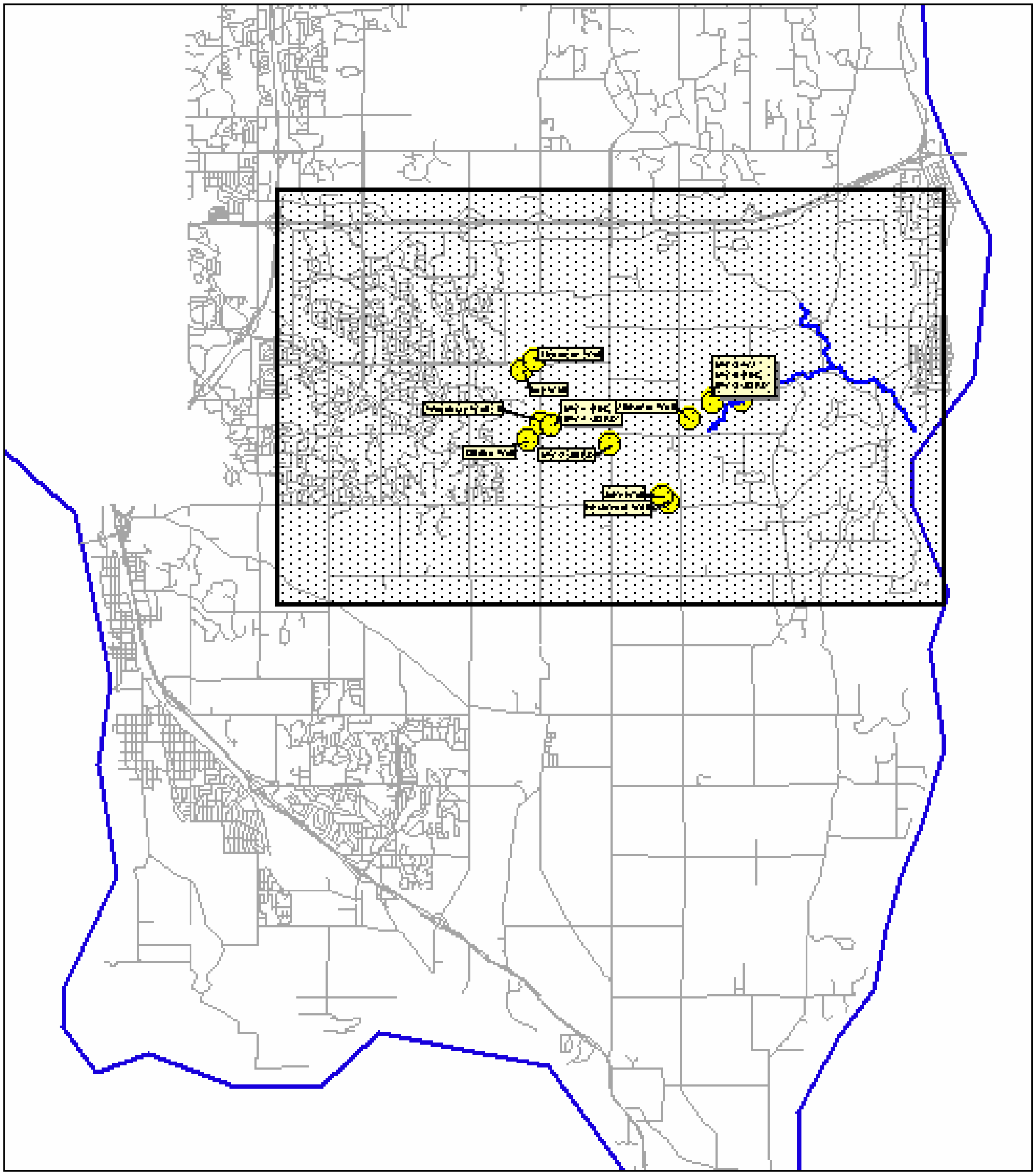

Figure 29

Location of Sub-Regional TMR Model: Woodbury Well 15 Pumping Test

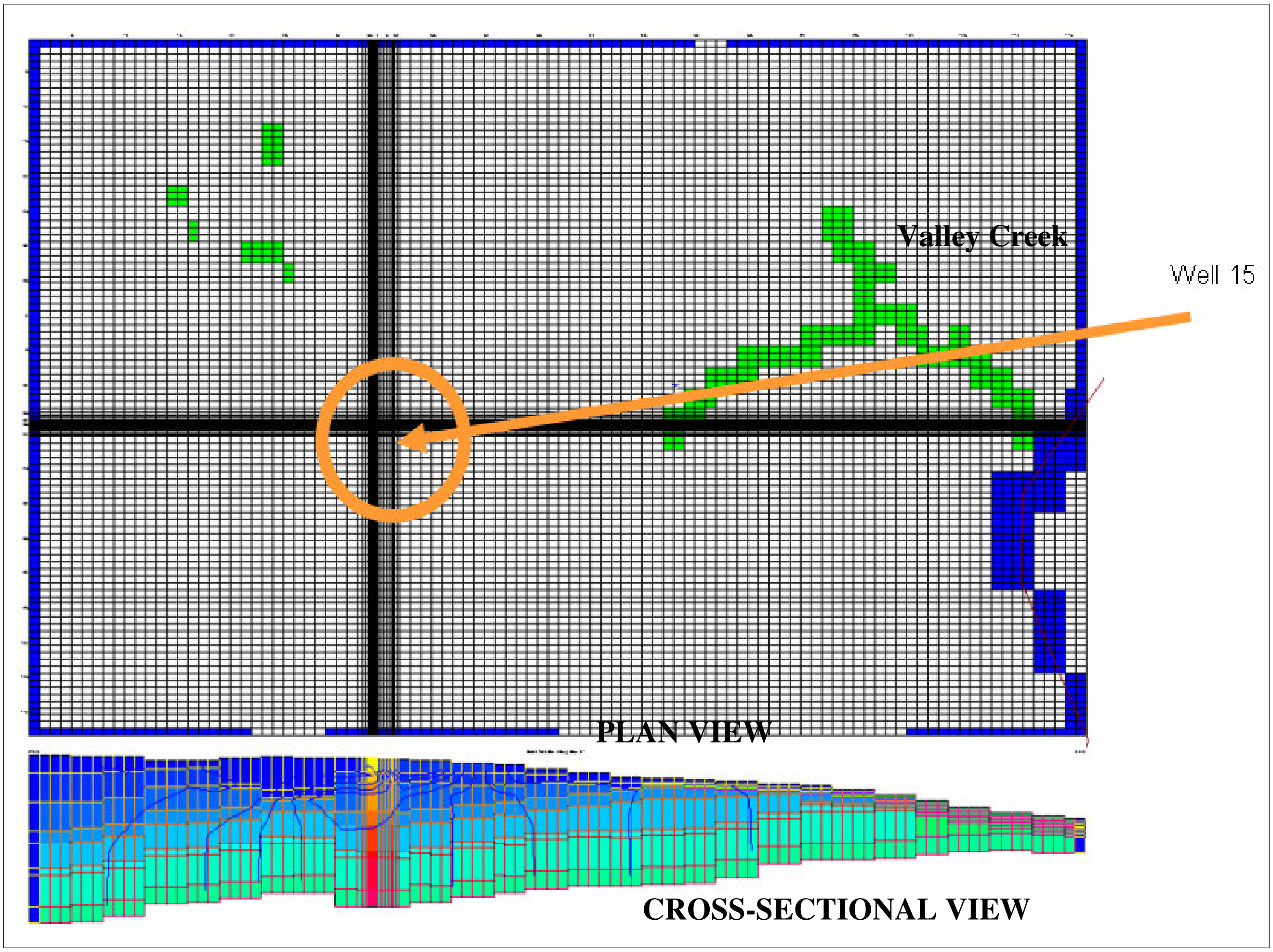

Figure 30

Discretization of the TMR Model for Optimizing to the Woodbury Well 15 Pumping Test

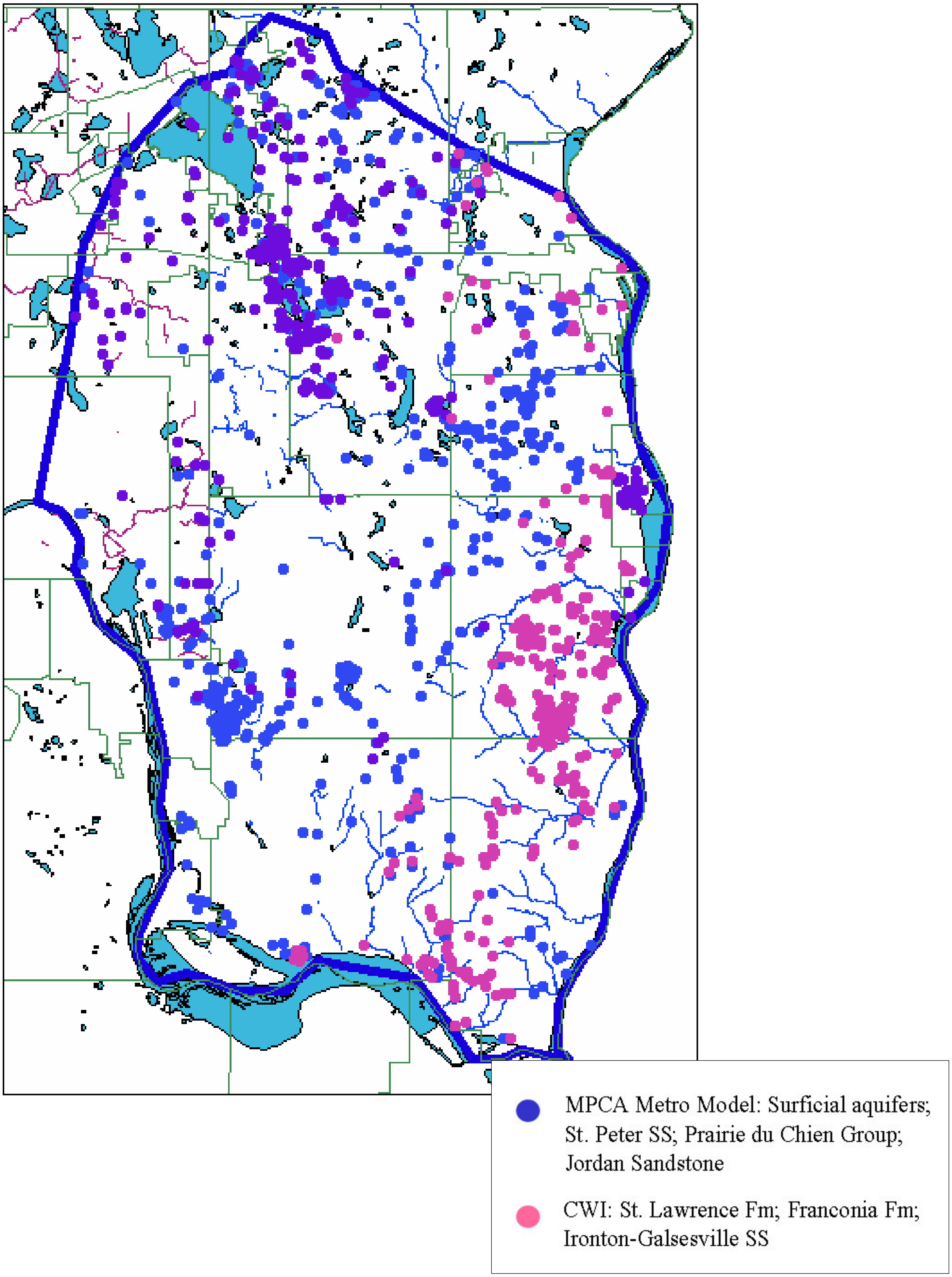

Figure 31

Sources for Regional Steady-State Calibration Targets

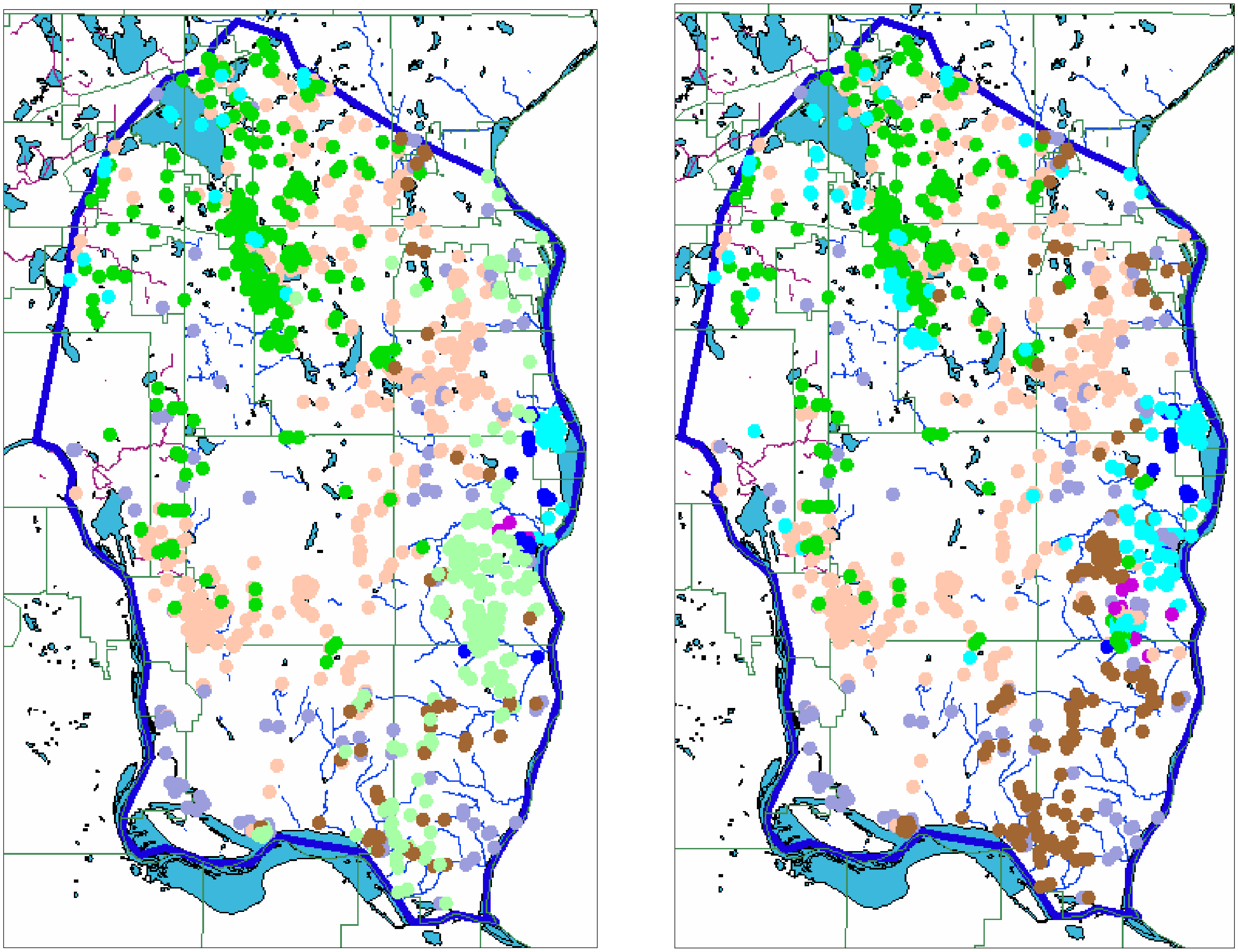

Top Layer **Bottom Layer**

Several calibration targets are in multiple layers

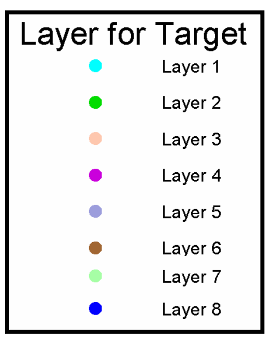

Figure 32

Model Layers Containing Calibration Targets for Regional Model

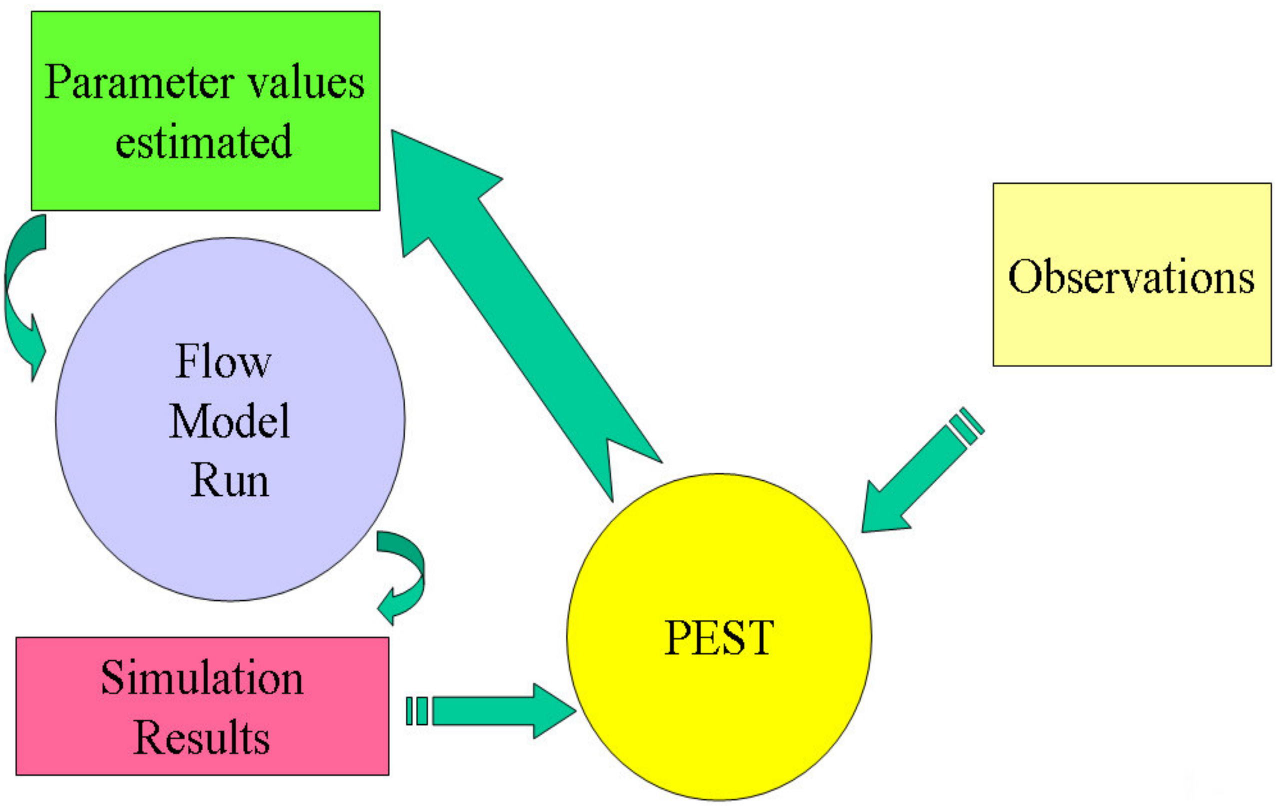

Figure 33

Flow Chart of Inverse Optimization Procedures

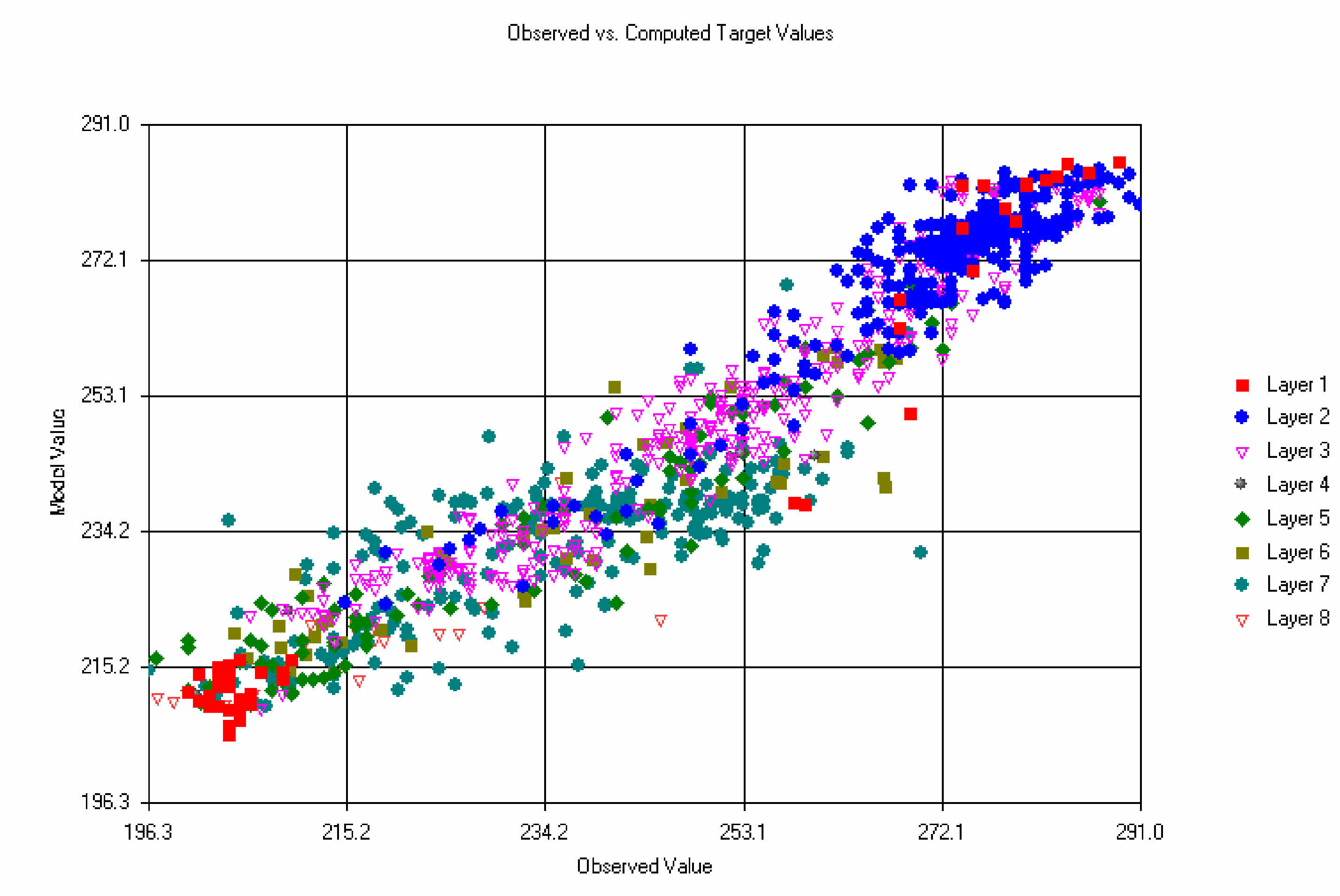

Figure 34

Plot of Simulated and Observed Heads for Steady-State Optimization

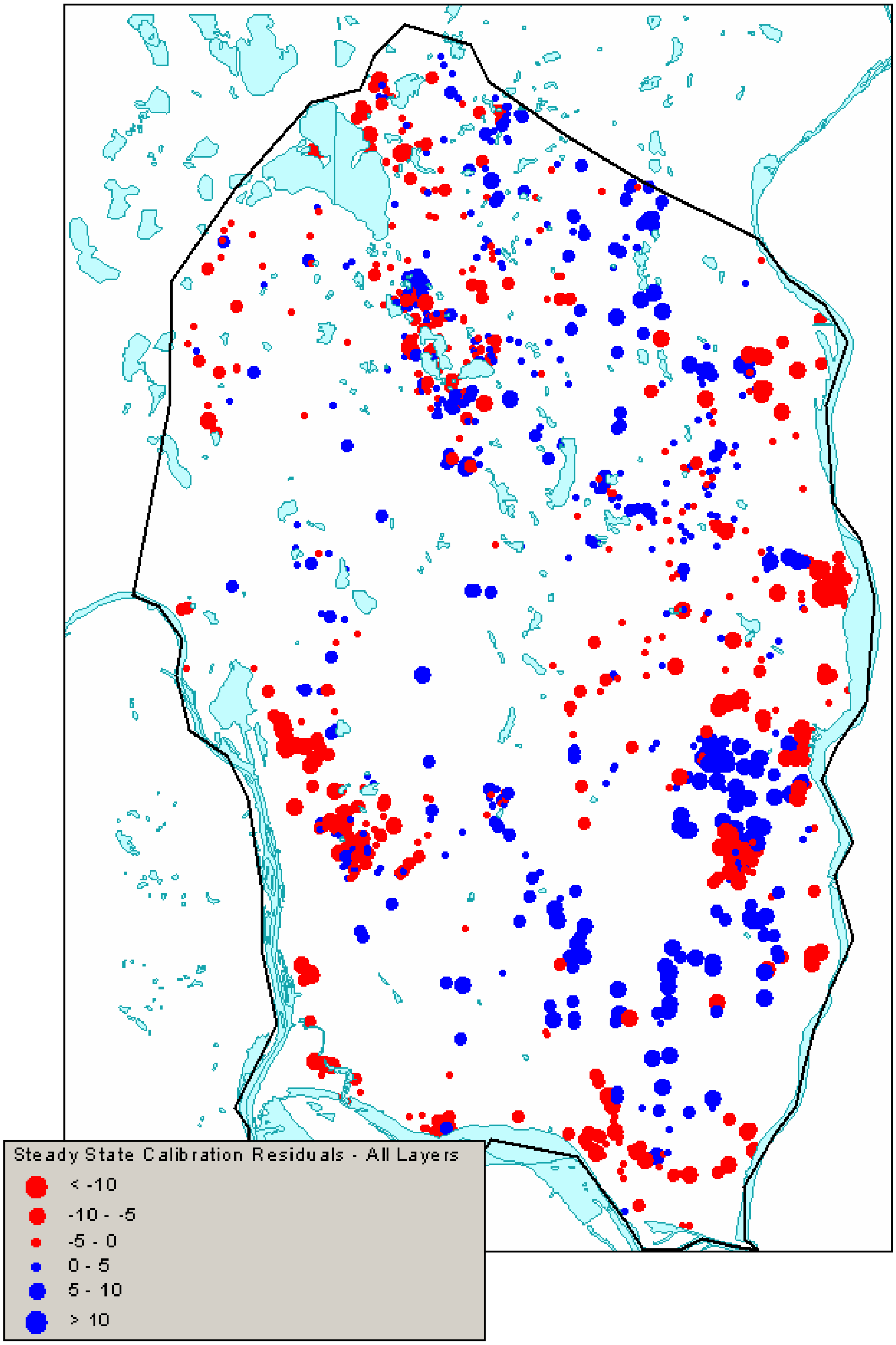

Figure 35

Map of Steady-State Optimization Residuals (meters) for All Layers

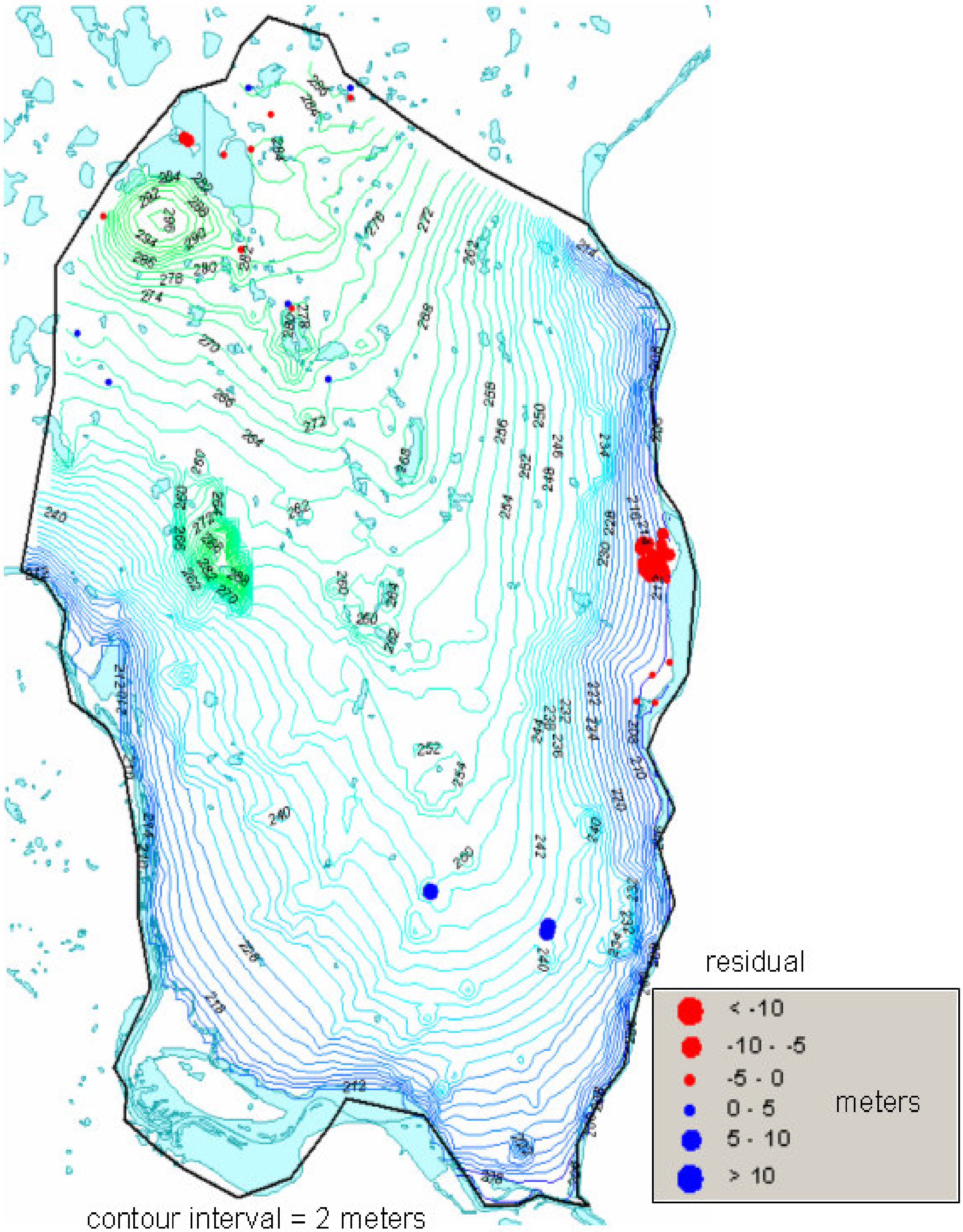

Figure 36

Contours of Steady-State Hydraulic Head and Plot of Optimization Residual for Layer 1

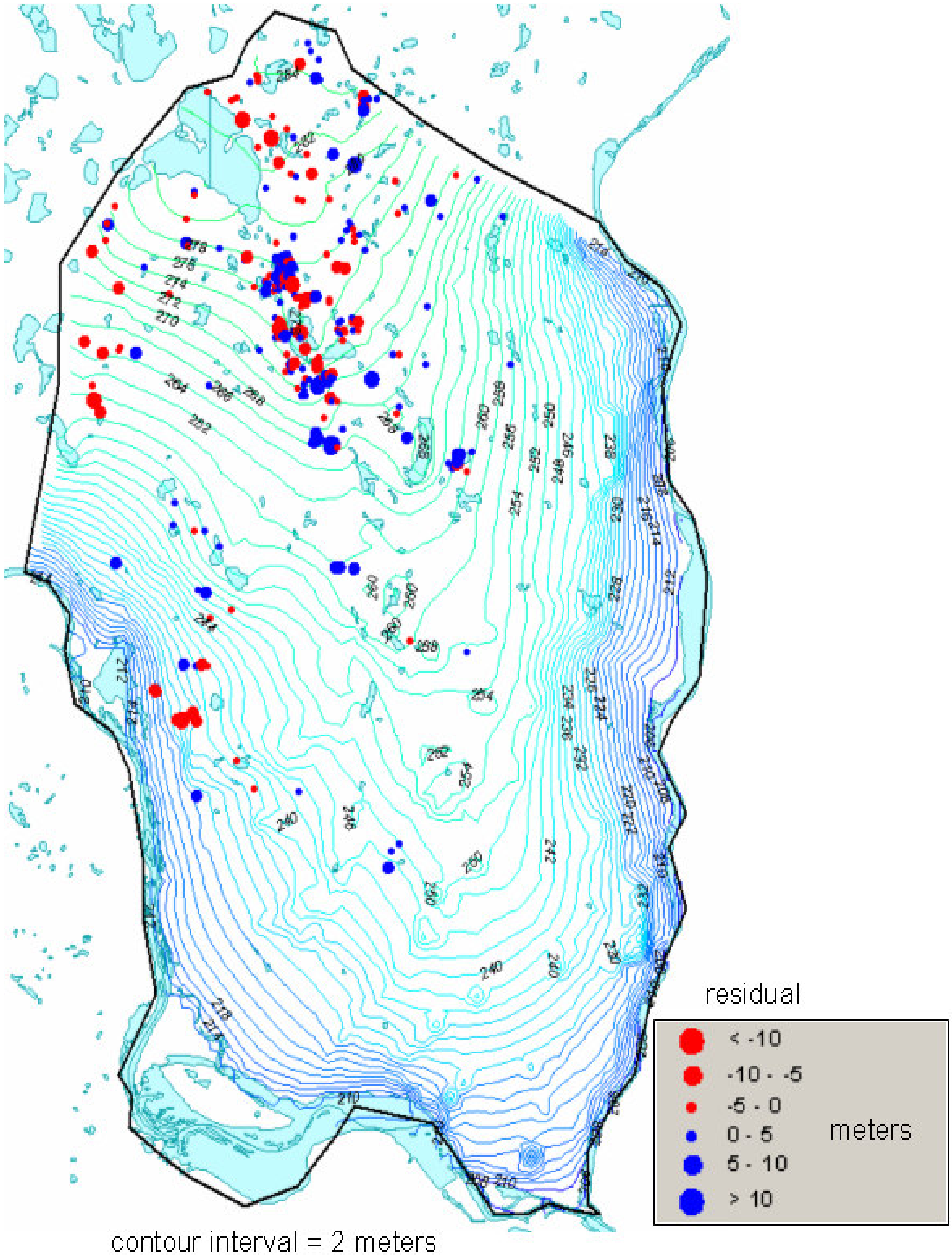

Figure 37

Contours of Steady-State Hydraulic Head and Plot of Optimization Residual for Layer 2

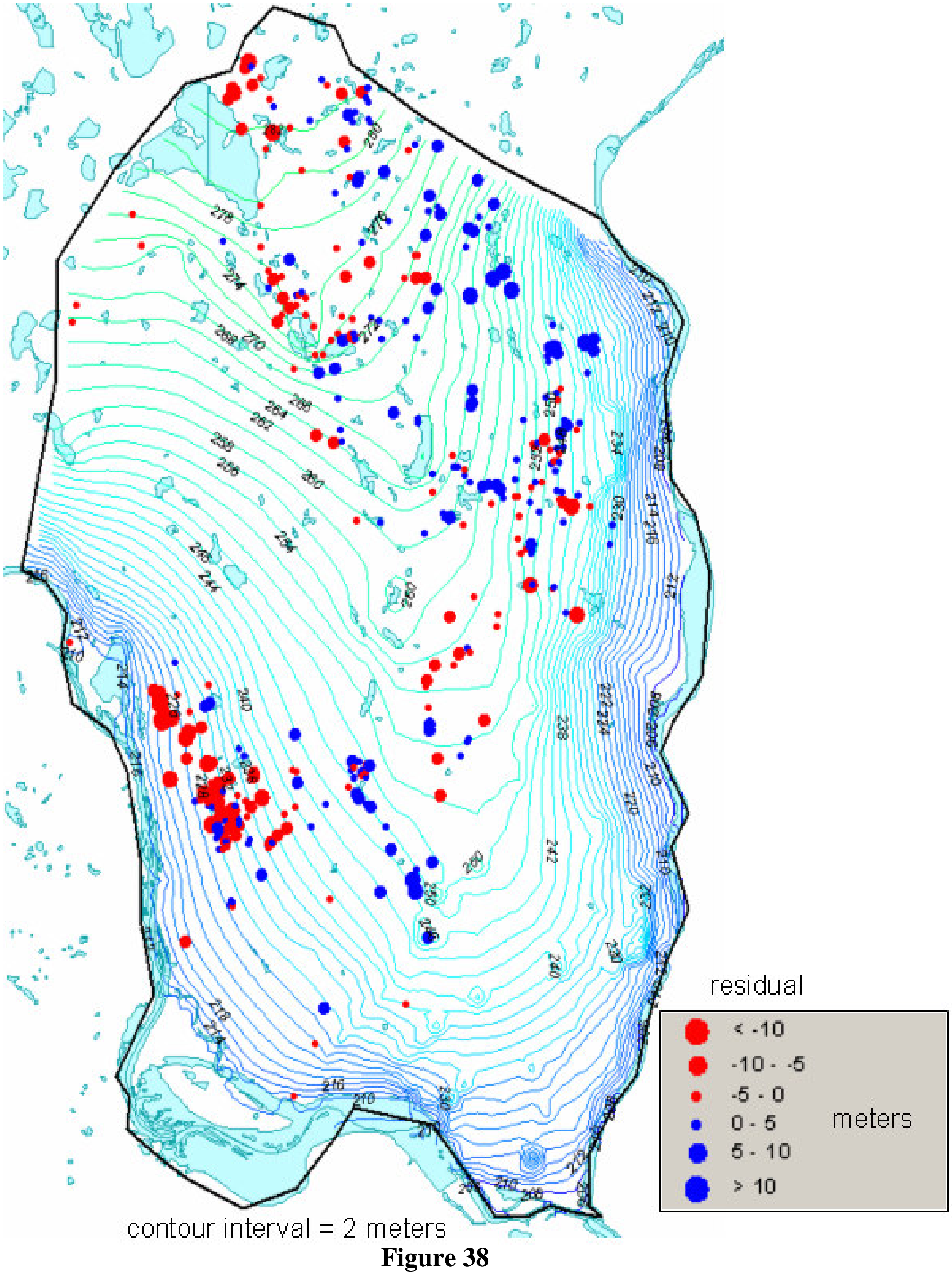

Figure 38

Contours of Steady-State Hydraulic Head and Plot of Optimization Residual for Layer 3

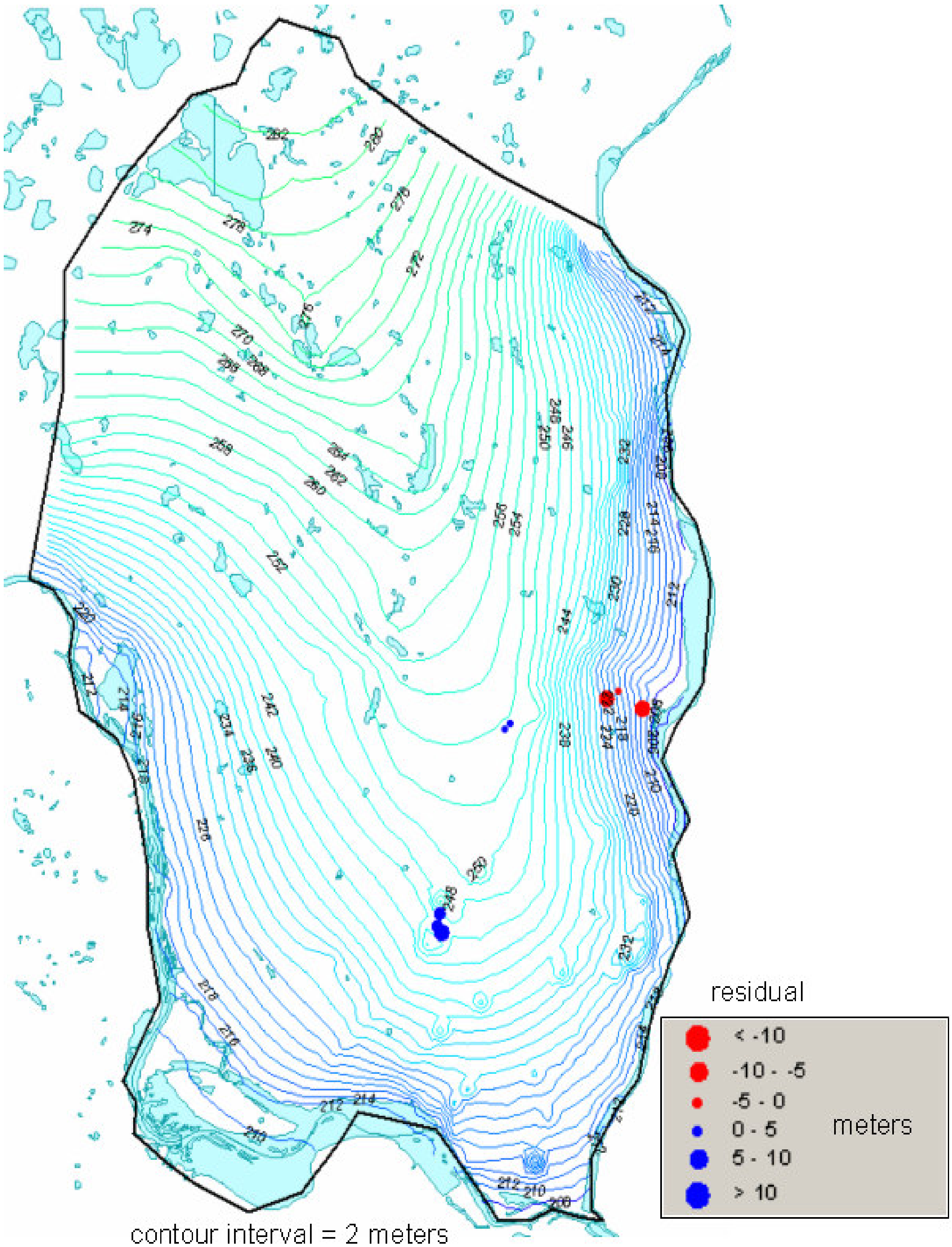

Figure 39

Contours of Steady-State Hydraulic Head and Plot of Optimization Residual for Layer 4

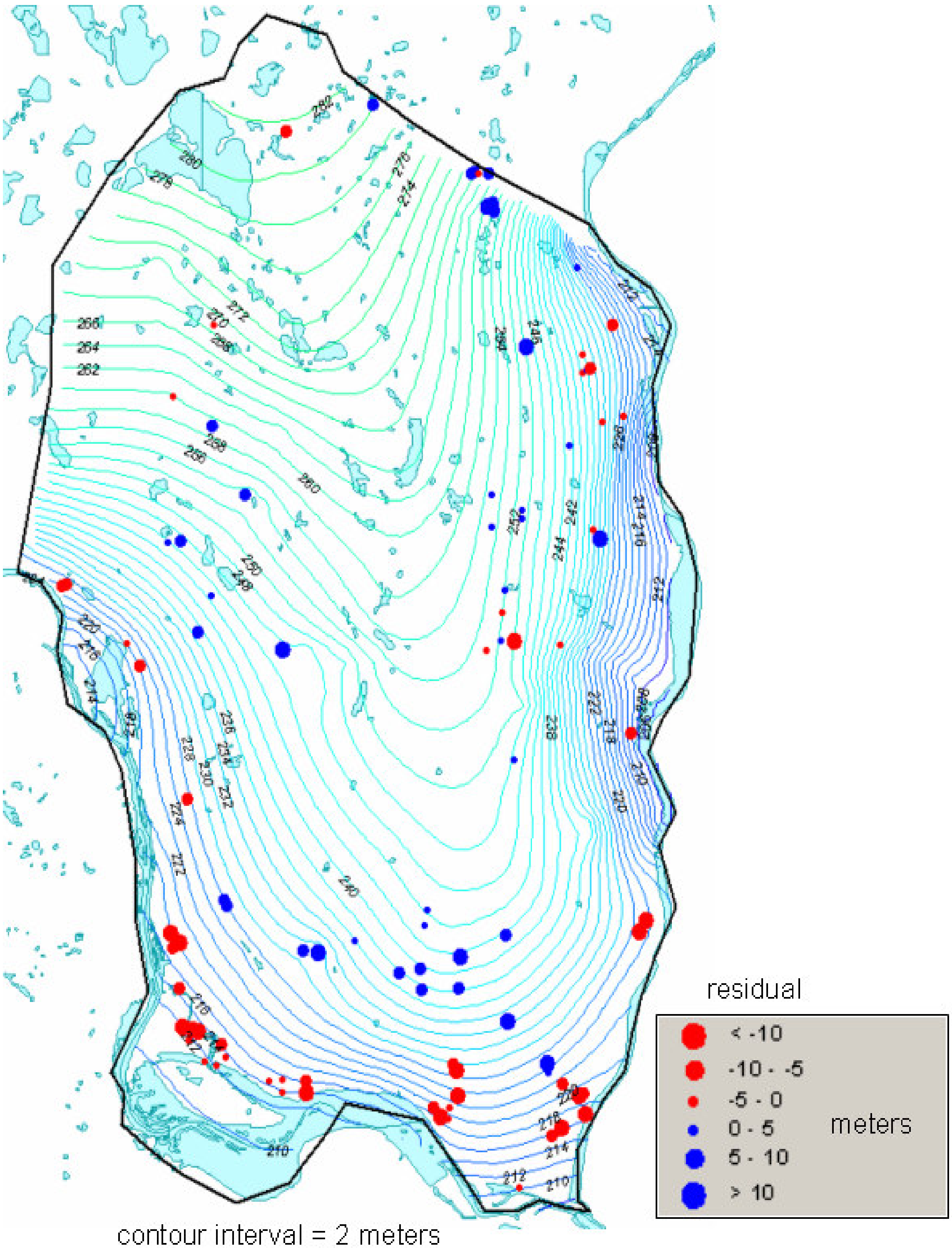

Figure 40

Contours of Steady-State Hydraulic Head and Plot of Optimization Residual for Layer 5

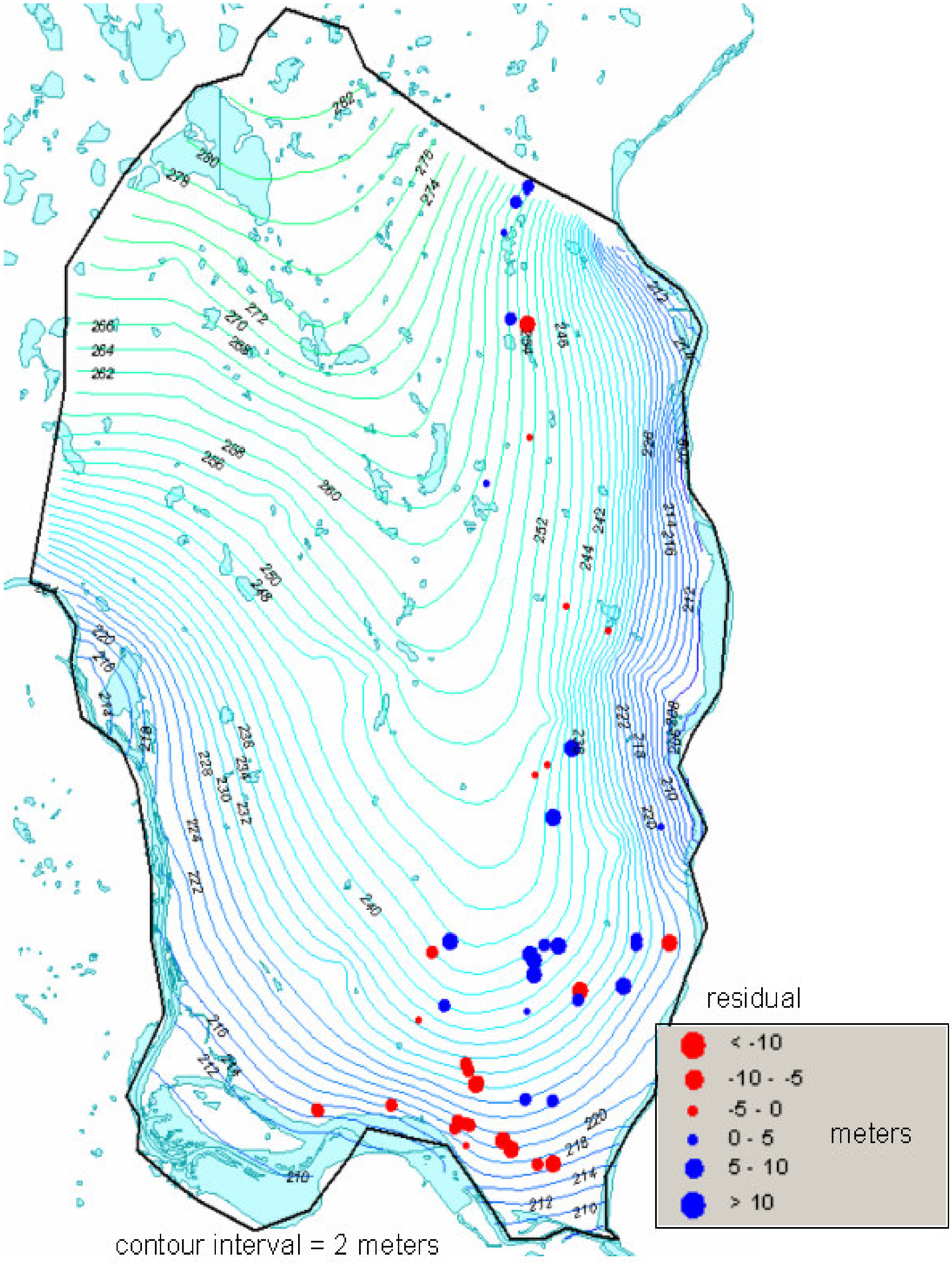

Figure 41

Contours of Steady-State Hydraulic Head and Plot of Optimization Residual for Layer 6

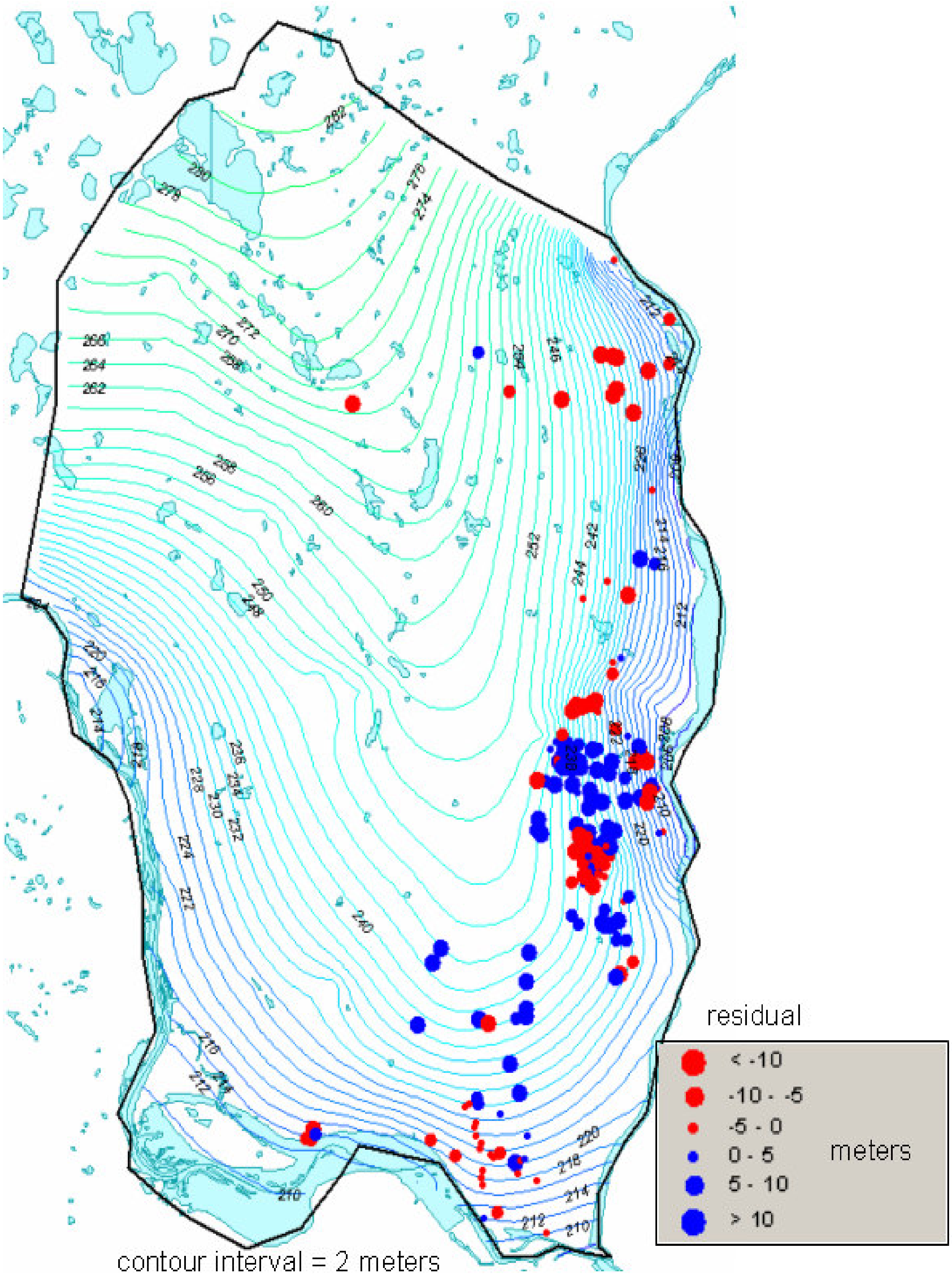

Figure 42

Contours of Steady-State Hydraulic Head and Plot of Optimization Residual for Layer 7

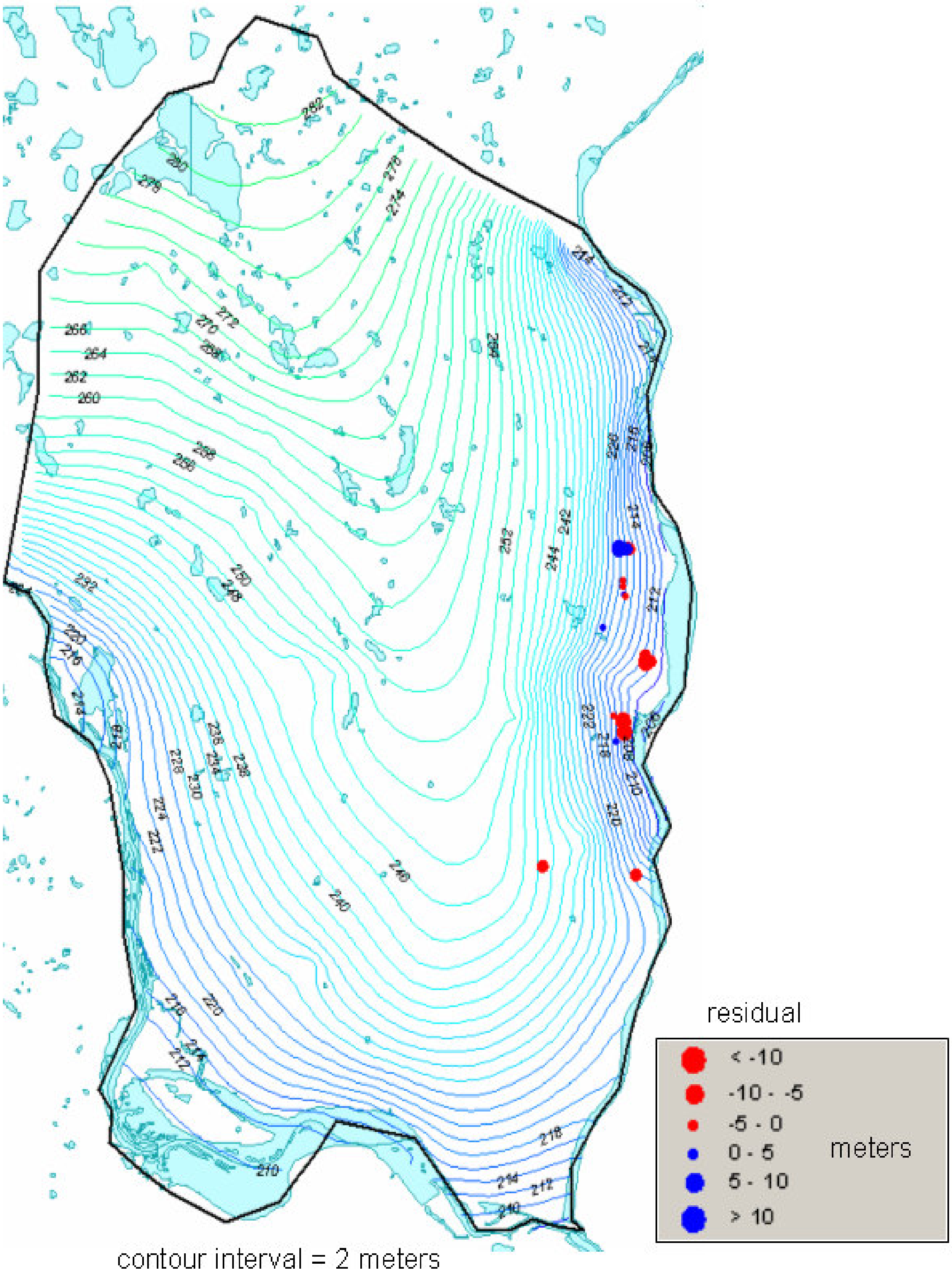

Figure 43

Contours of Steady-State Hydraulic Head and Plot of Optimization Residual for Layer 8

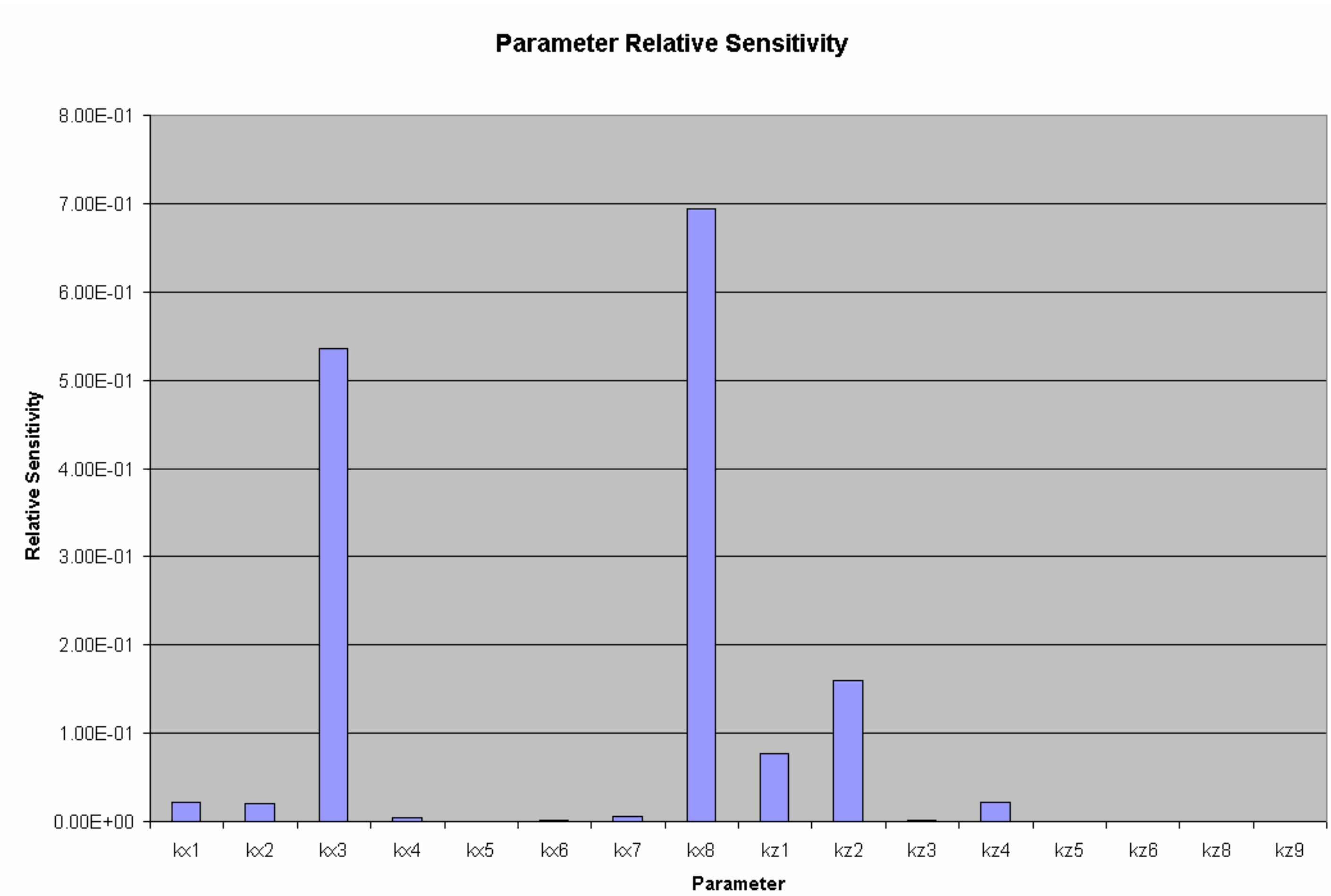

Figure 44

Plot of Relative Parameter Sensitivities for Regional Optimization

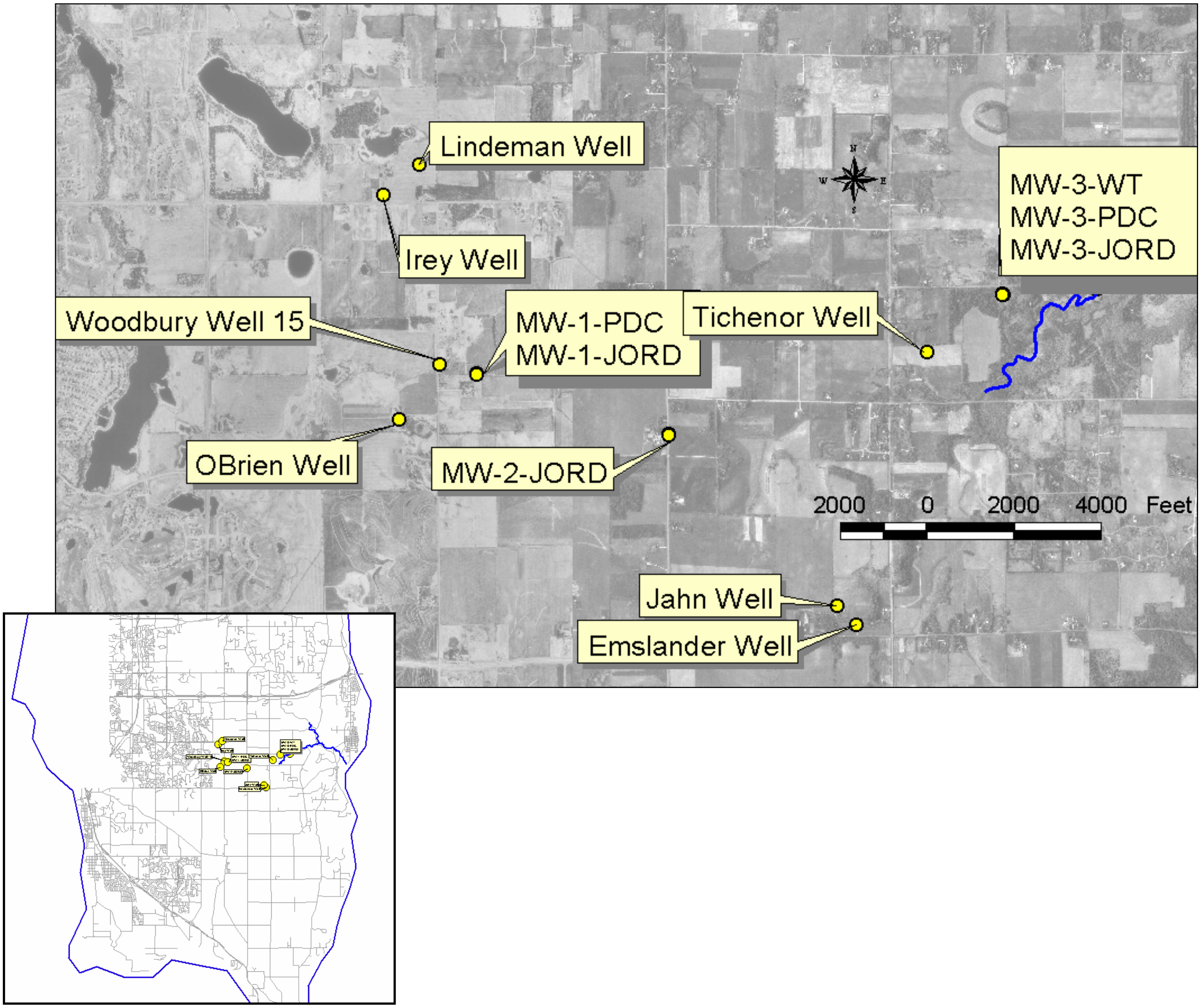

Figure 45

Location of Wells for Woodbury Well 15 Aquifer Tests

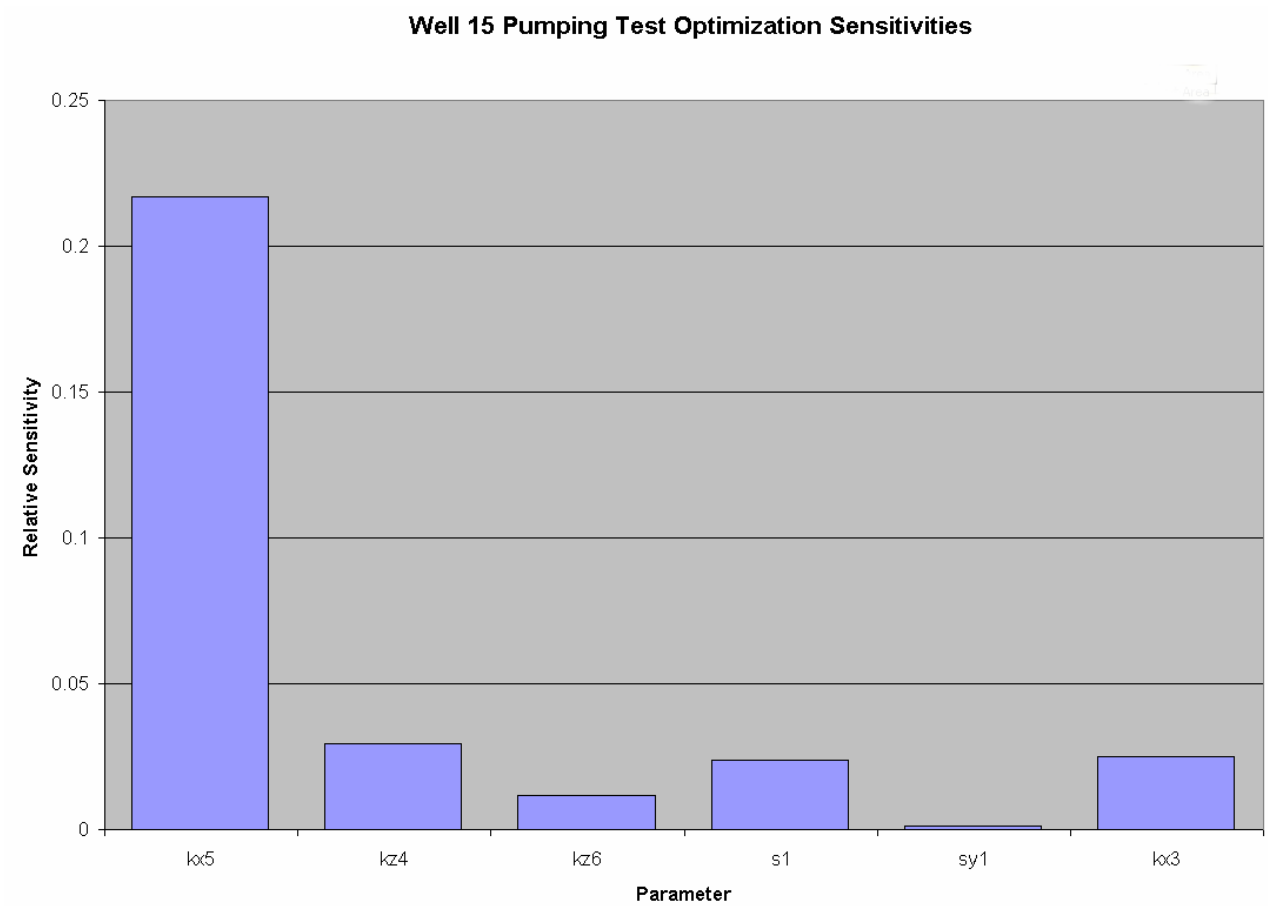

Figure 46

Plot of Relative Parameter Sensitivities for Woodbury Well 15 Aquifer Test Optimization

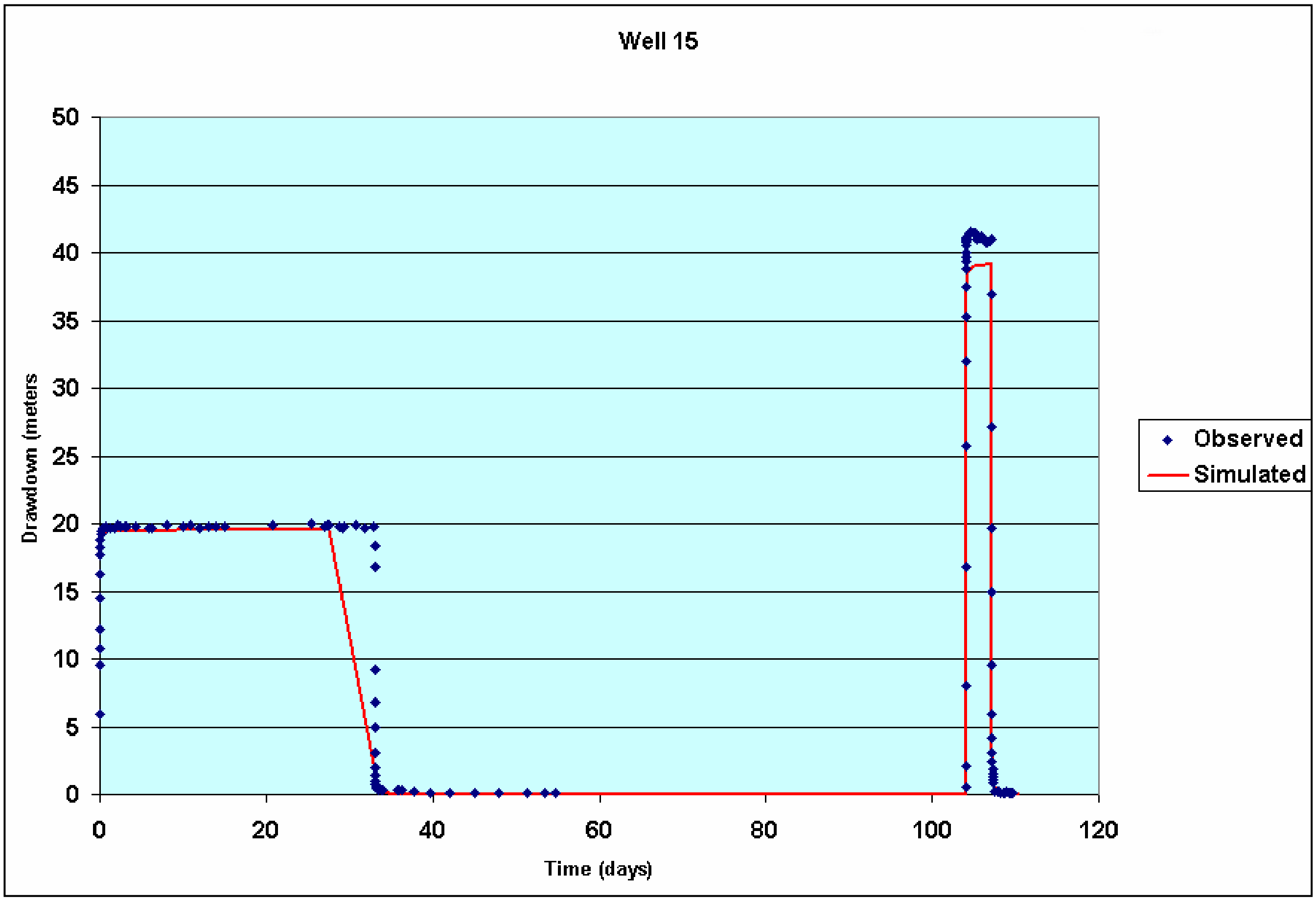

Figure 47

Comparison of Simulated and Observed Drawdowns at Well 15 for Aquifer Test Optimization

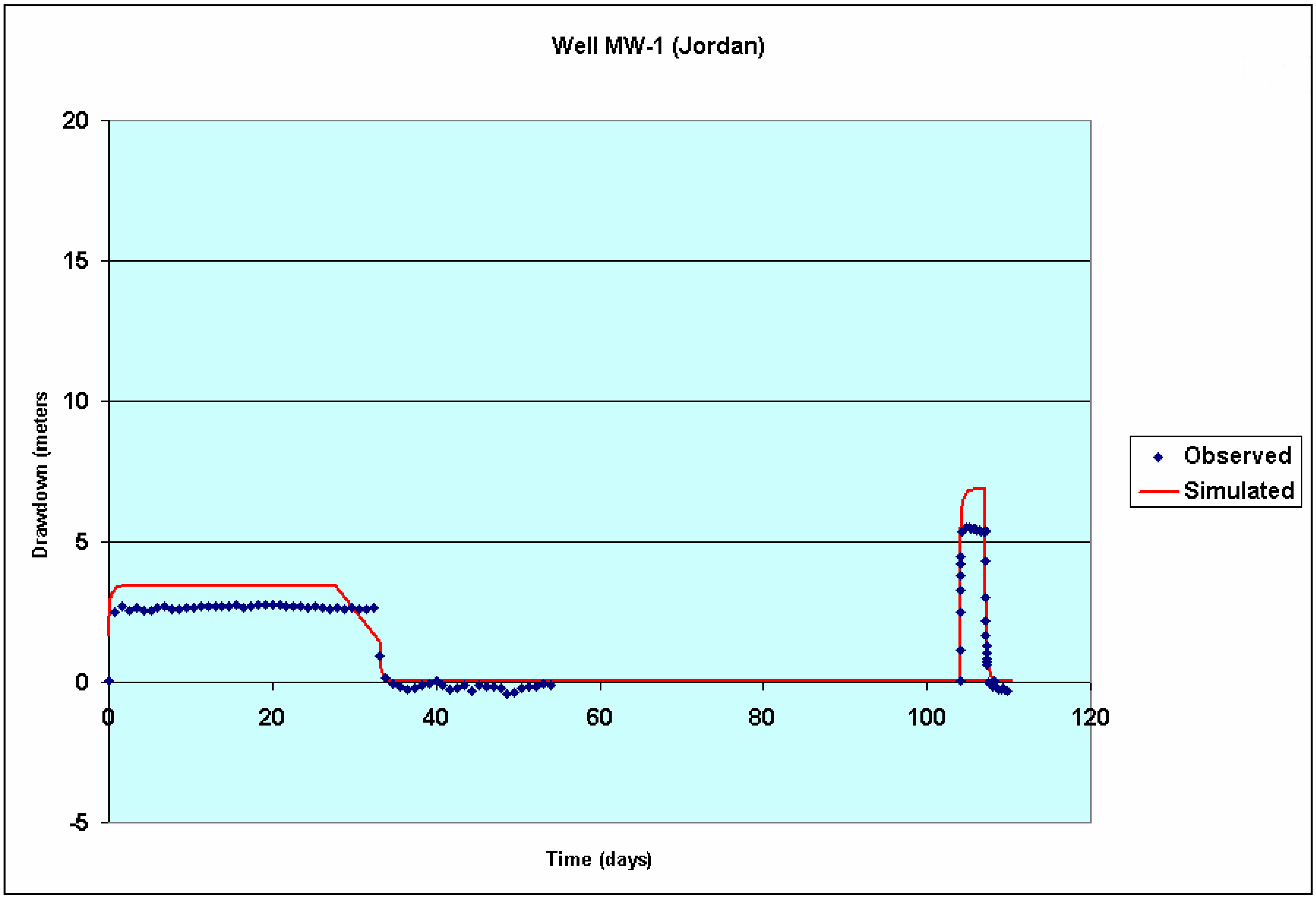

Figure 48

Comparison of Simulated and Observed Drawdowns at Monitoring Well MW-1-Jordan for Aquifer Test Optimization

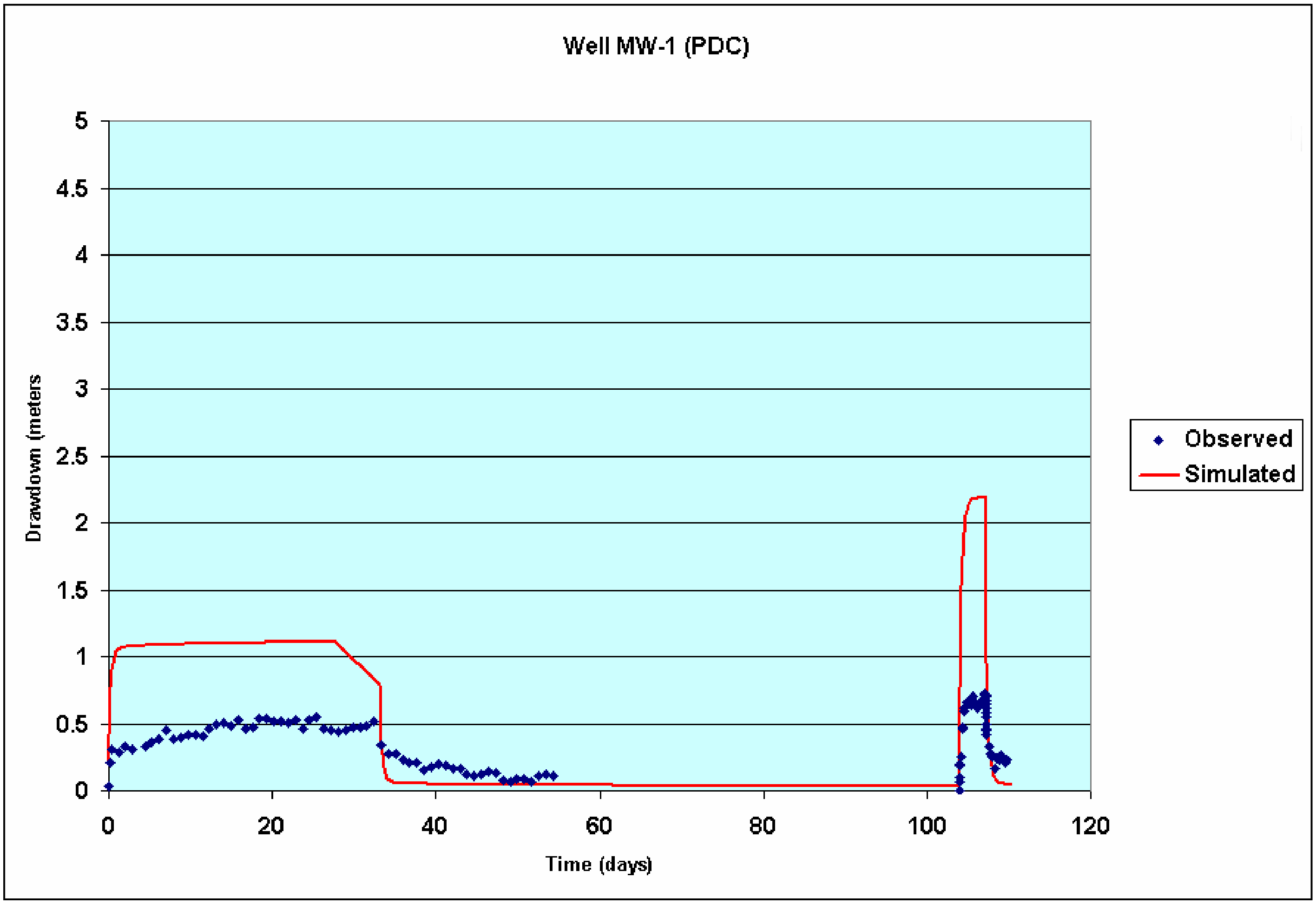

Figure 49

Comparison of Simulated and Observed Drawdowns at Monitoring Well MW-1-PDC for Aquifer Test Optimization

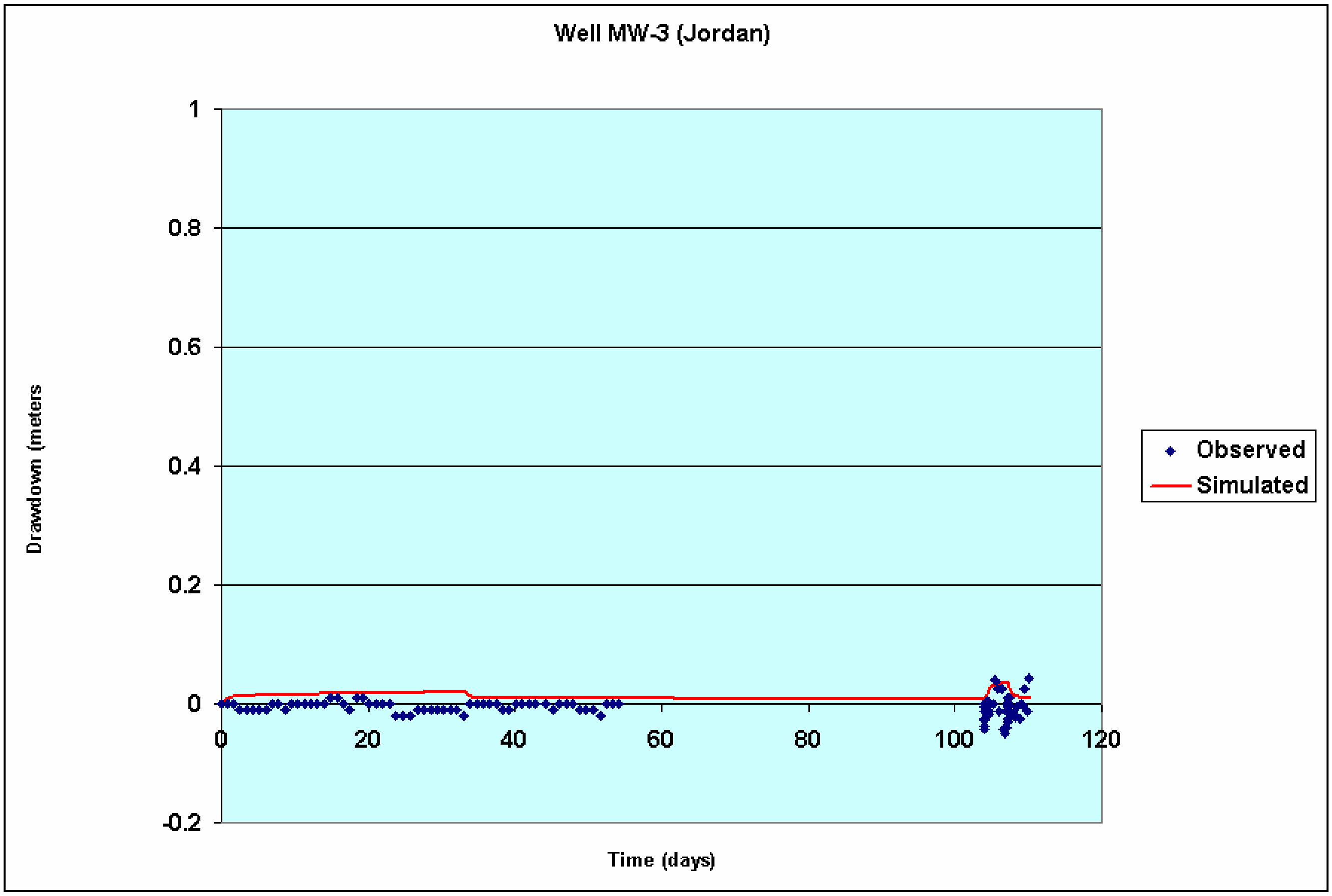

Figure 50

Comparison of Simulated and Observed Drawdowns at Monitoring Well MW-3-Jordan for Aquifer Test Optimization

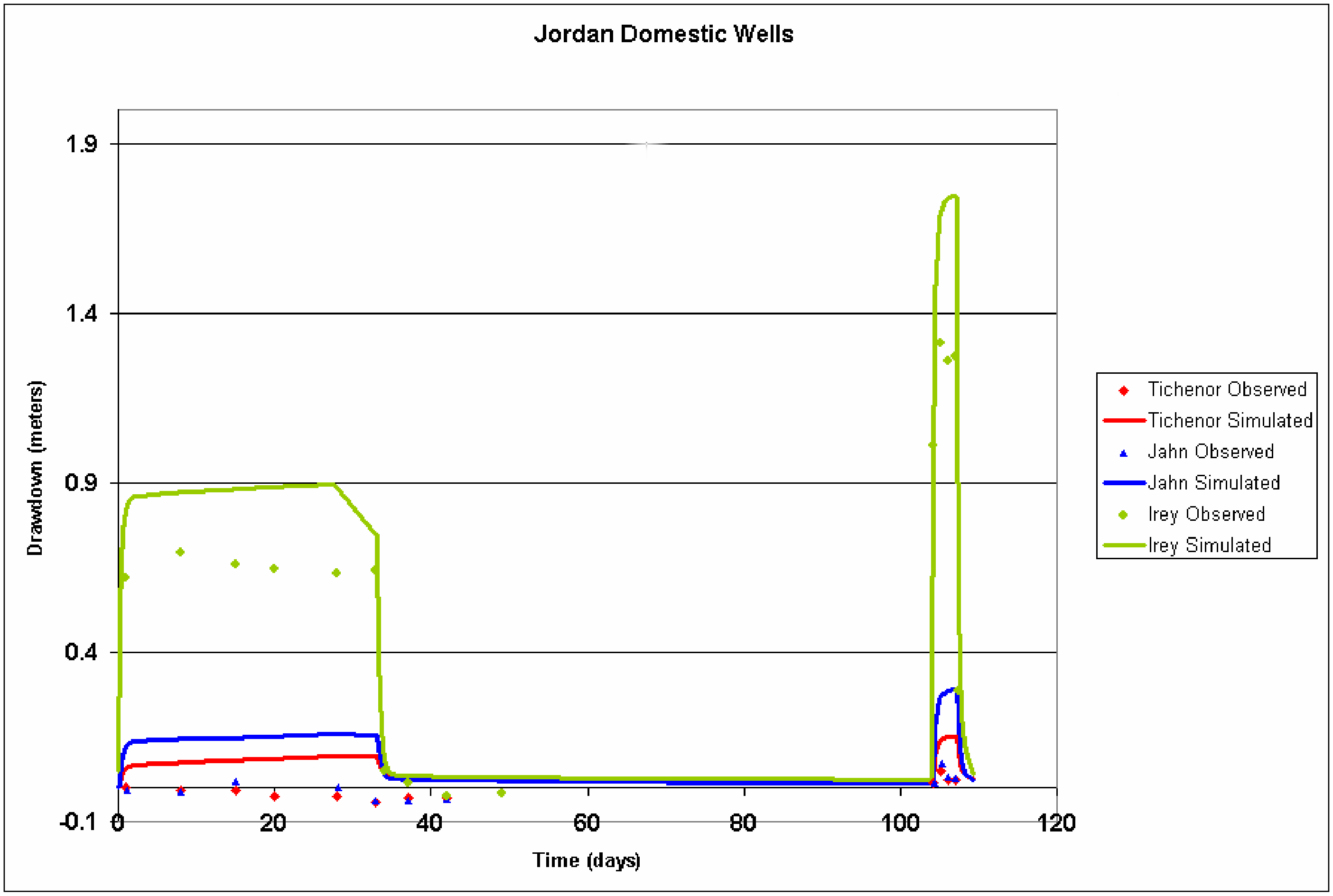

Figure 51

Comparison of Simulated and Observed Drawdowns at Jordan Domestic Wells for Aquifer Test Optimization

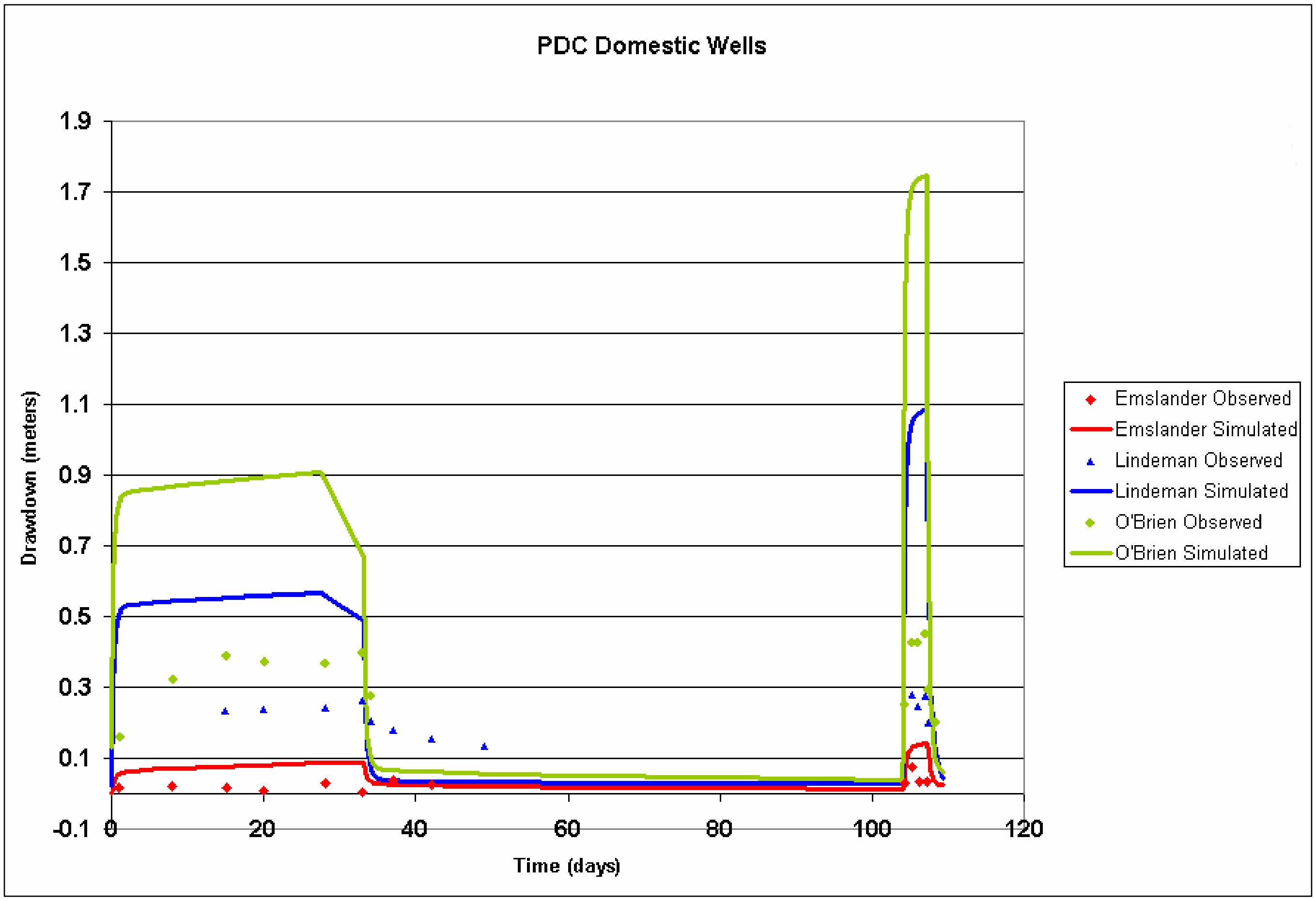

Figure 52

Comparison of Simulated and Observed Drawdowns at Prairie du Chien Group Domestic Wells for Aquifer Test Optimization

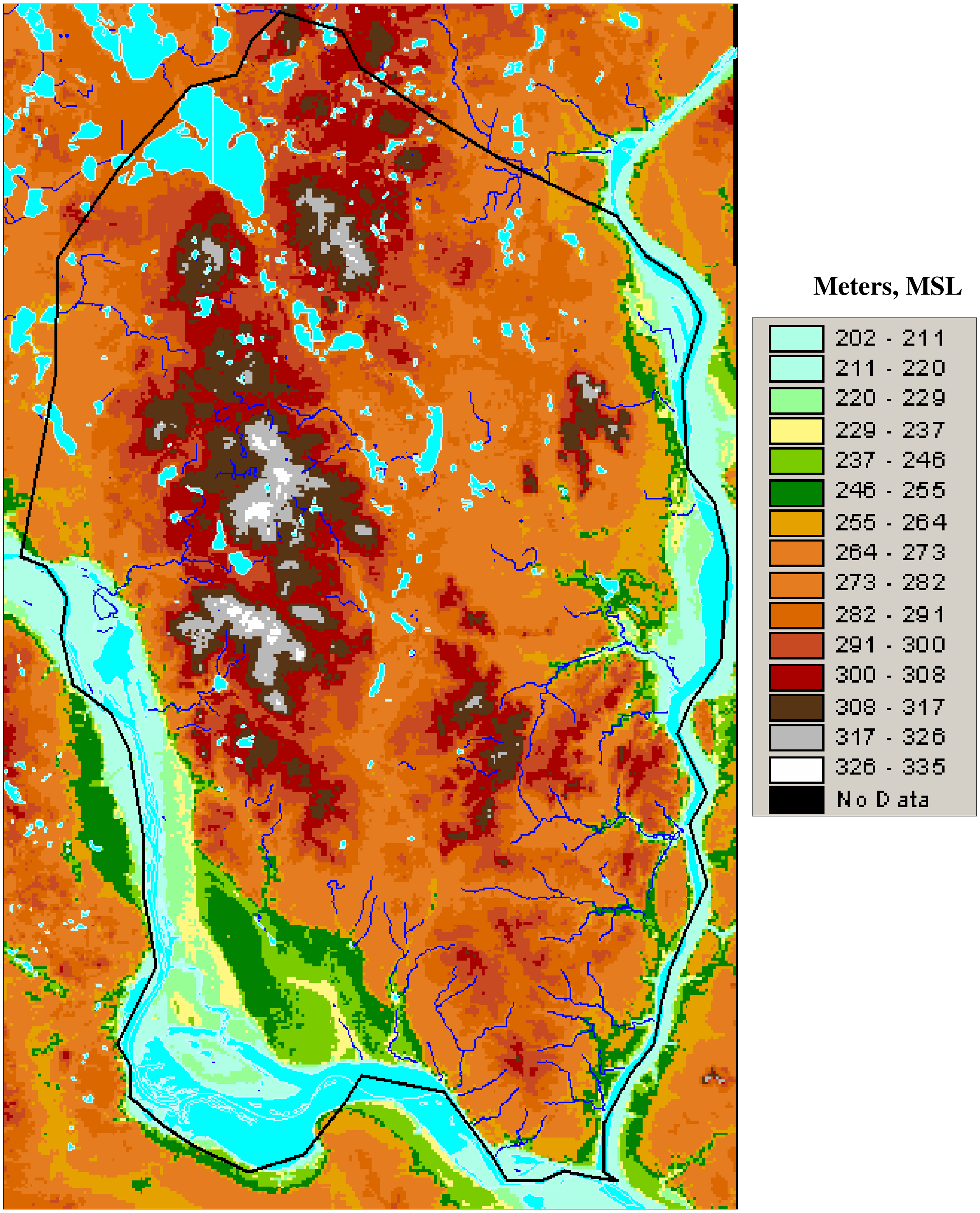

Figure 53

100-Meter Grid of Ground-Surface Topography Used in MIKE SHE Simulations

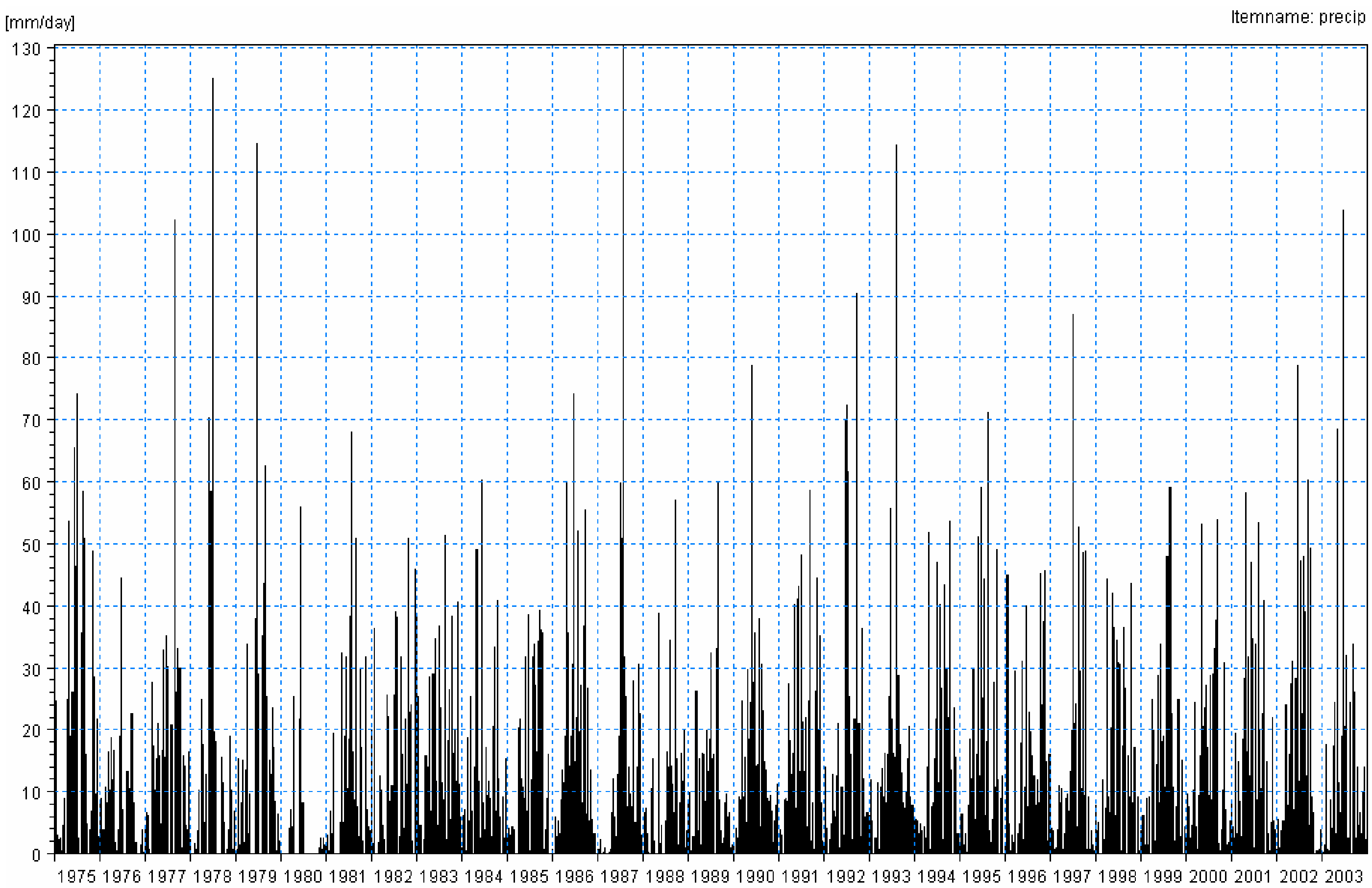

Figure 54

Daily Precipitation, mm, (St. Paul, Minnesota) Used in MIKE SHE Simulations for Period 1975-2003

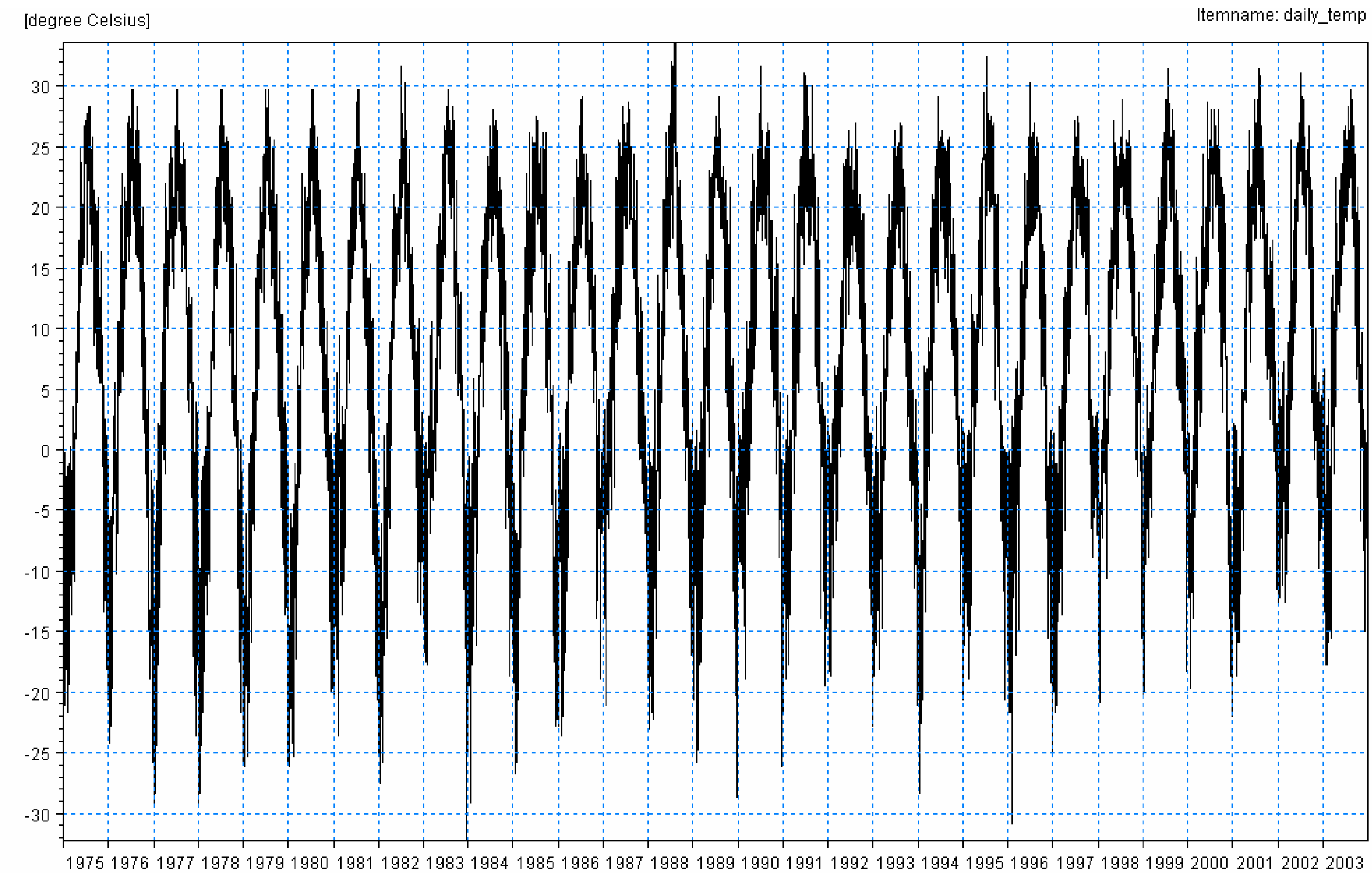

Figure 55

Daily Mean Temperature (^{o}C) (St. Paul, Minnesota) Used in MIKE SHE Simulations for Period 1975-2003

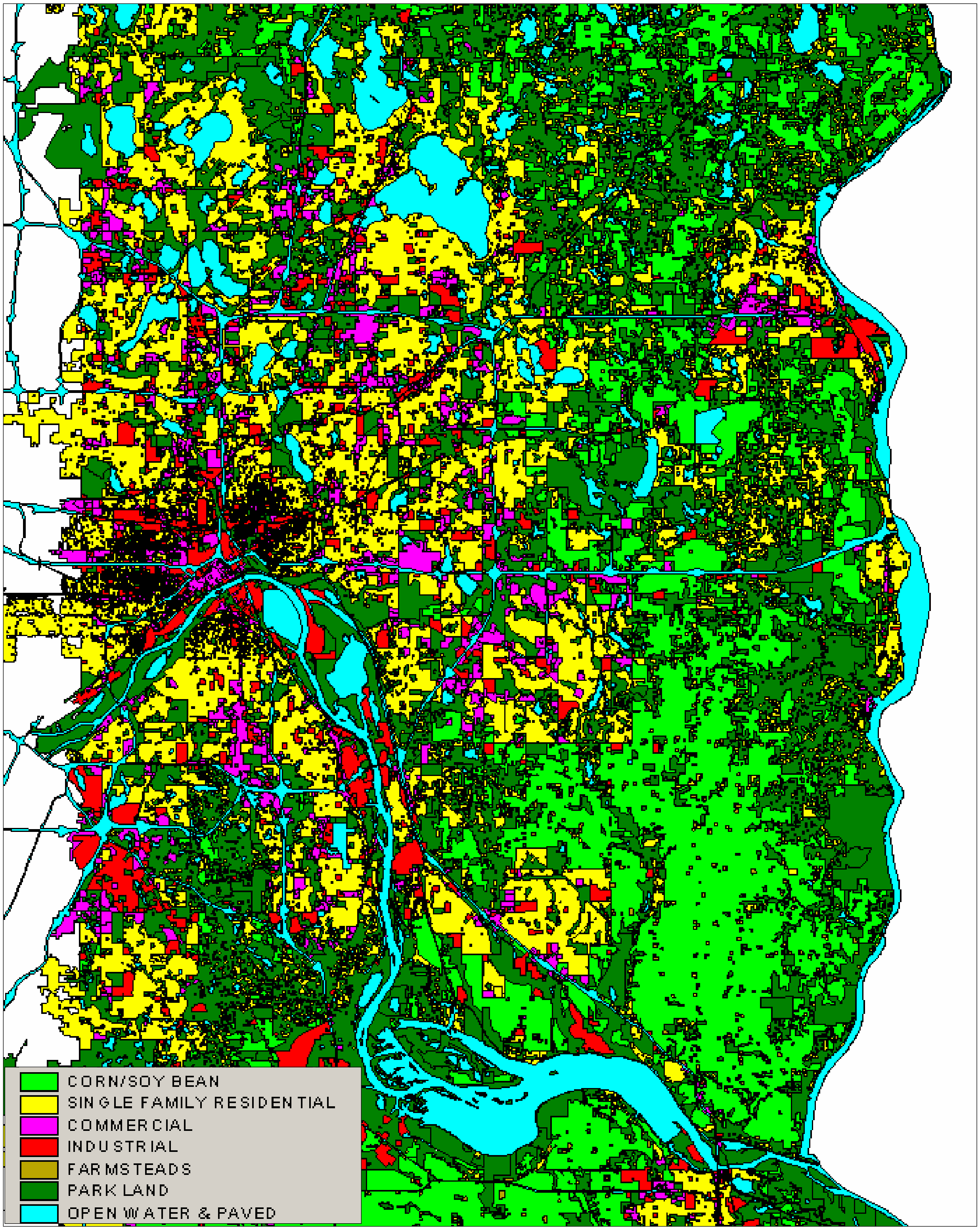

Figure 56

Seven Land-Use/Vegetation Types Used in MIKE SHE Simulations

CORN/SOYBEAN

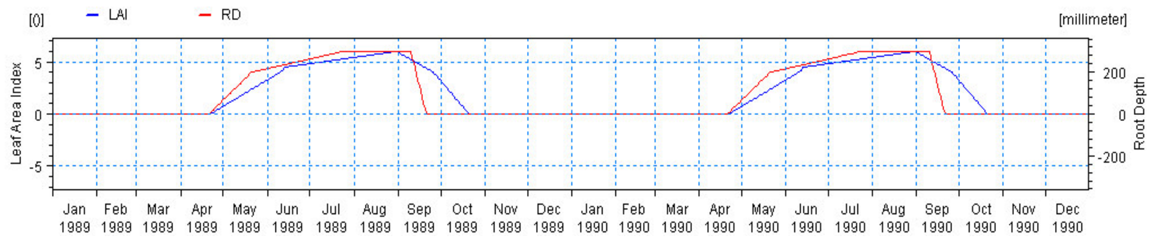

RESIDENTIAL/LAWN

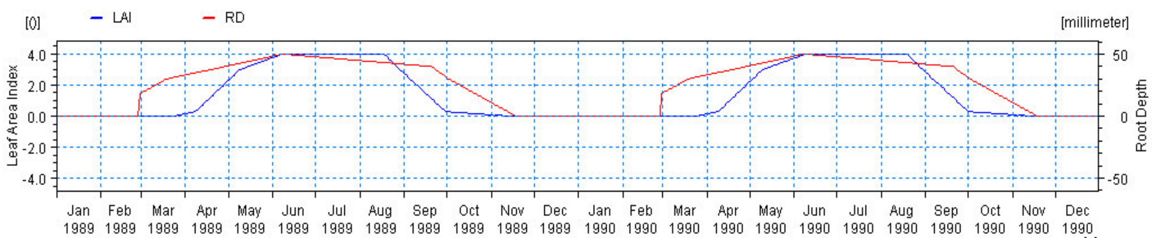

PARK LAND

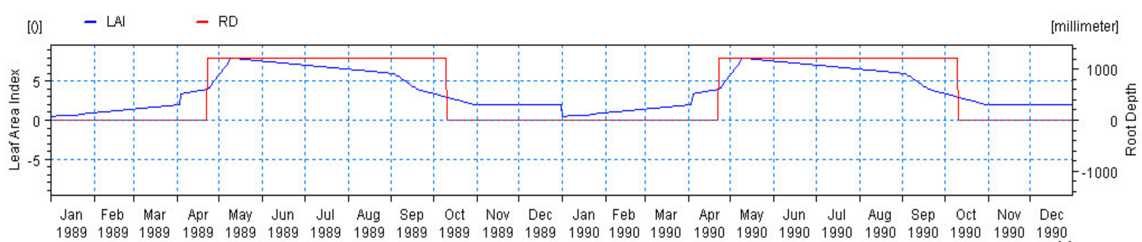

Figure 57

Example of Root Depth and Leaf Area Index Data Used in MIKE SHE Simulations

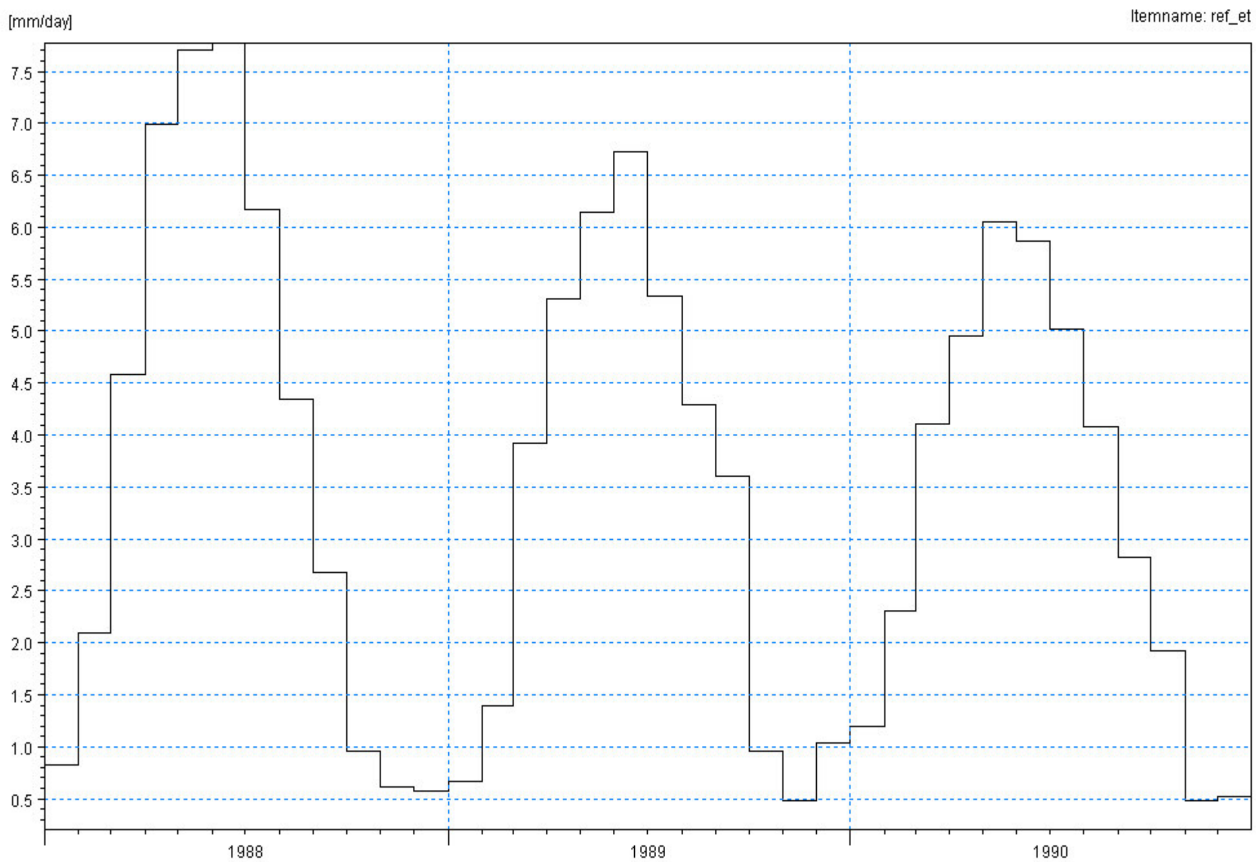

Figure 58

Reference Evapotranspiration Used in MIKE SHE for the period 1988 through 1990

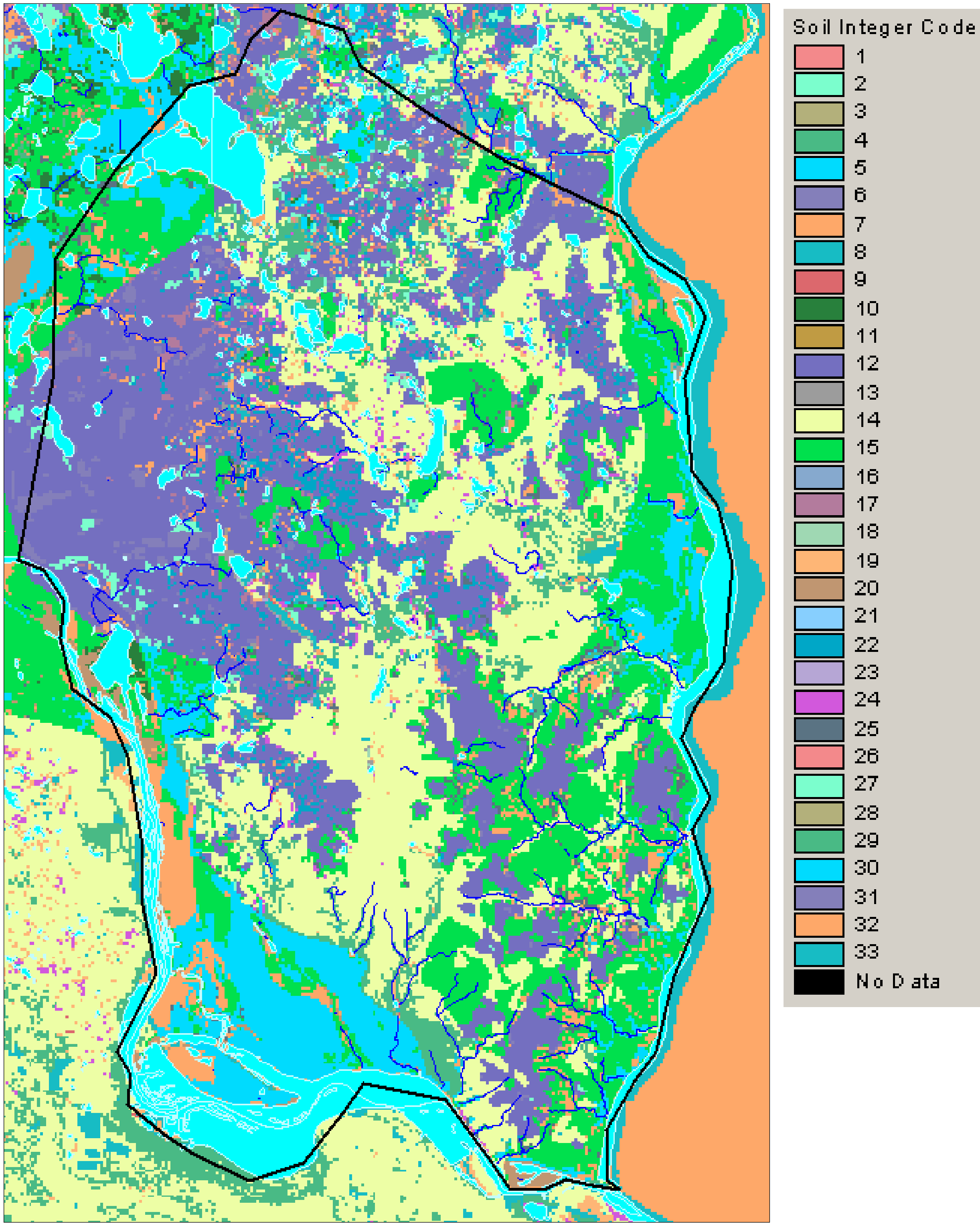

Figure 59

Soil Integer Codes Identifying Soil Profiles for MIKE SHE Unsaturated Flow Modeling

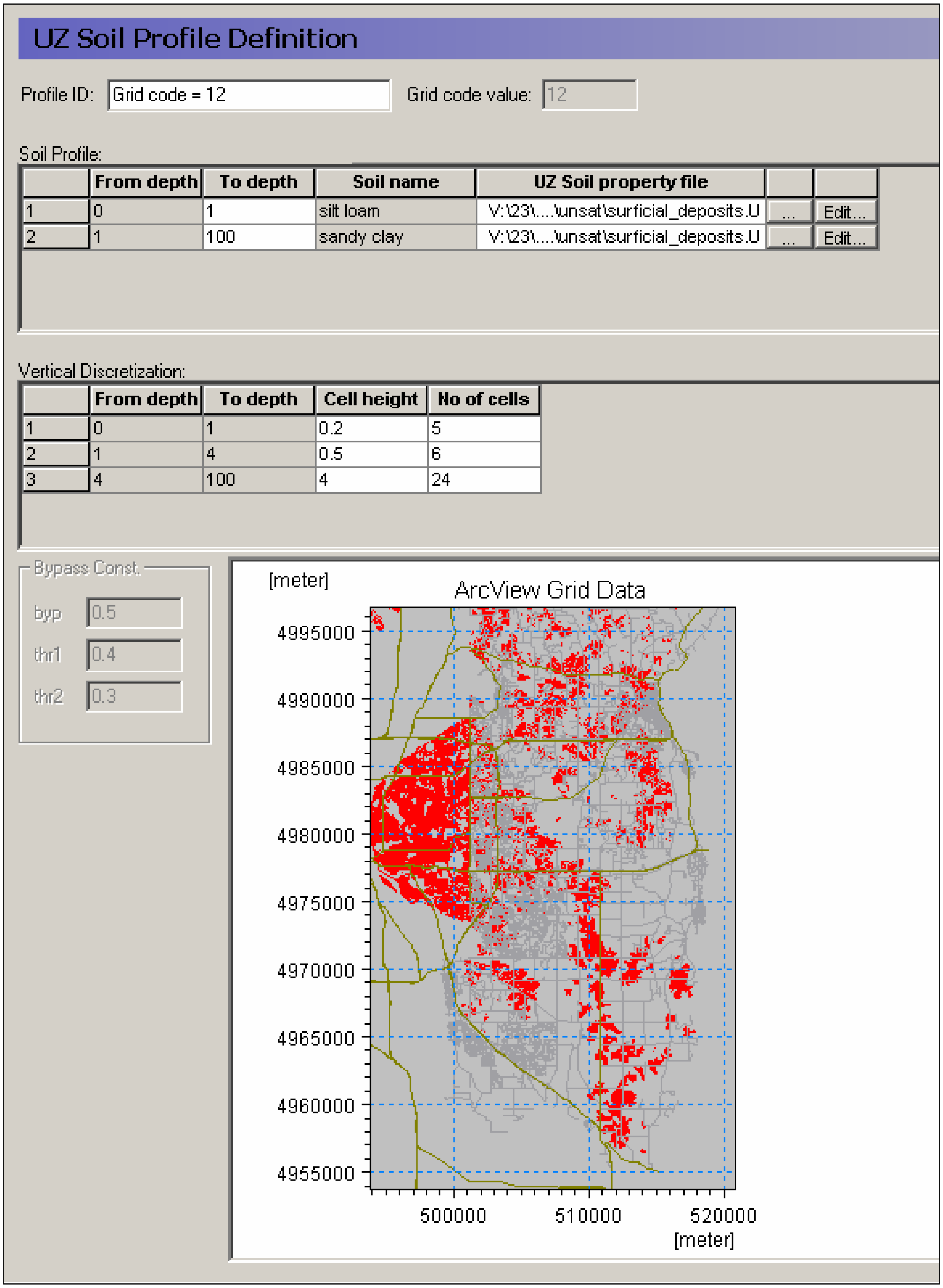

Figure 60

Example of Soil Profile Data

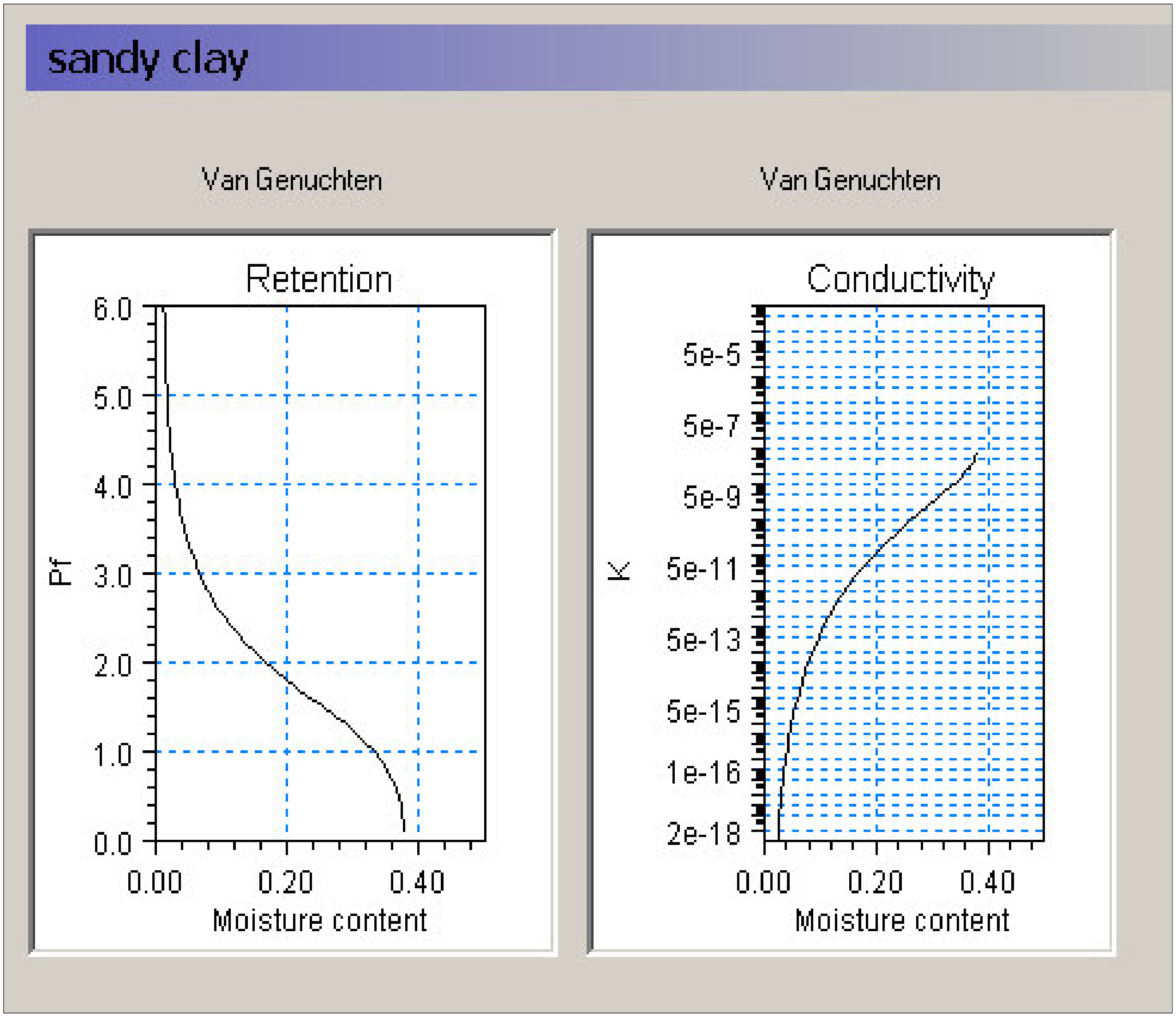

Figure 61

Example of van Genuchten Retention and Conductivity Relationships

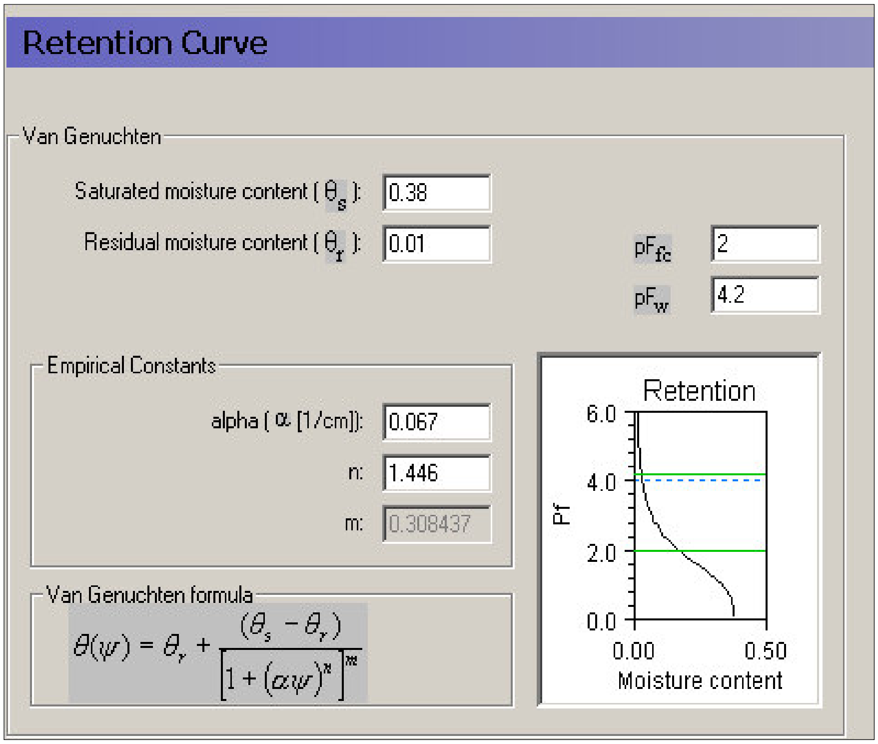

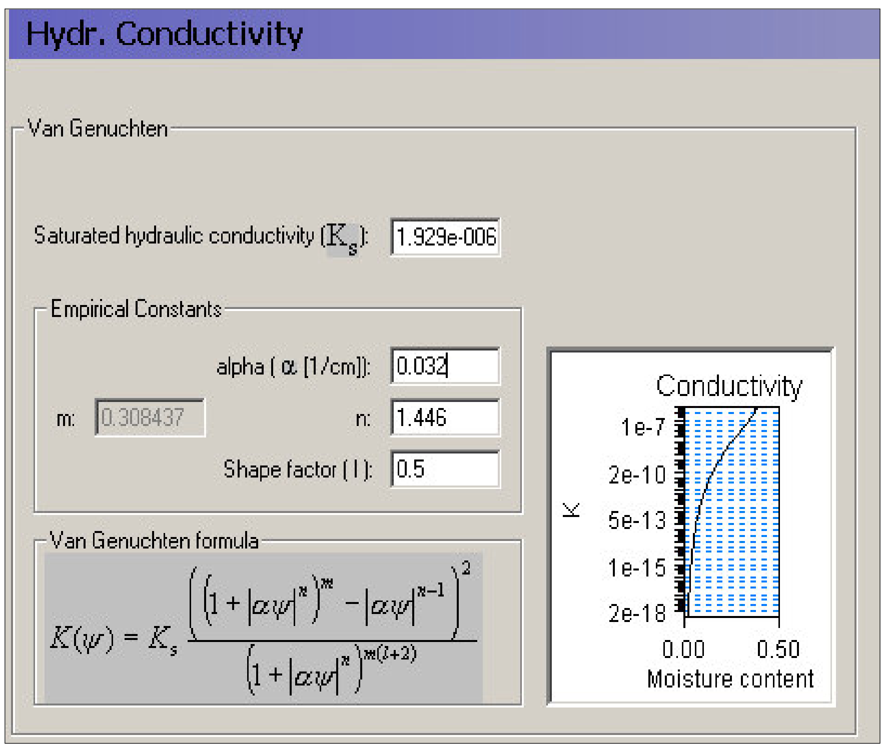

$$\theta(\psi) = \theta_r + \frac{(\theta_s - \theta_r)}{\left[1 + (\alpha\psi)^n\right]^m}$$

$$K(\psi) = K_s \frac{\left(\left(1 + |\alpha\psi|^n\right)^m - |\alpha\psi|^{n-1}\right)^2}{\left(1 + |\alpha\psi|^n\right)^{m(l+2)}}$$

Figure 62

Example of van Genuchten Variables for Soil

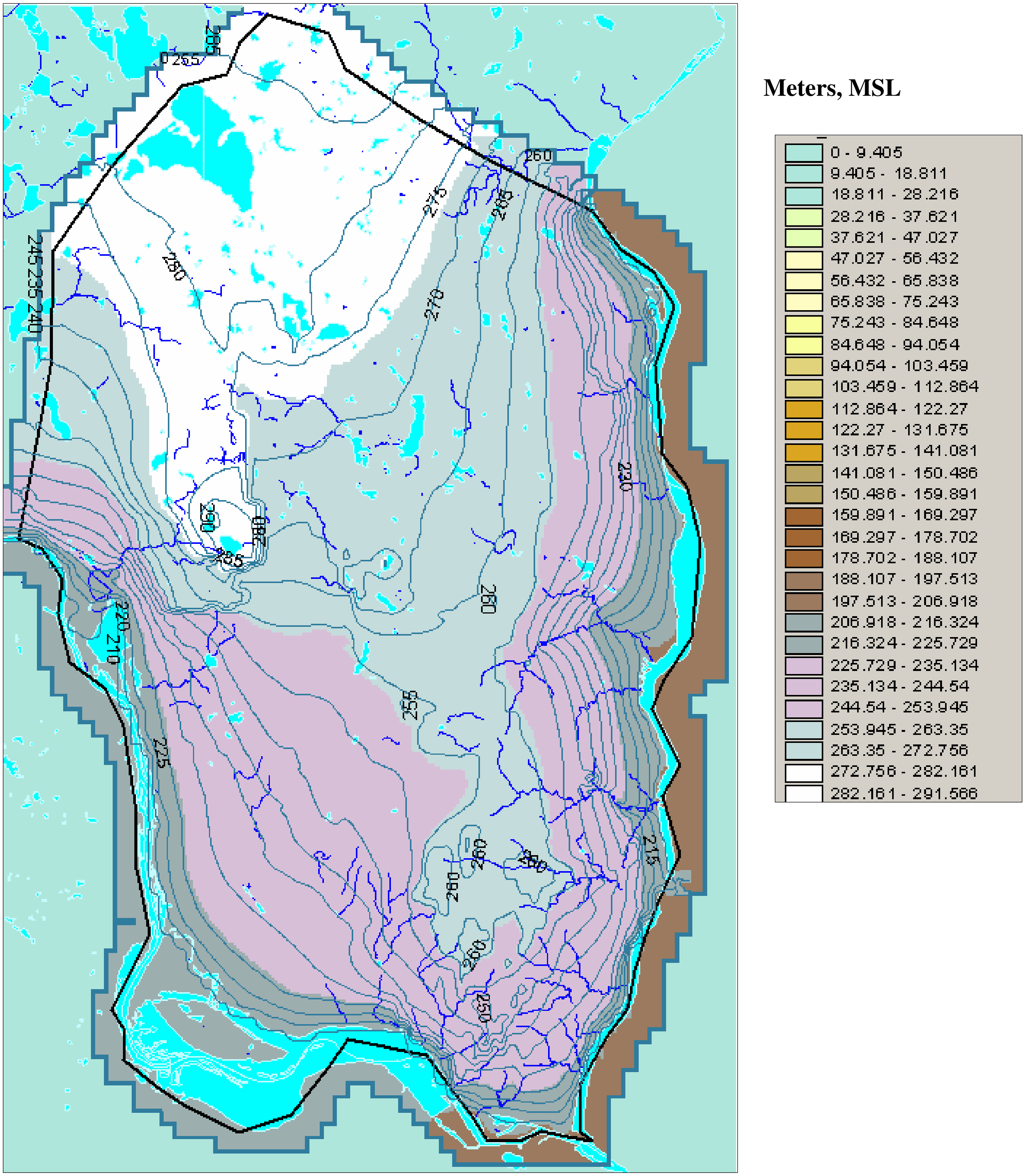

Figure 63

Water Table Elevation for Unsaturated Flow Computations

565 total classifications

Figure 64

Soil Column Classification for Unsaturated Flow Computations

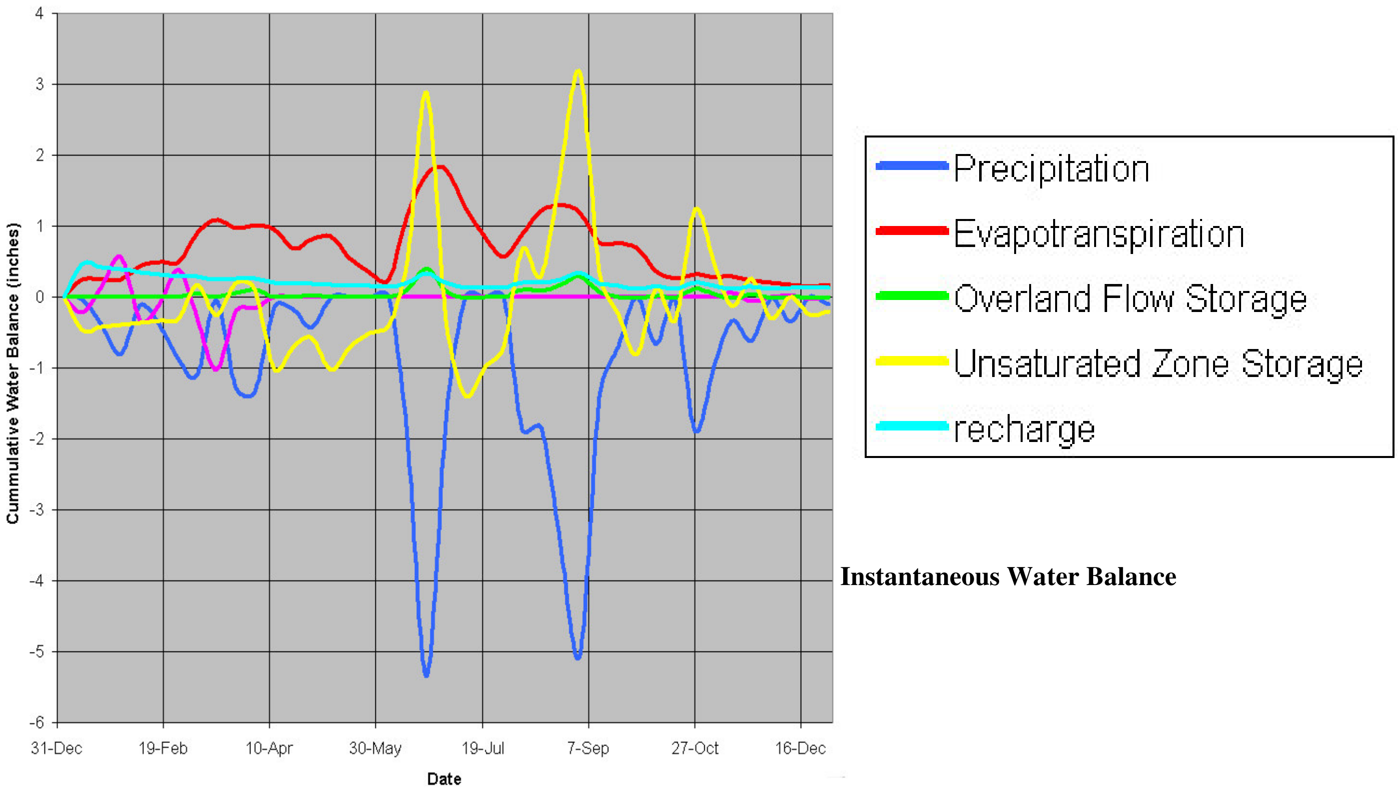

Instantaneous Water Balance

Cumulative Water Balance

Negative values indicate flows into the unsaturated zone and positive values indicate losses out of the unsaturated zone.

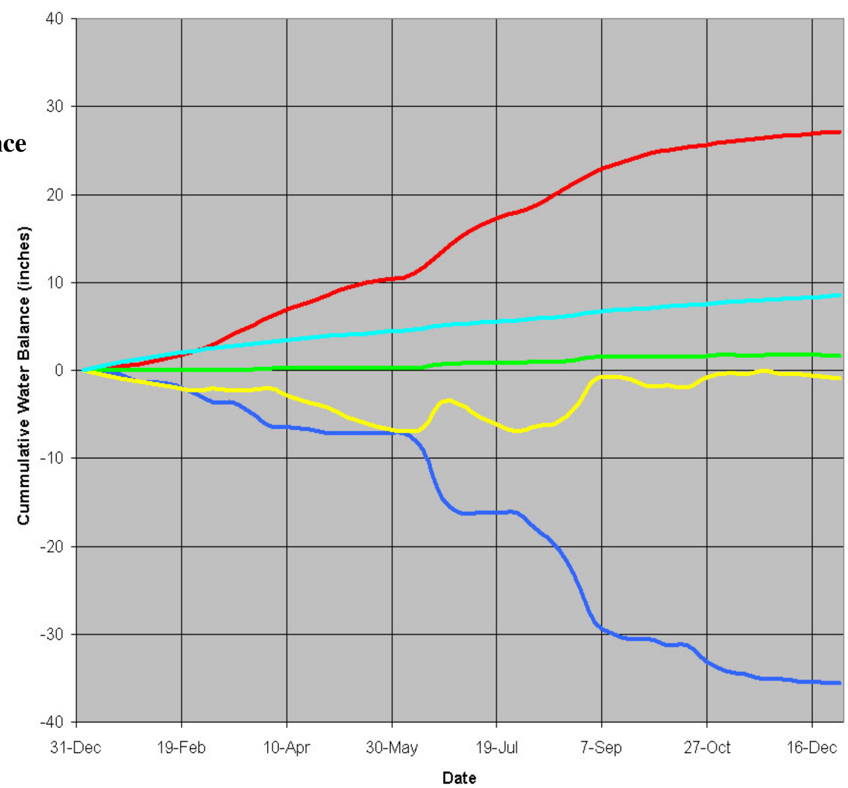

Figure 65

MIKE SHE Water Balance over Entire Model Domain for "Typical Year" (1979)

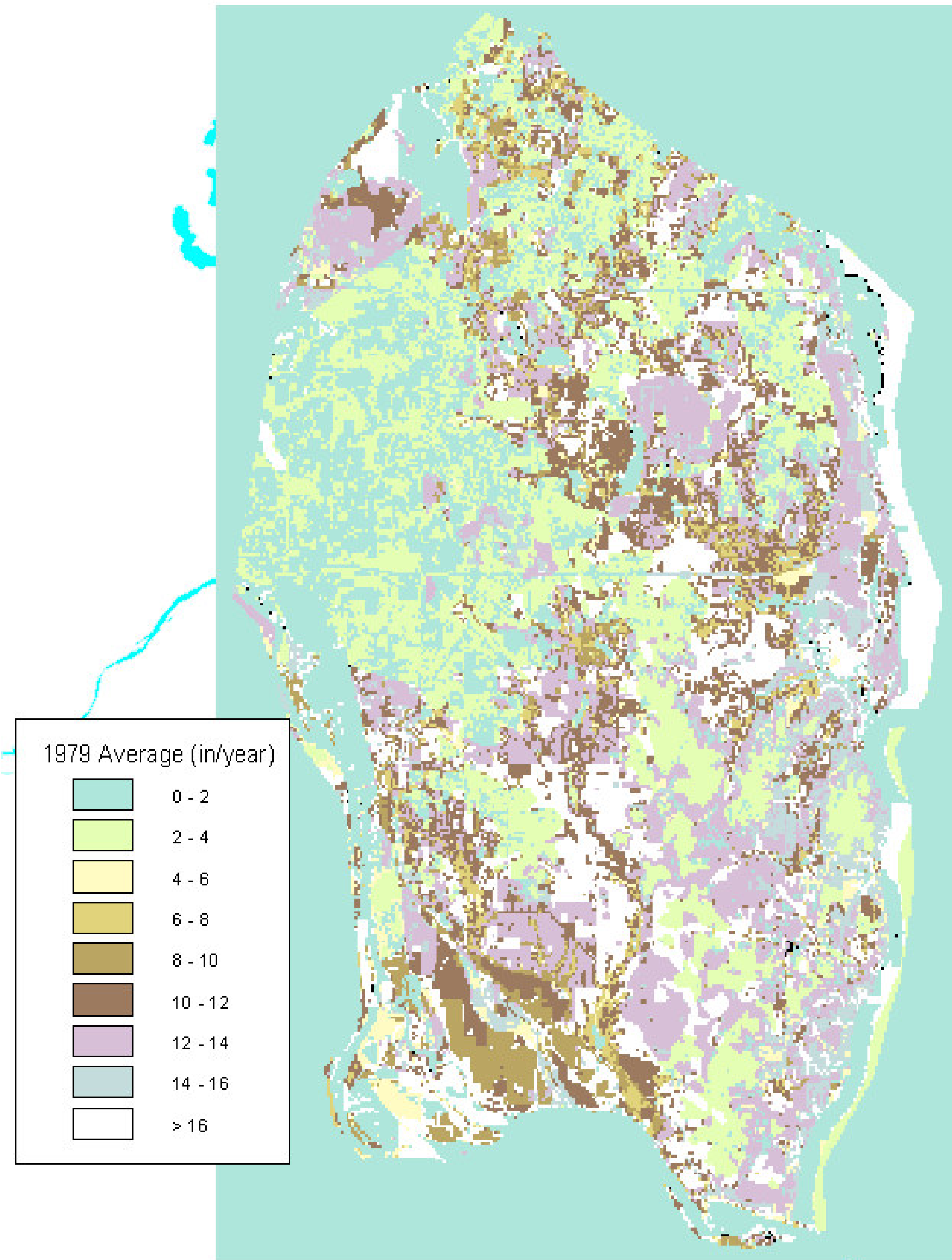

Figure 66

MIKE SHE Simulation of Annually Averaged Recharge for a Typical Year (1979)

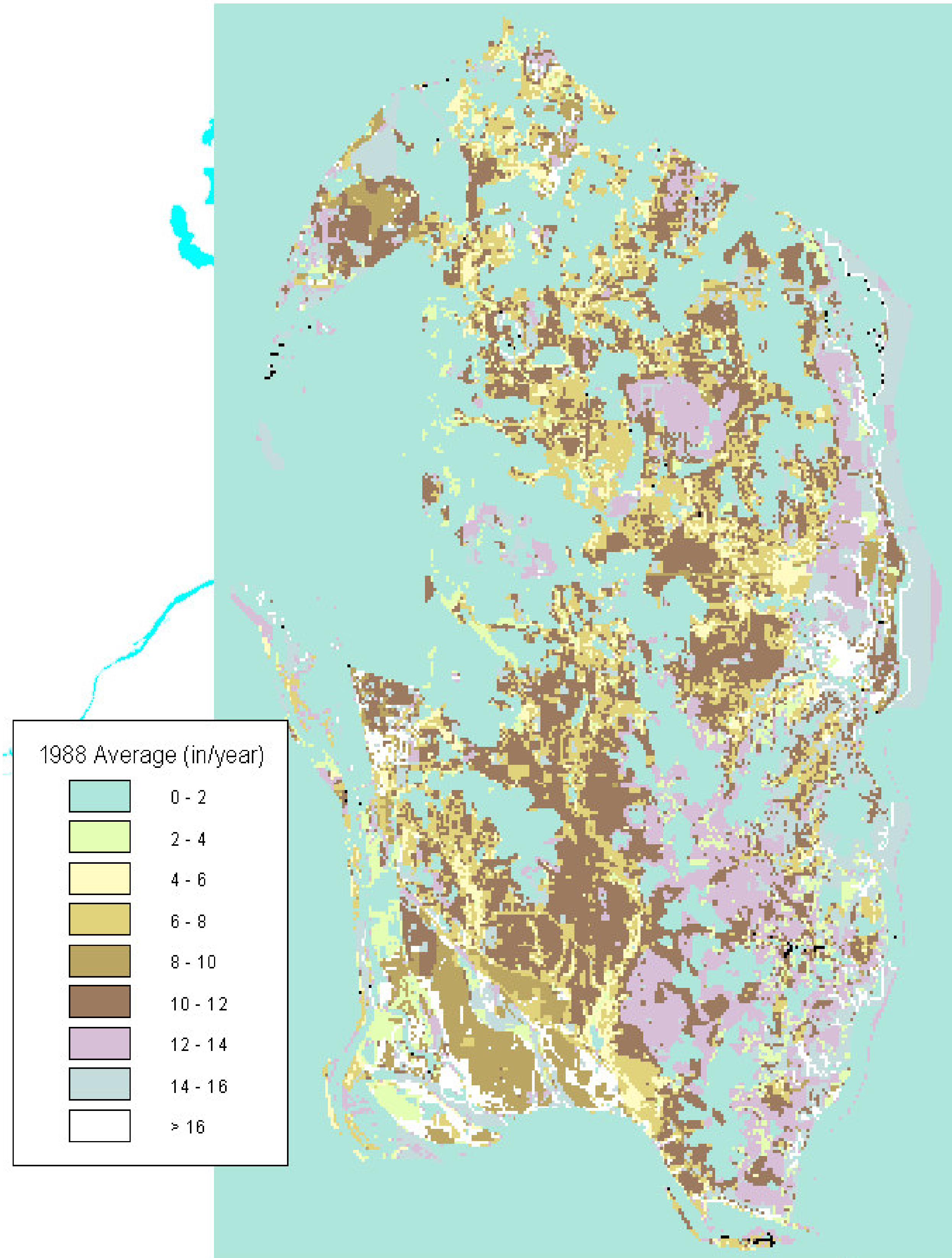

Figure 67

MIKE SHE Simulation of Annually Averaged Recharge for a Dry Year (1988)

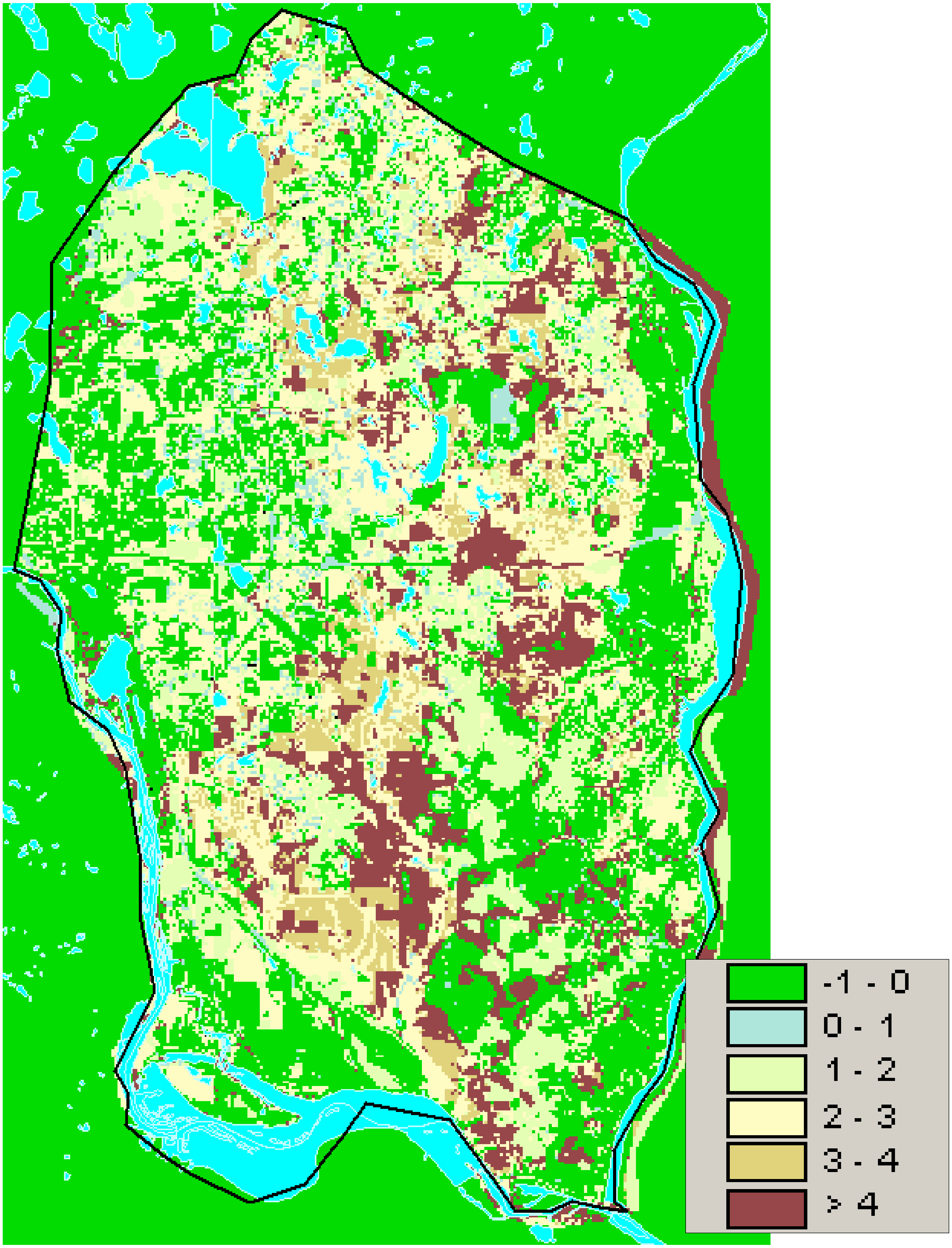

Figure 68

MIKE SHE Simulation of Deficit (in/yr) Between Dry Year and Typical Year Infiltration

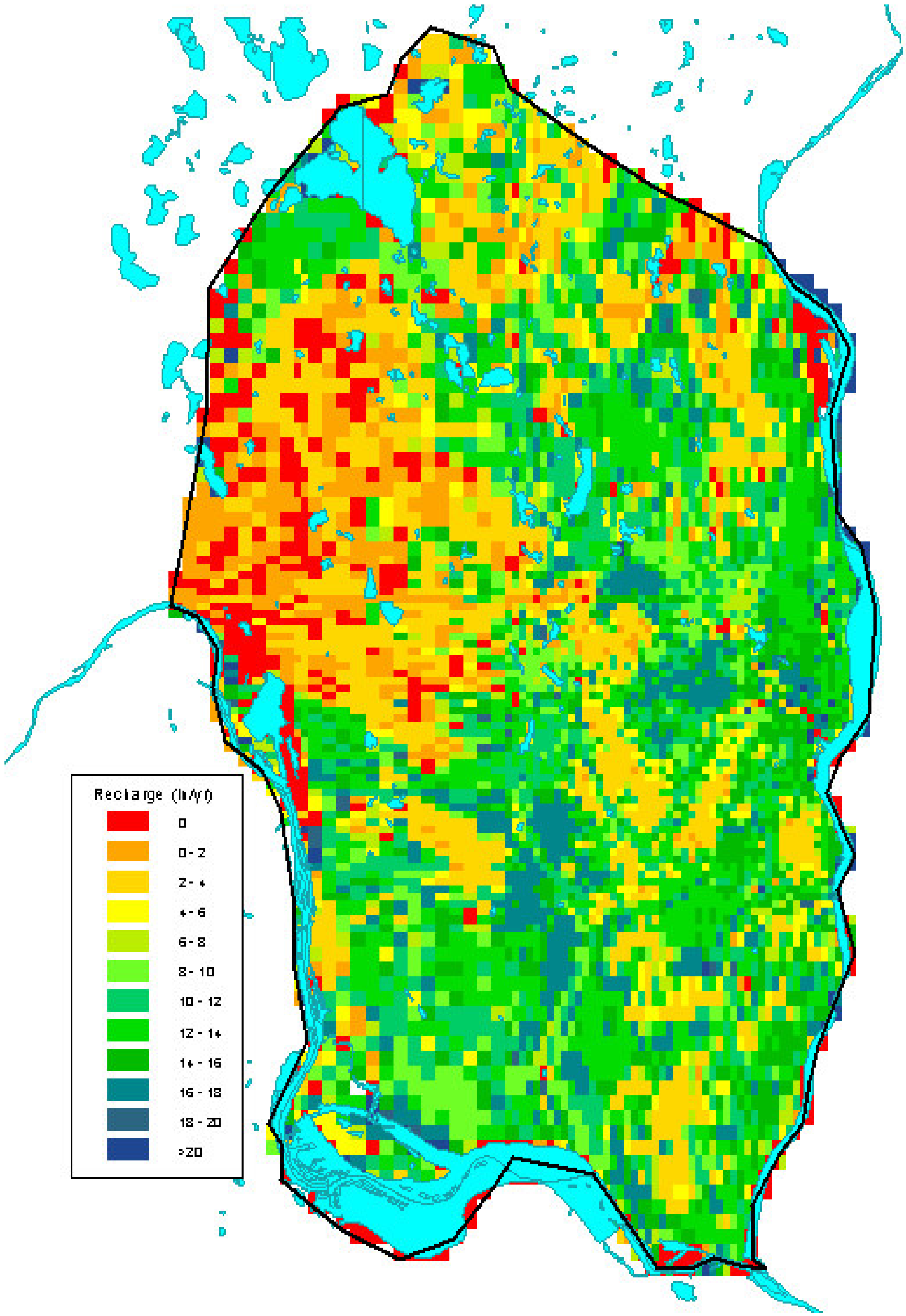

Figure 69

MODFLOW Steady-State Recharge (in/yr) for Typical Conditions

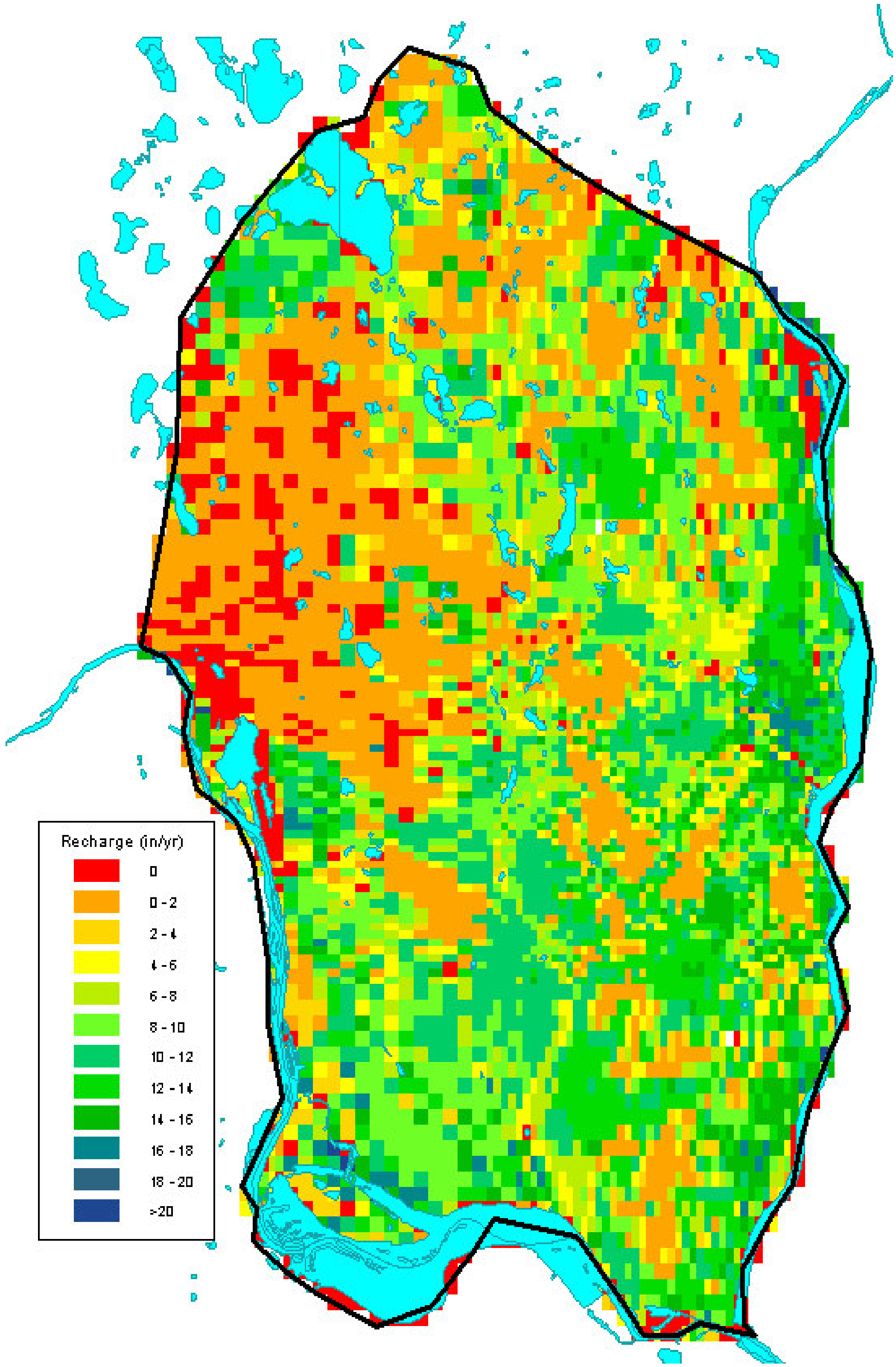

Figure 70

MODFLOW Steady-State Recharge (in/yr) for Dry (1988) Conditions

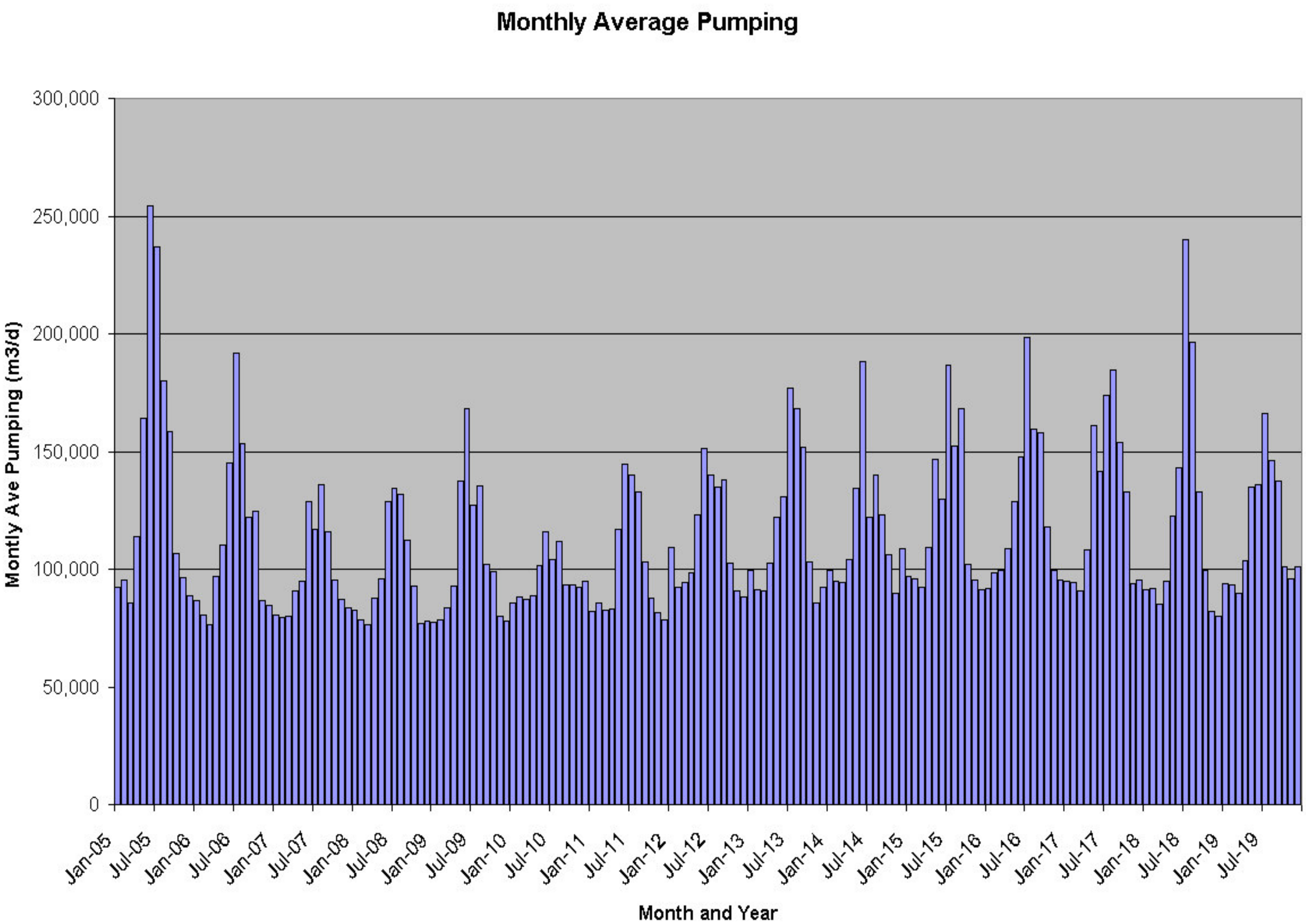

Figure 71

Projected Average Monthly Pumping of non-Woodbury Wells for Transient Simulations (based on pumping records for 1988-2003)

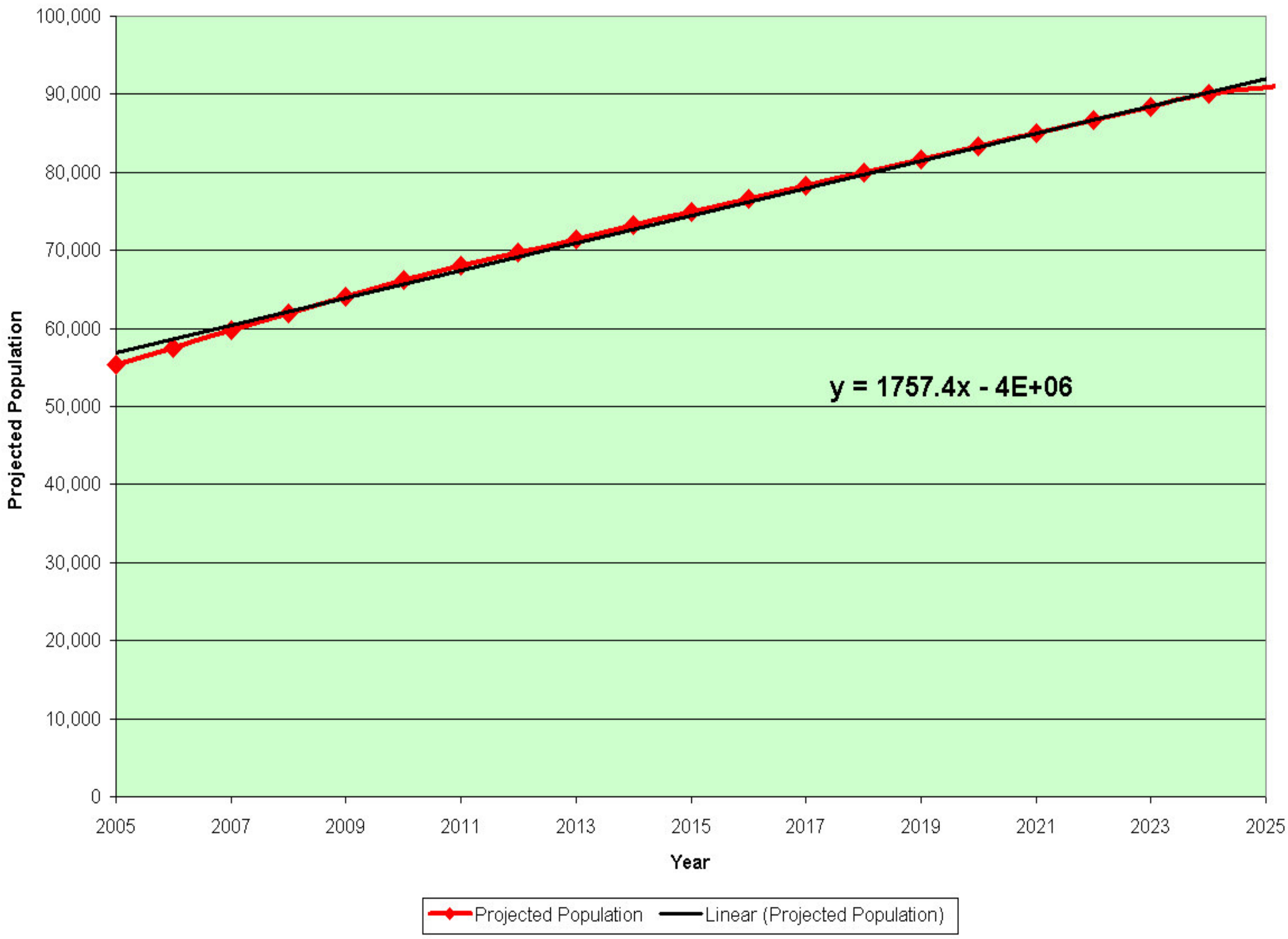

Figure 72

Projected Population for City of Woodbury: 2005-2025

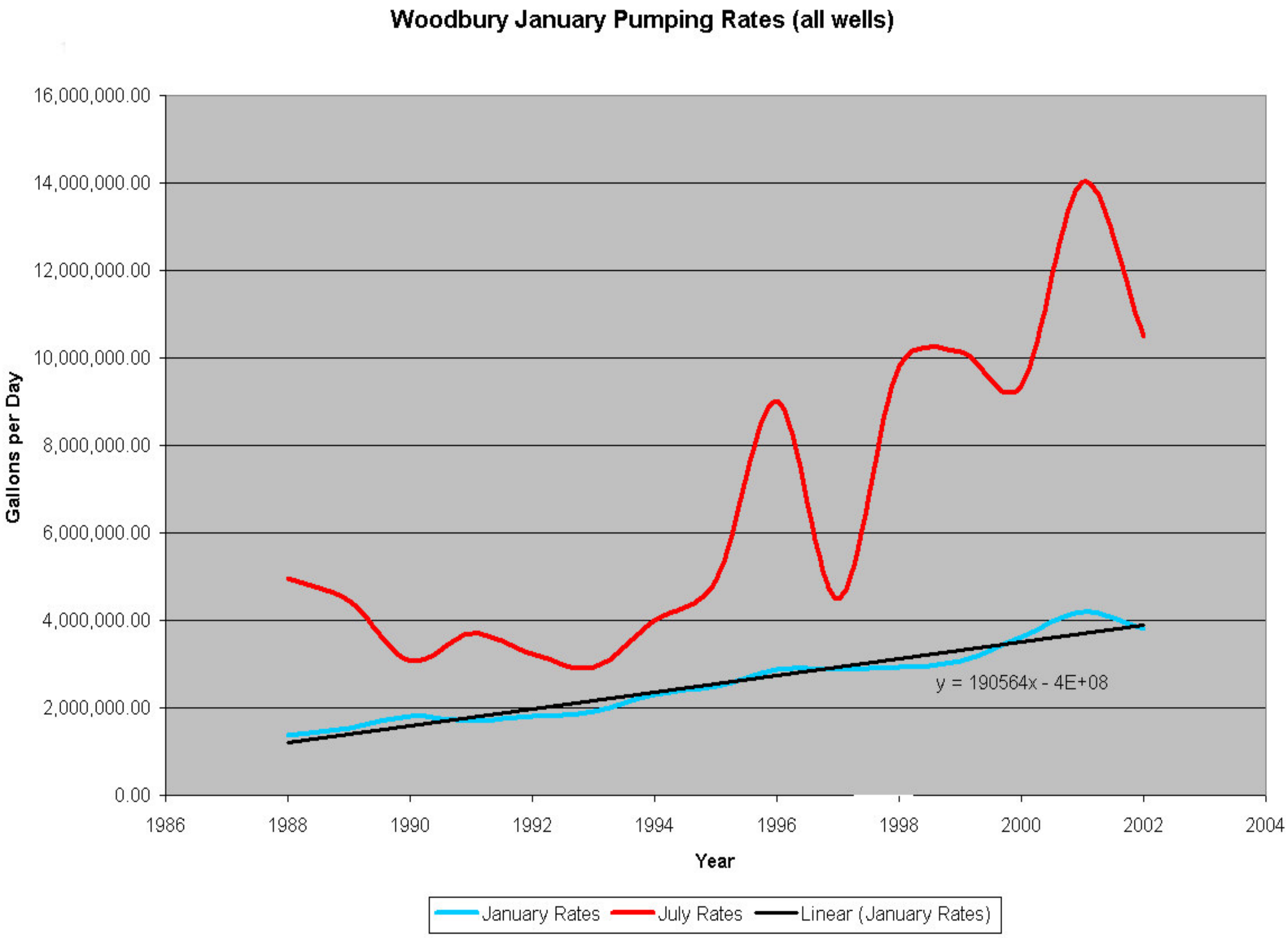

Figure 73

Woodbury Pumping Comparison: June vs. January – 1988 to 2002

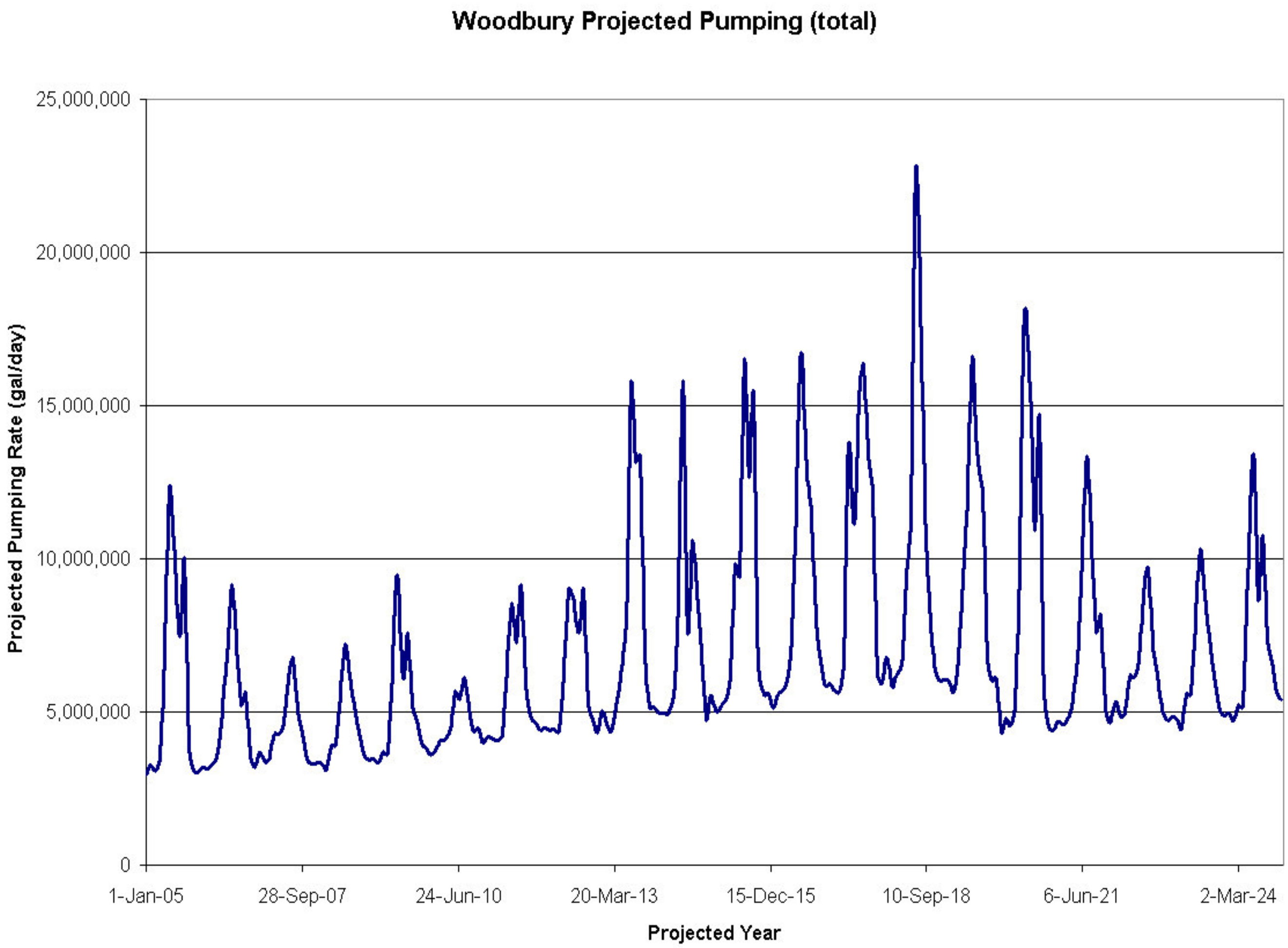

Figure 74

Projected Month-By-Month Water Demand for Woodbury

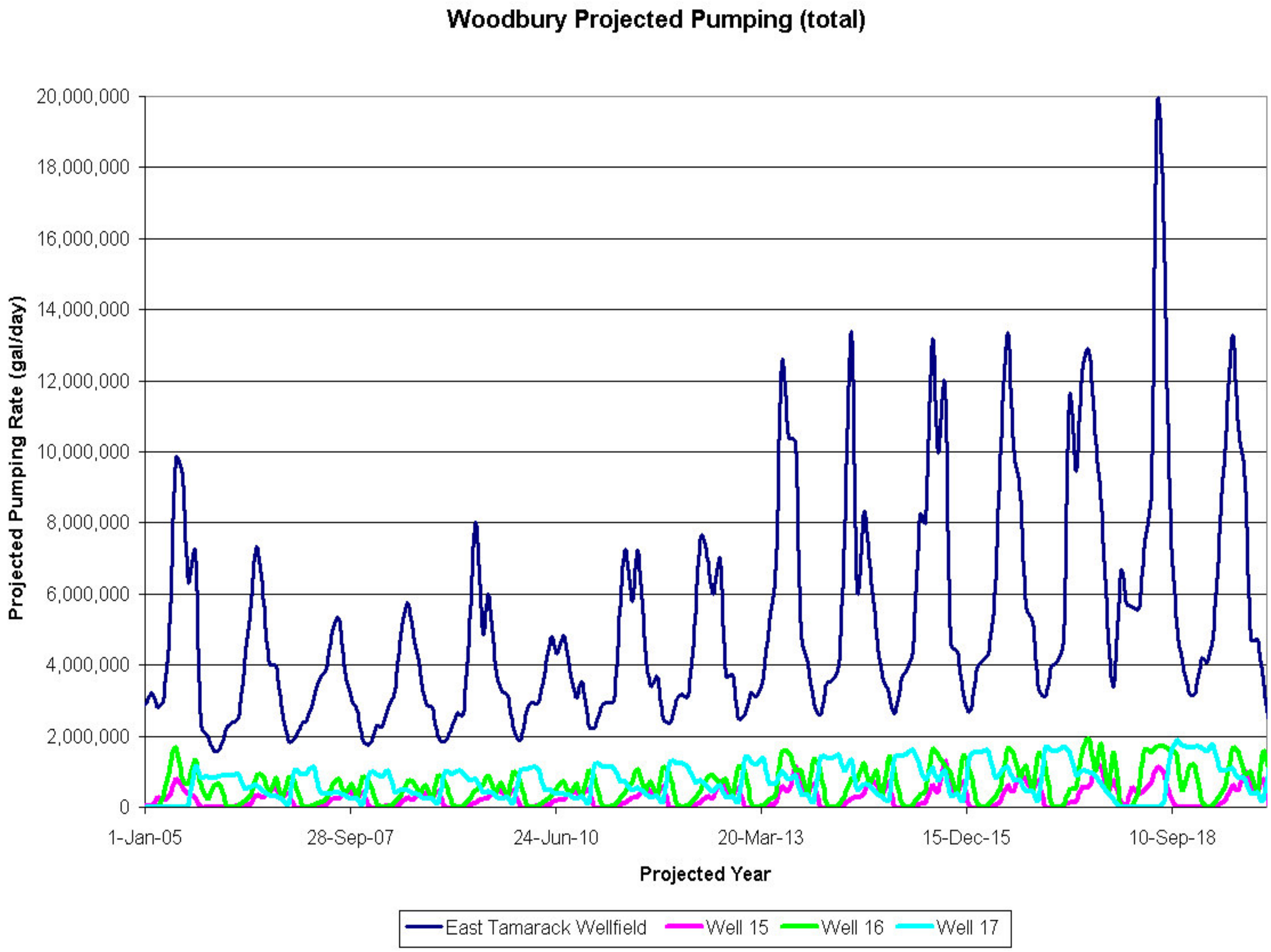

Figure 75

Projected Month-By-Month Water Demand for Woodbury East Tamarack Well Field, Well 15, Well 16, and Well 17

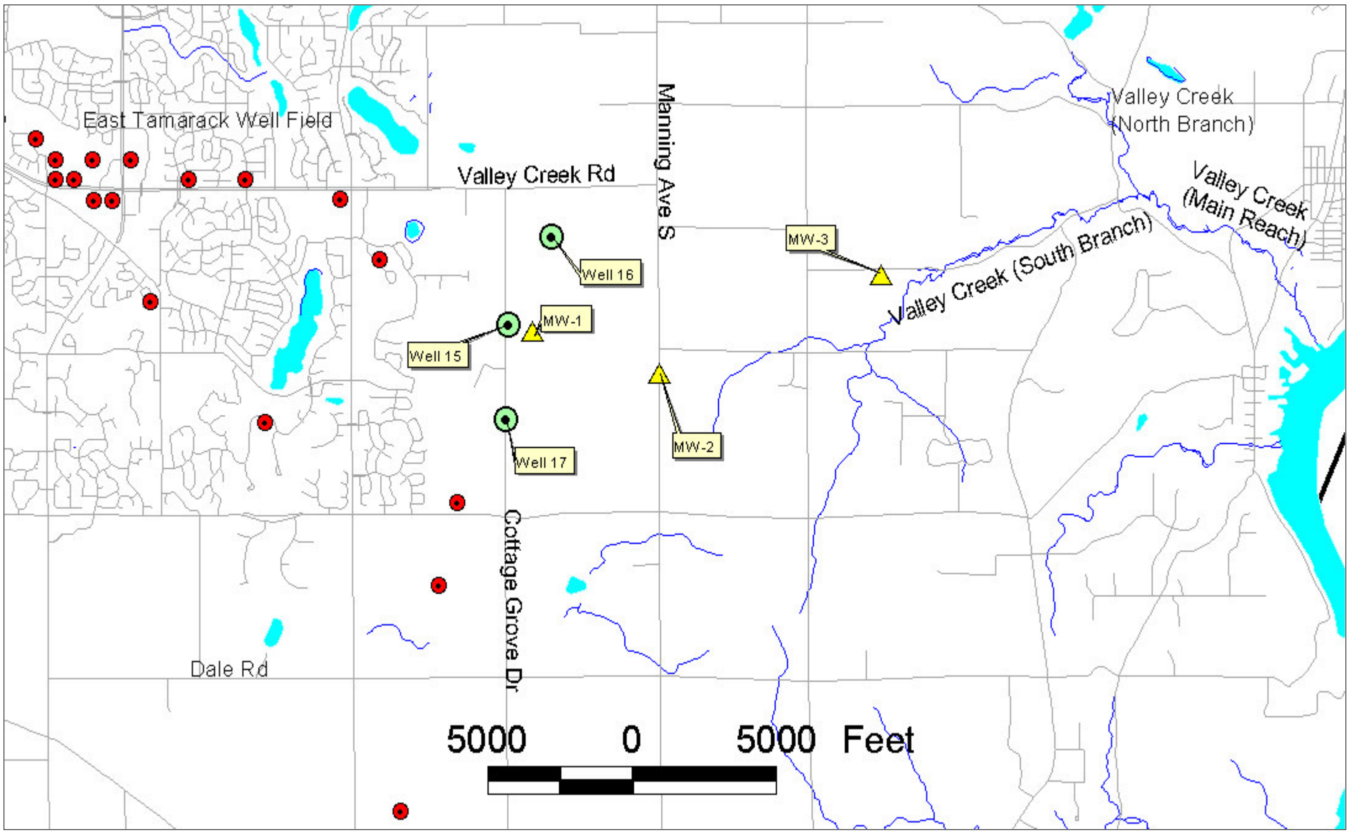

Figure 76

Locations of Pumping Wells, Monitoring Wells, and Stream Reaches of Valley Creek for Transient Simulations

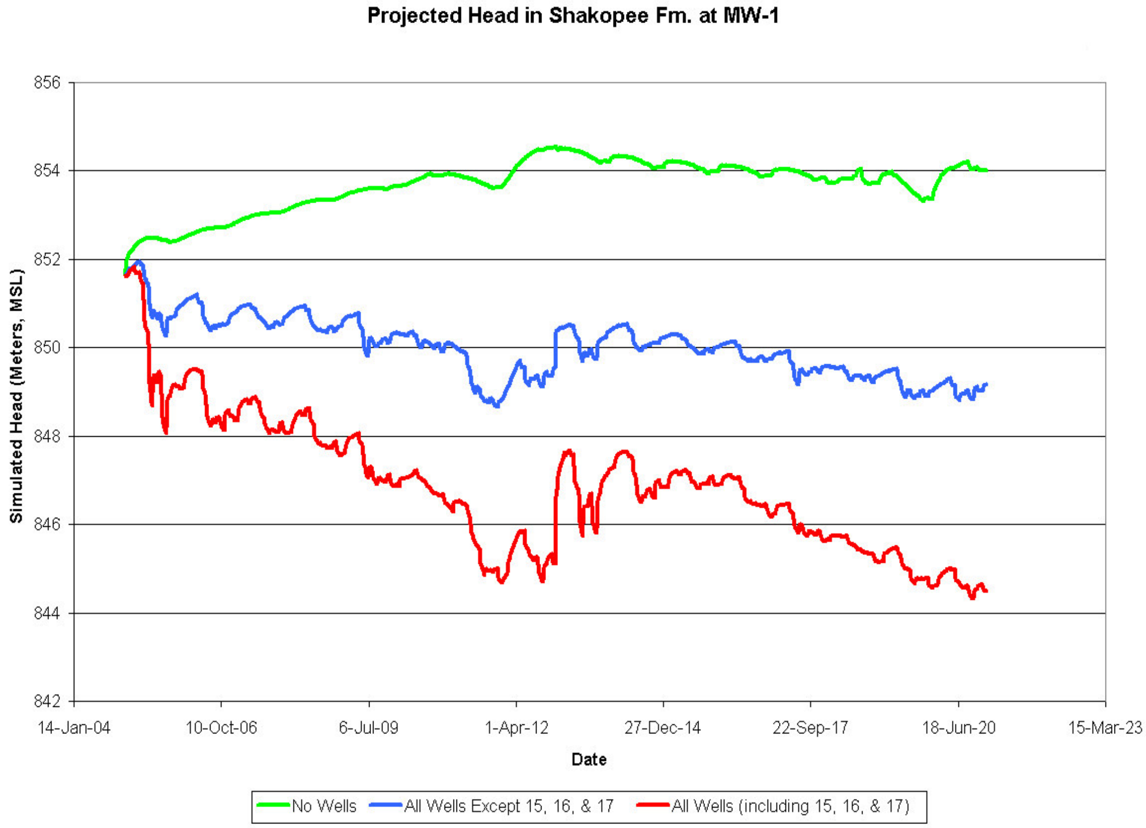

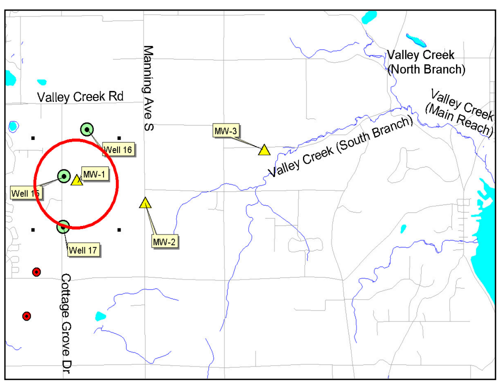

Figure 77

Simulation of Groundwater Levels in Shakopee Formation at Well Nest MW-1: 2005-2020

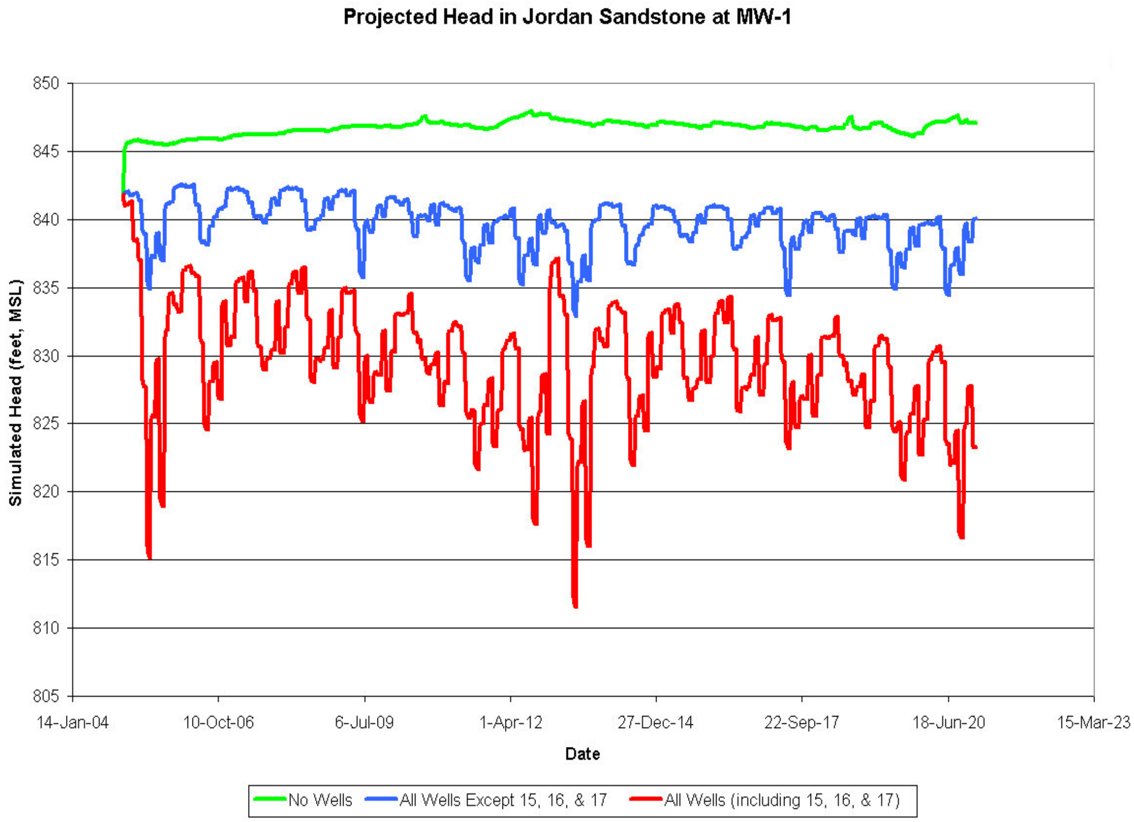

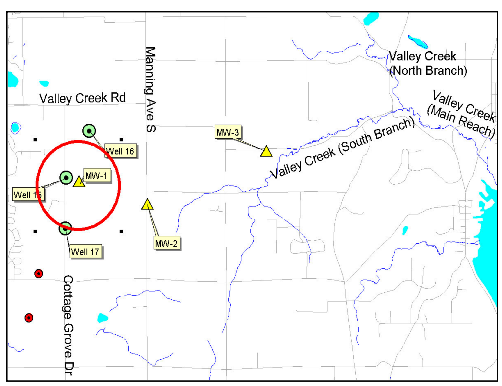

Figure 78

Simulation of Groundwater Levels in Jordan Sandstone at Well Nest MW-1: 2005-2020

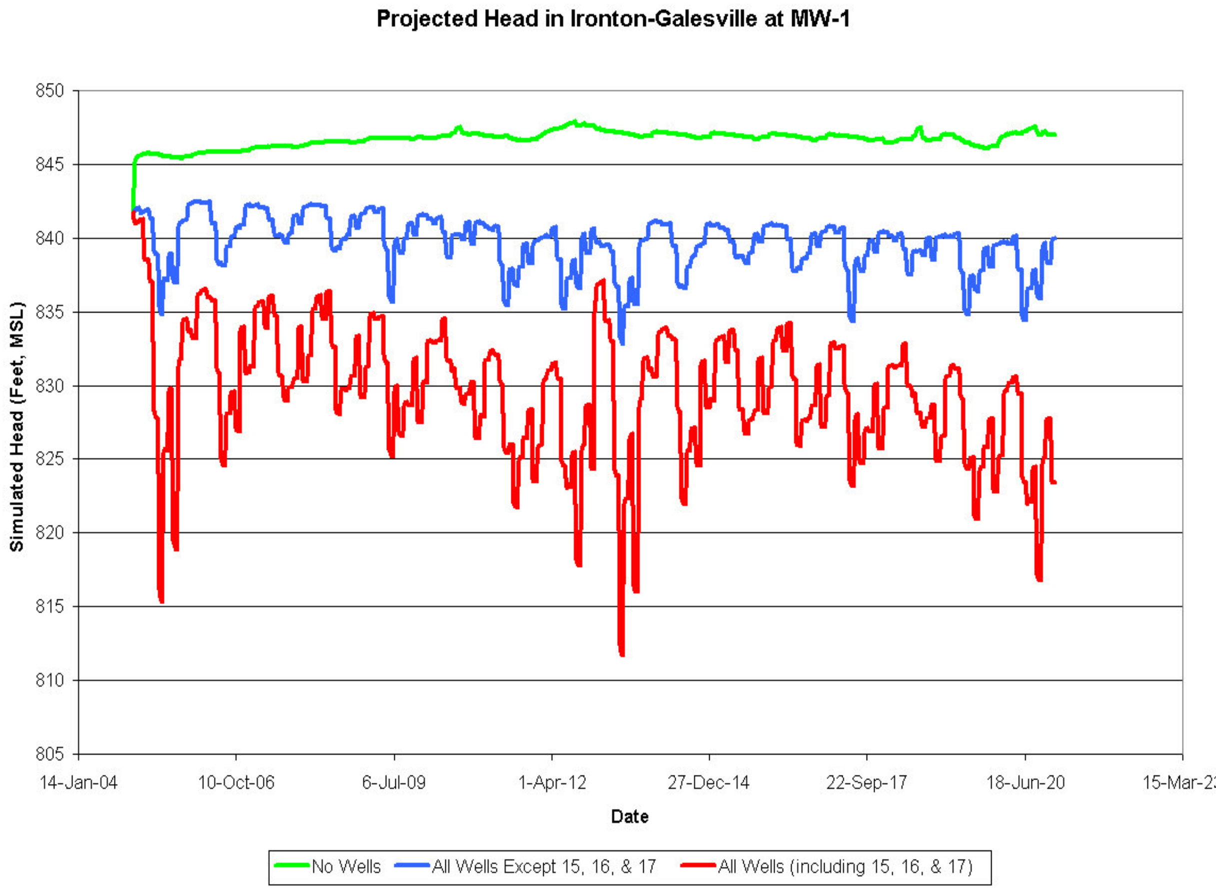

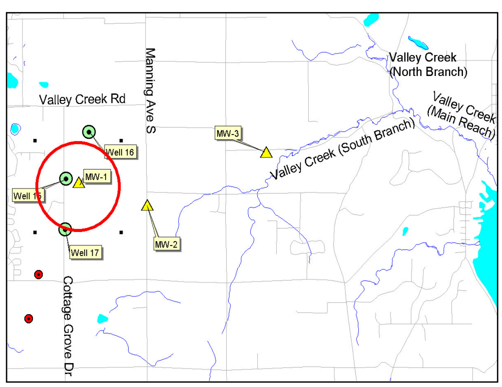

Figure 79

Simulation of Groundwater Levels in Ironton-Galesville Sandstones at Well Nest MW-1: 2005-2020

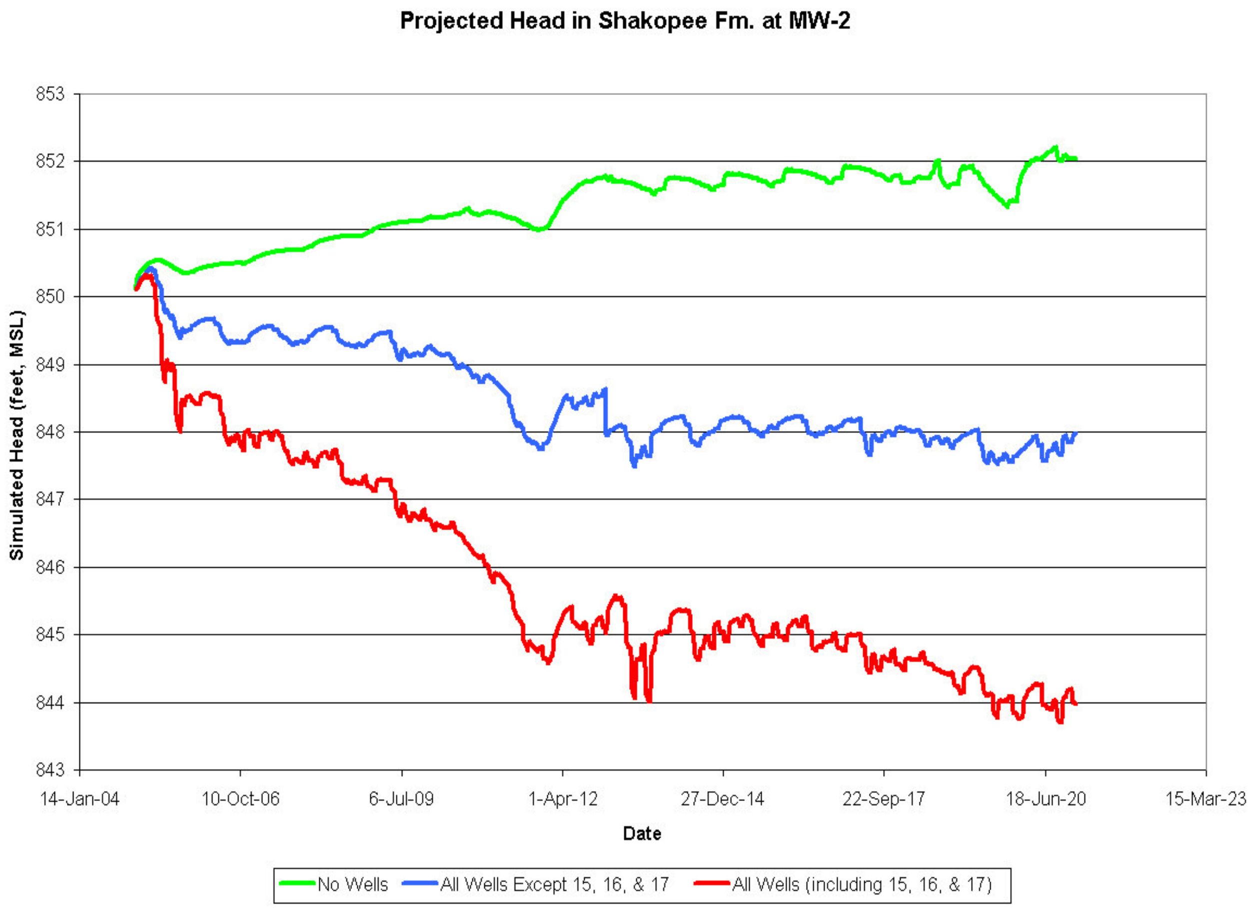

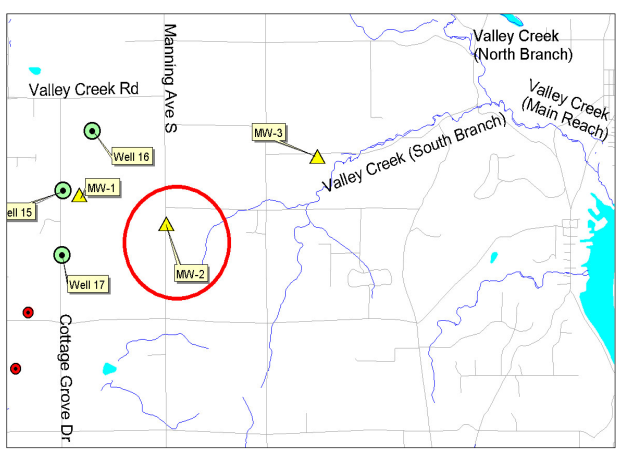

Figure 80

Simulation of Groundwater Levels in Shakopee Formation at Well Nest MW-2: 2005-2020

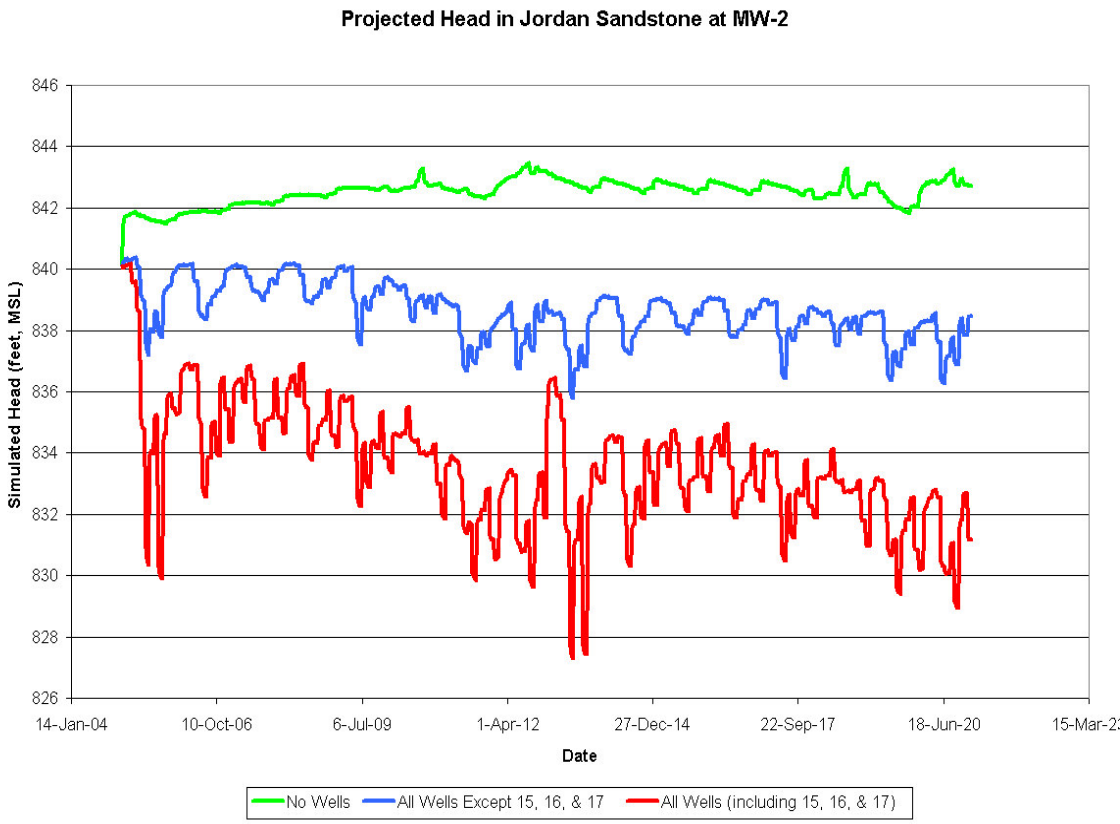

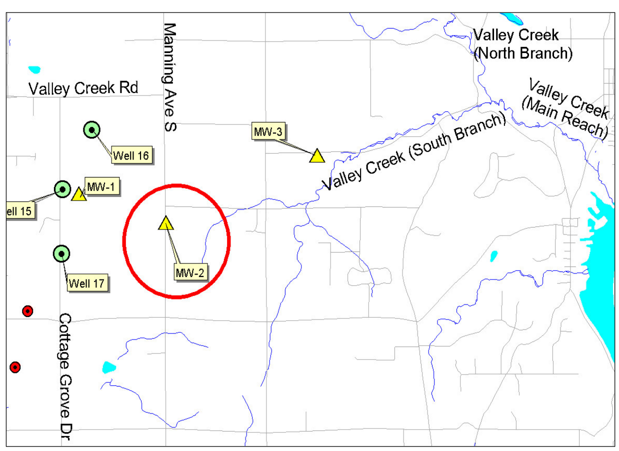

Figure 81

Simulation of Groundwater Levels in Jordan Sandstone at Well Nest MW-2: 2005-2020

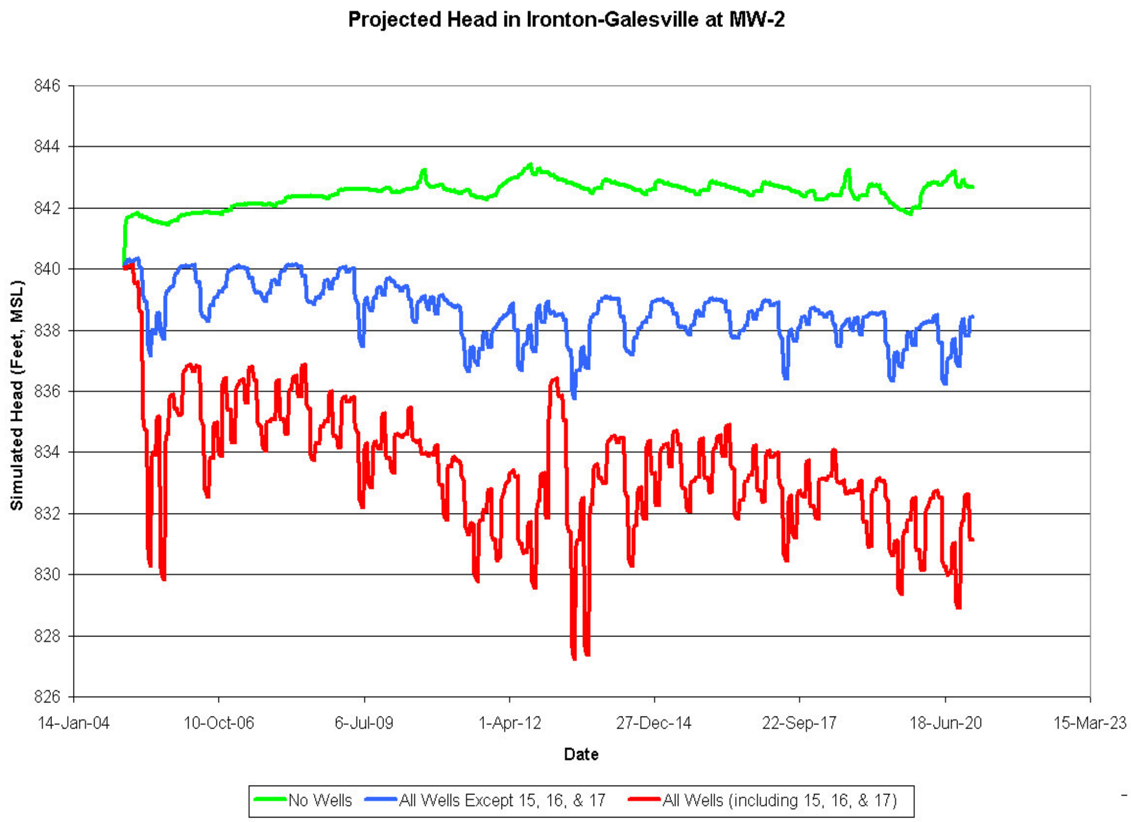

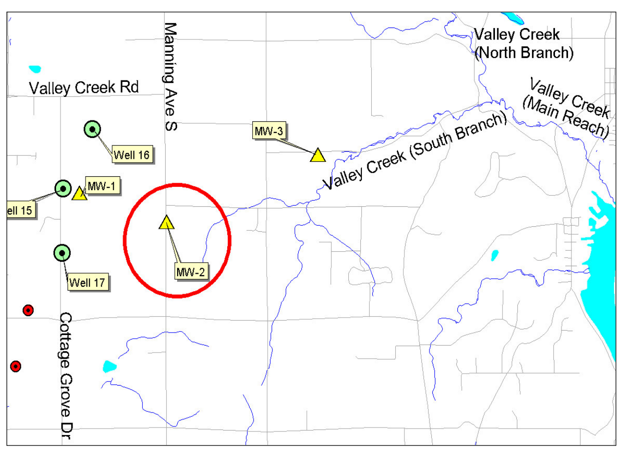

Figure 82

Simulation of Groundwater Levels in Ironton-Galesville Sandstones at Well Nest MW-2: 2005-2020

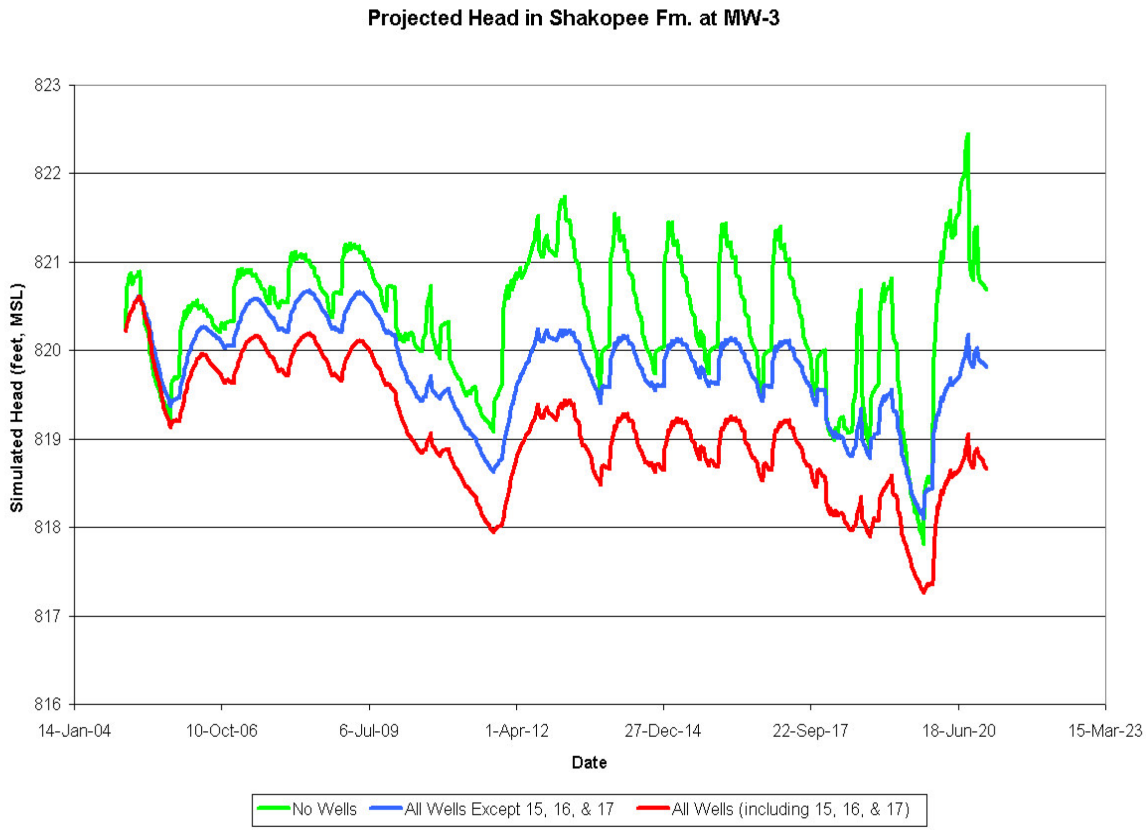

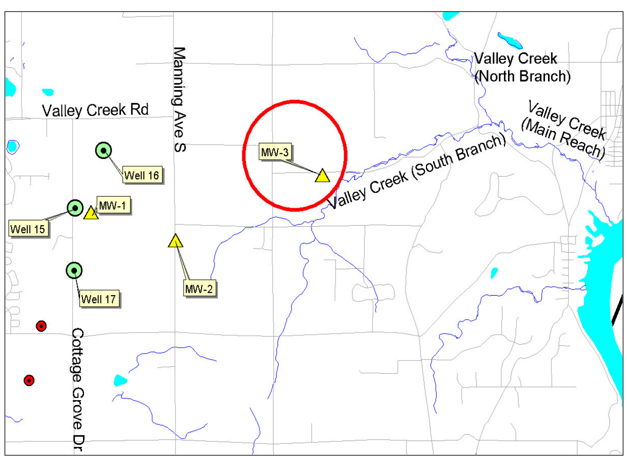

Figure 83

Simulation of Groundwater Levels in Shakopee Formation at Well Nest MW-3: 2005-2020

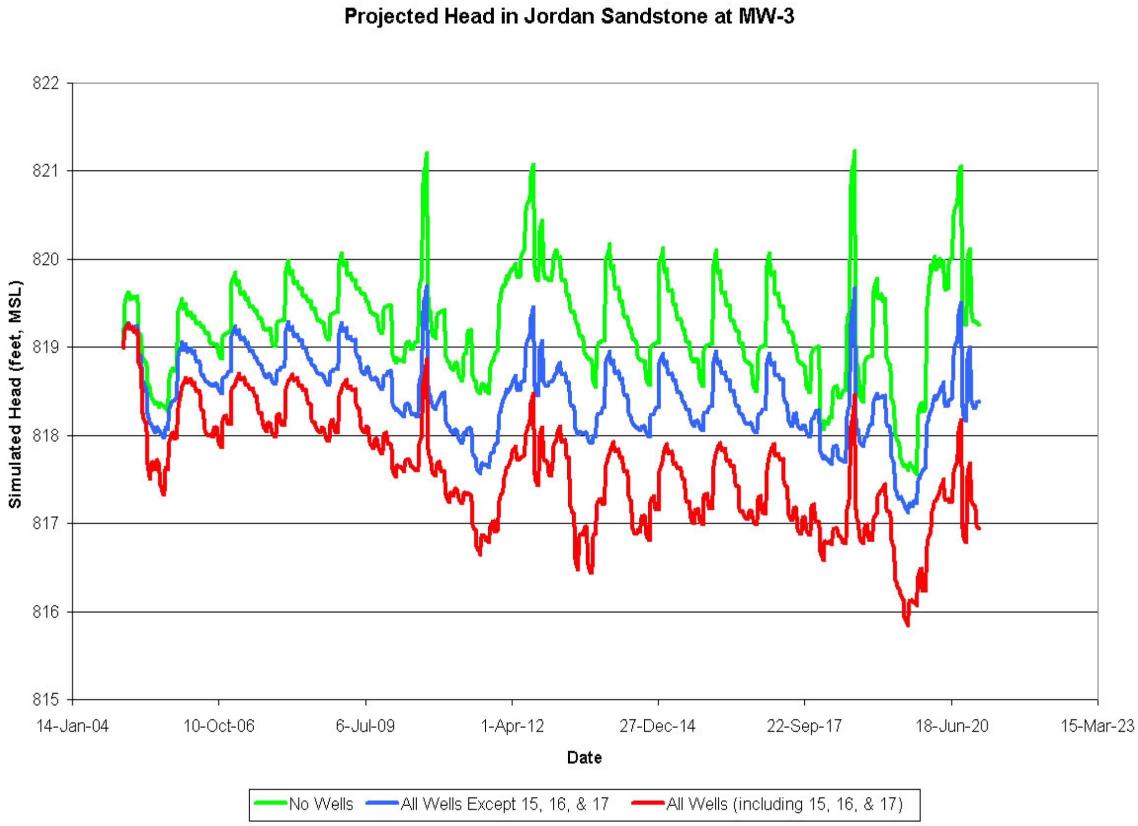

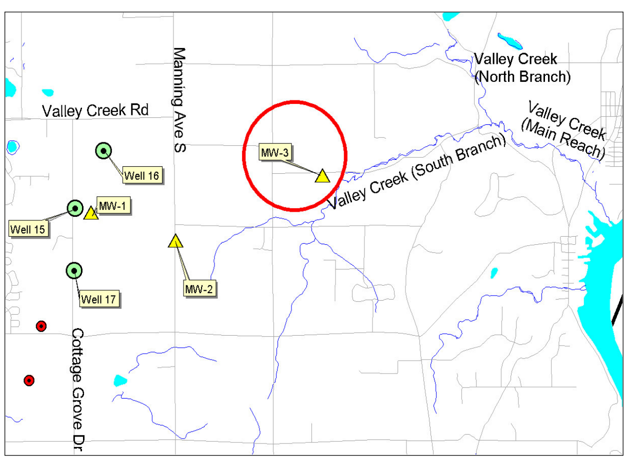

Figure 84

Simulation of Groundwater Levels in Jordan Sandstone at Well Nest MW-3: 2005-2020

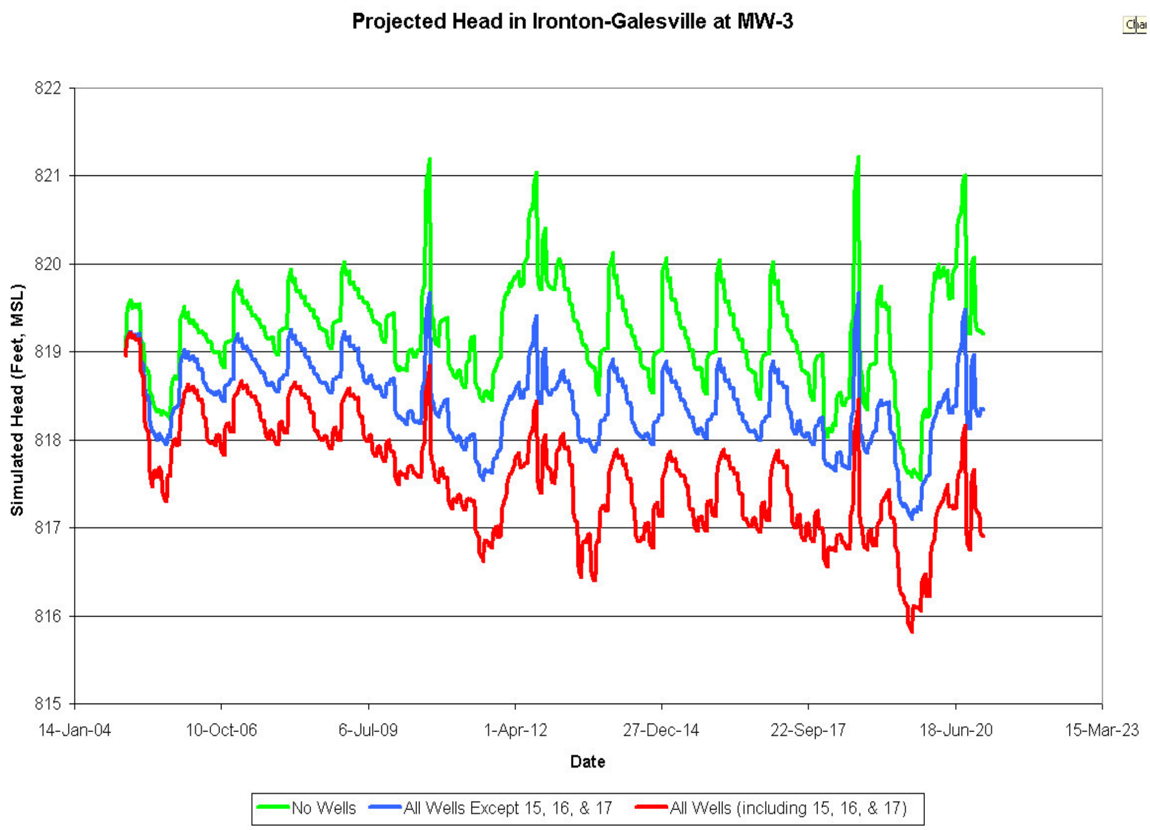

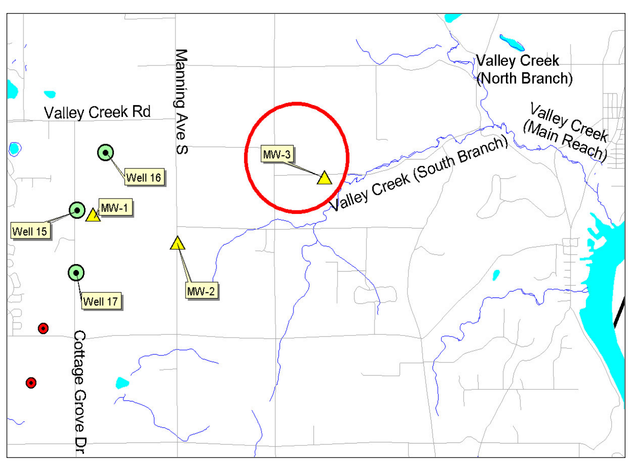

Figure 85

Simulation of Groundwater Levels in Ironton-Galesville Sandstones at Well Nest MW-3: 2005-2020

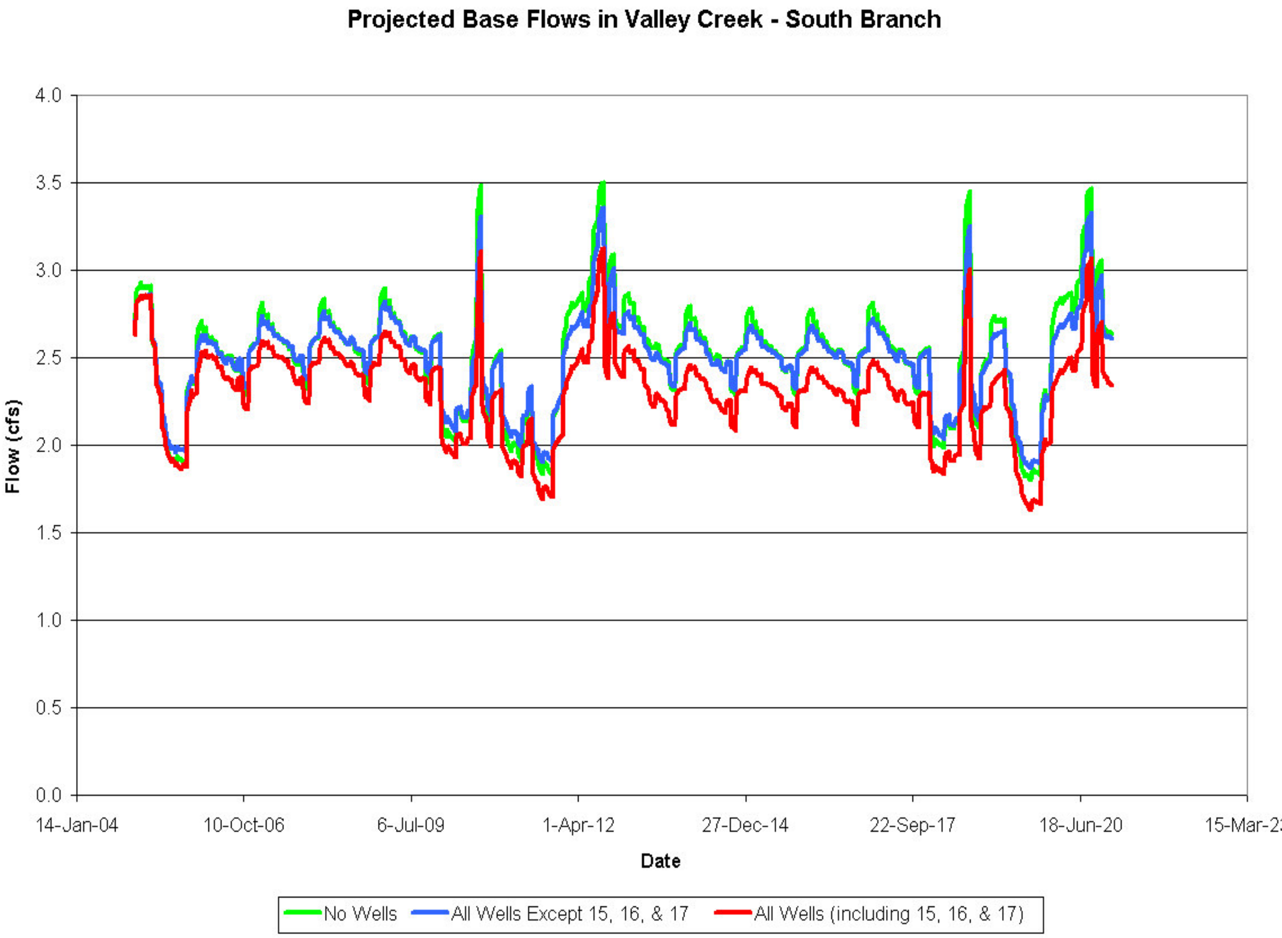

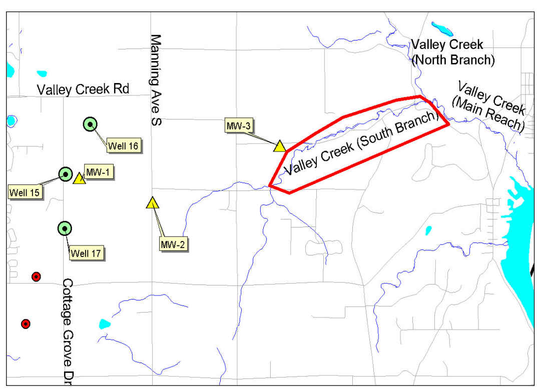

Figure 86

Simulation of Base Flows in South Branch of Valley Creek: 2002-2025

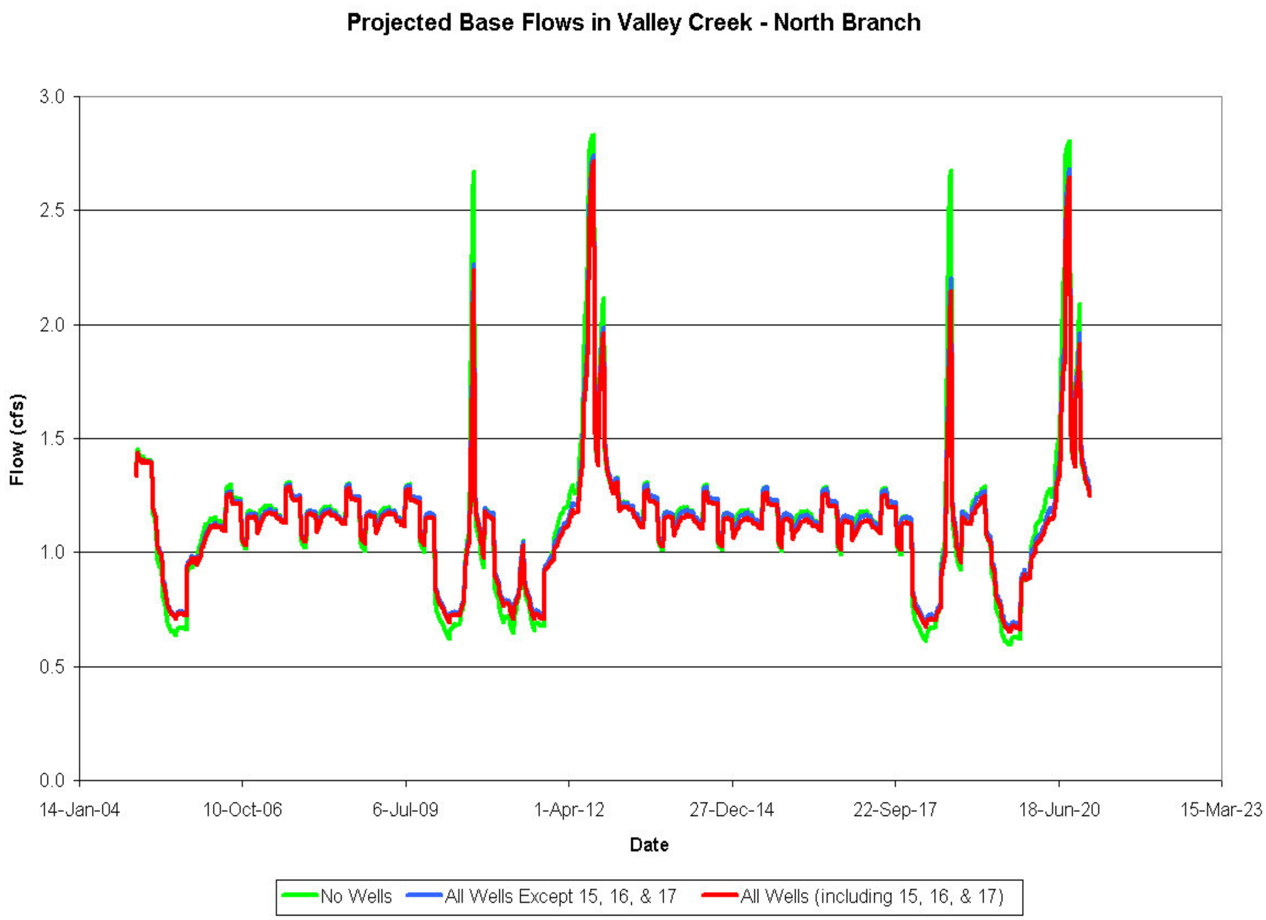

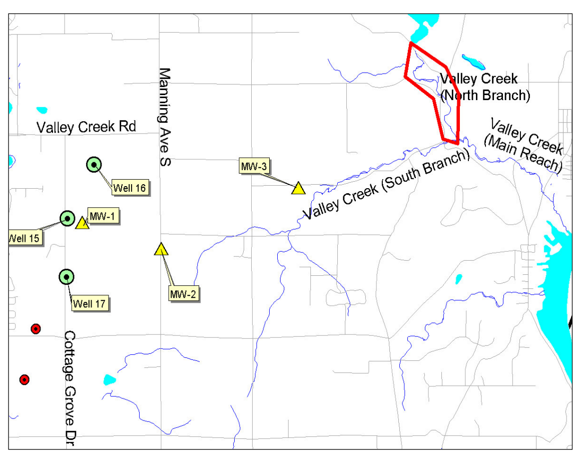

Figure 87

Simulation of Base Flows in North Branch of Valley Creek: 2002-2025

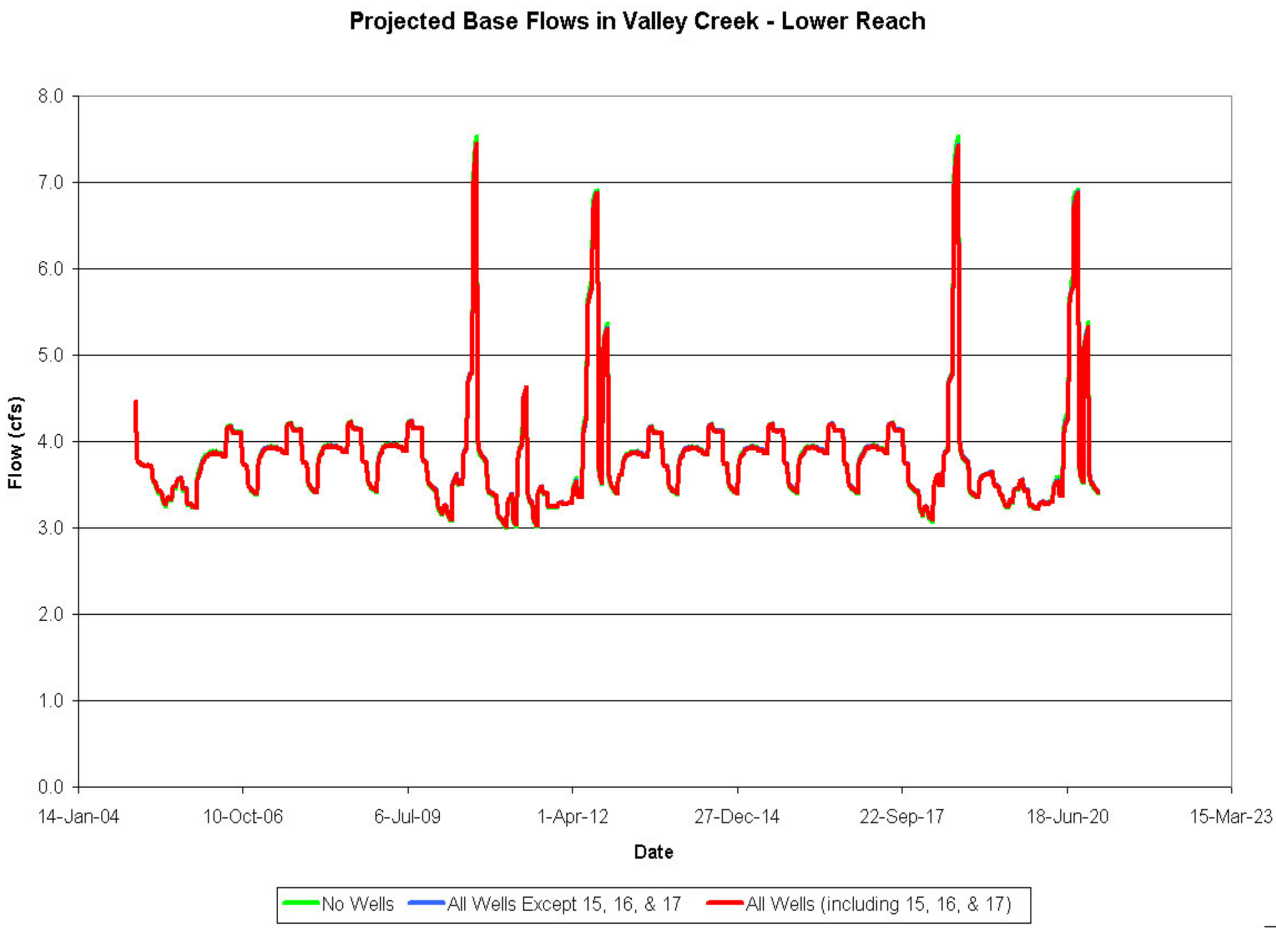

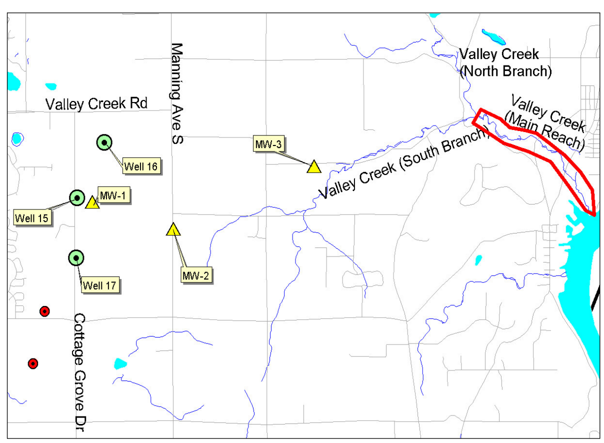

Figure 88

Simulation of Base Flows in Main Reach of Valley Creek: 2002-2025

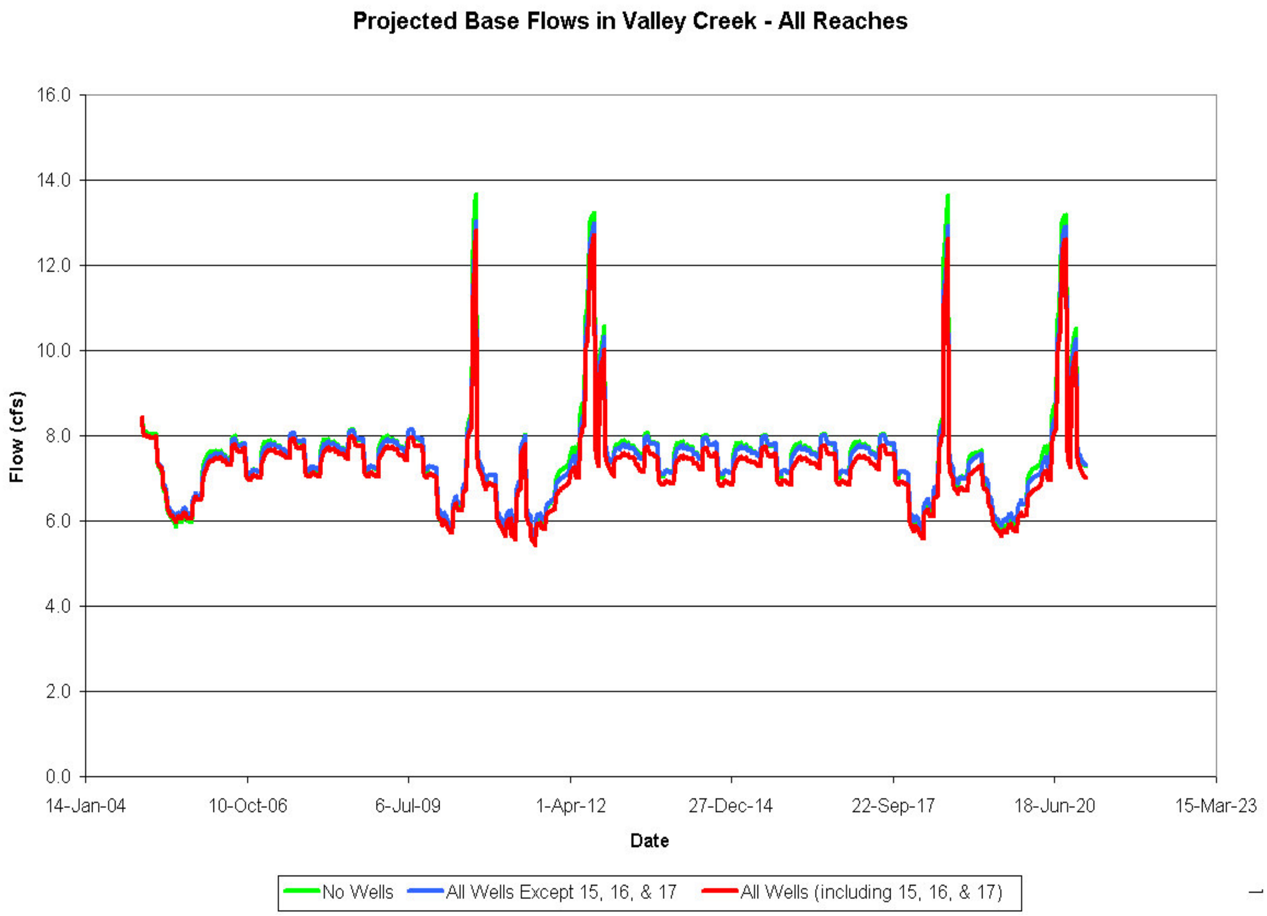

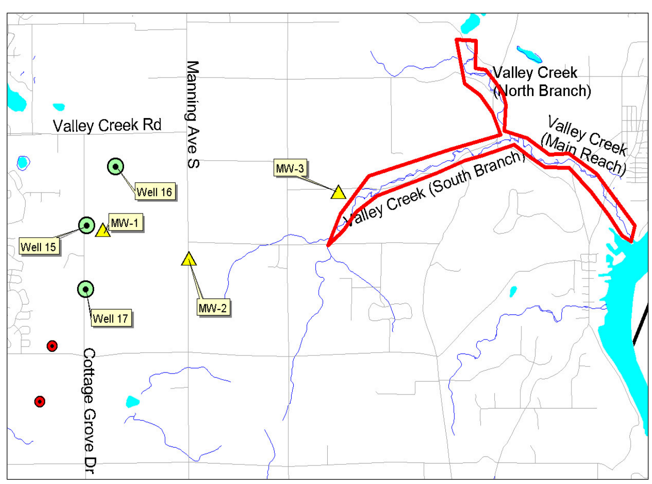

Figure 89

Simulation of Base Flows in All of Valley Creek: 2002-2025

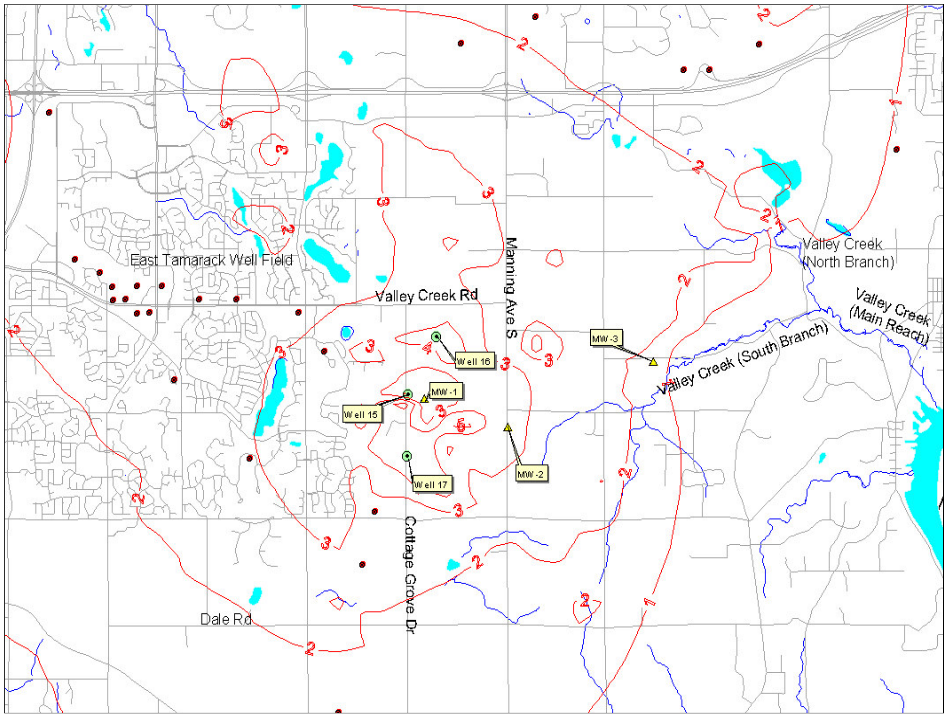

Water Table

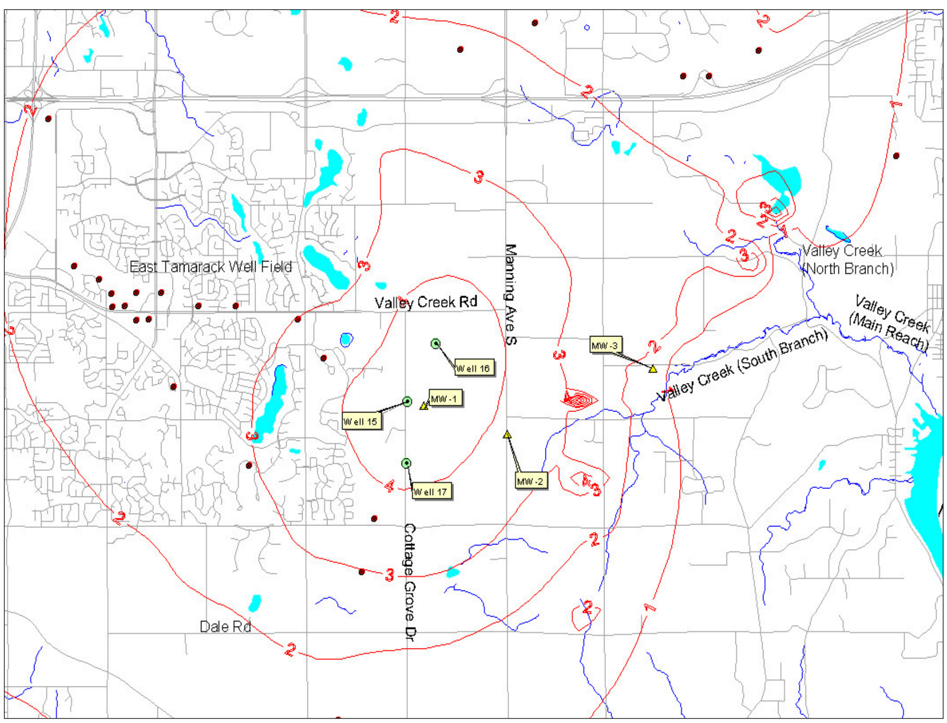

Shakopee Formation
(contour interval = 1 foot)

Figure 90

Predicted Lowering of Head (feet) for July 2012, Resulting from the Pumping of Wells 15, 16, and 17 – Water Table and Shakopee Formation

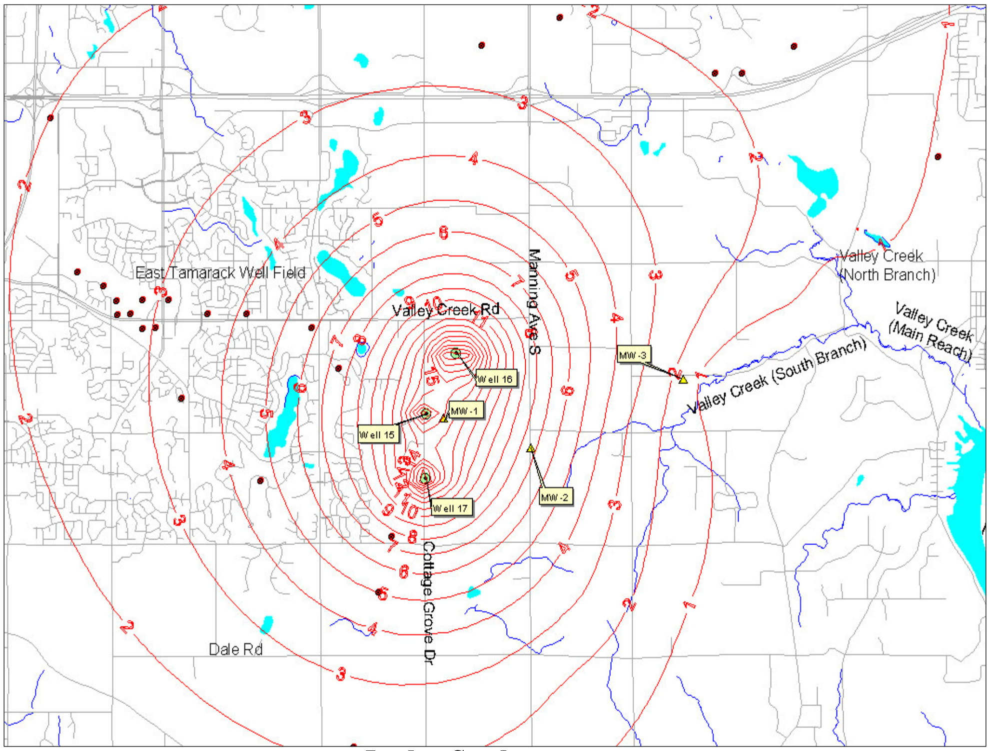

Jordan Sandstone

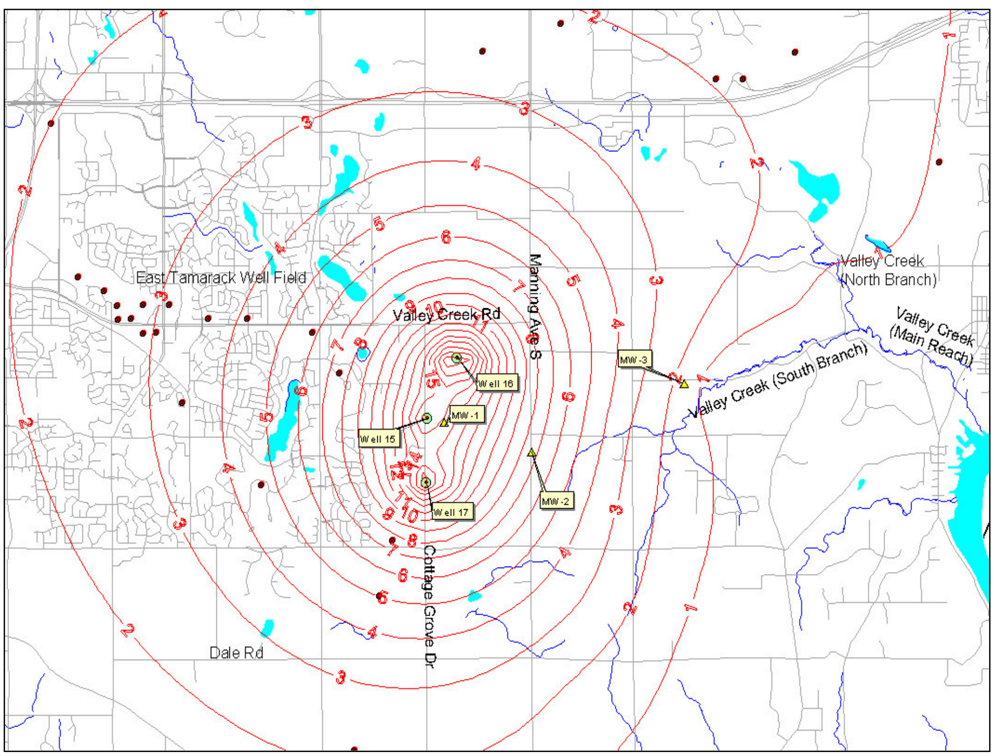

Ironton-Galesville Sandstones
(contour interval = 1 foot)

Figure 91

Predicted Lowering of Head (feet) for July 2012, Resulting from the Pumping of Wells 15, 16, and 17 – Jordan Sandstone and Ironton-Galesville Sandstones

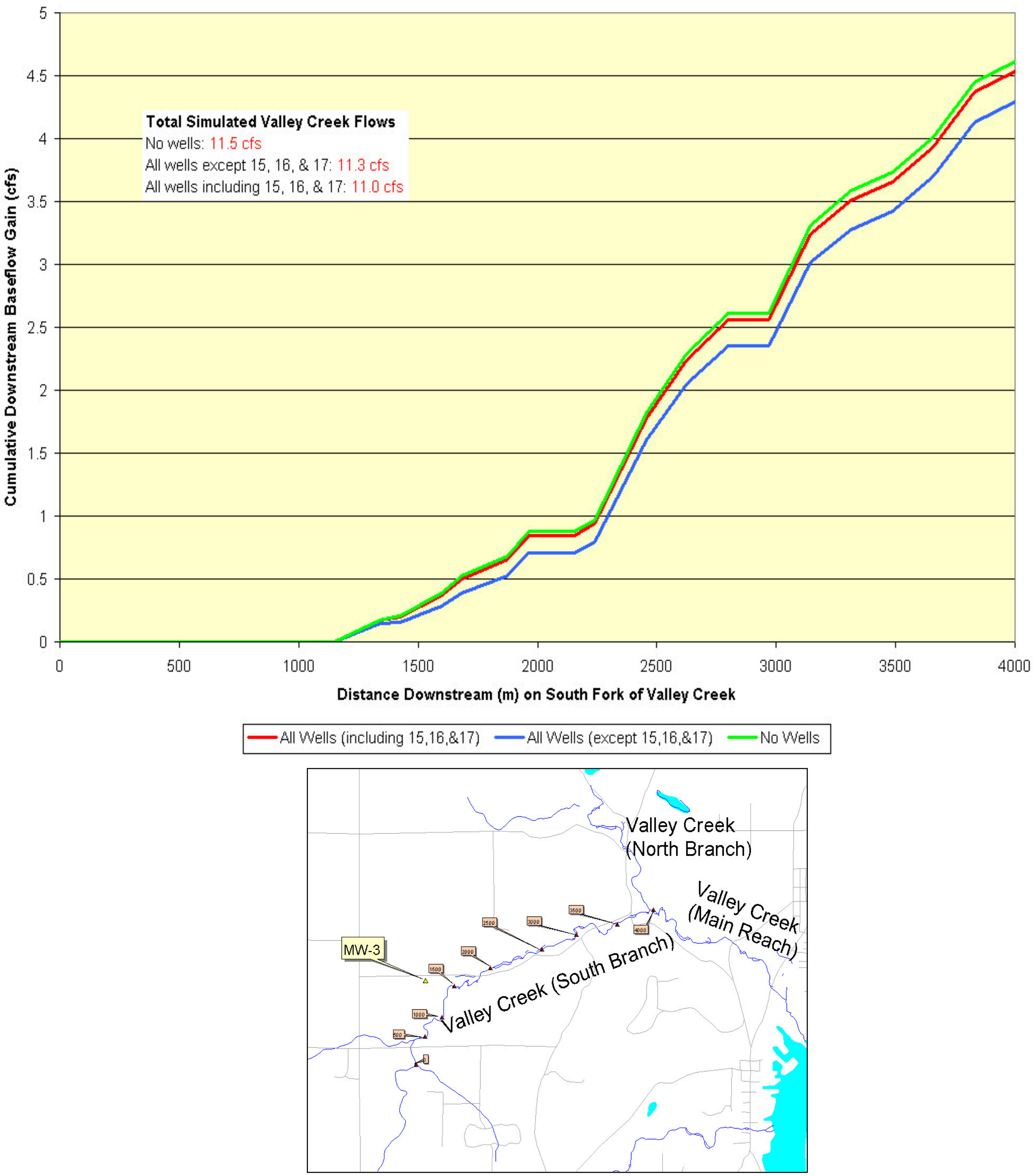

Figure 92

Predictions of Cumulative Base flow with Downstream Distance (meters) Along South Fork of Valley Creek: July 2012

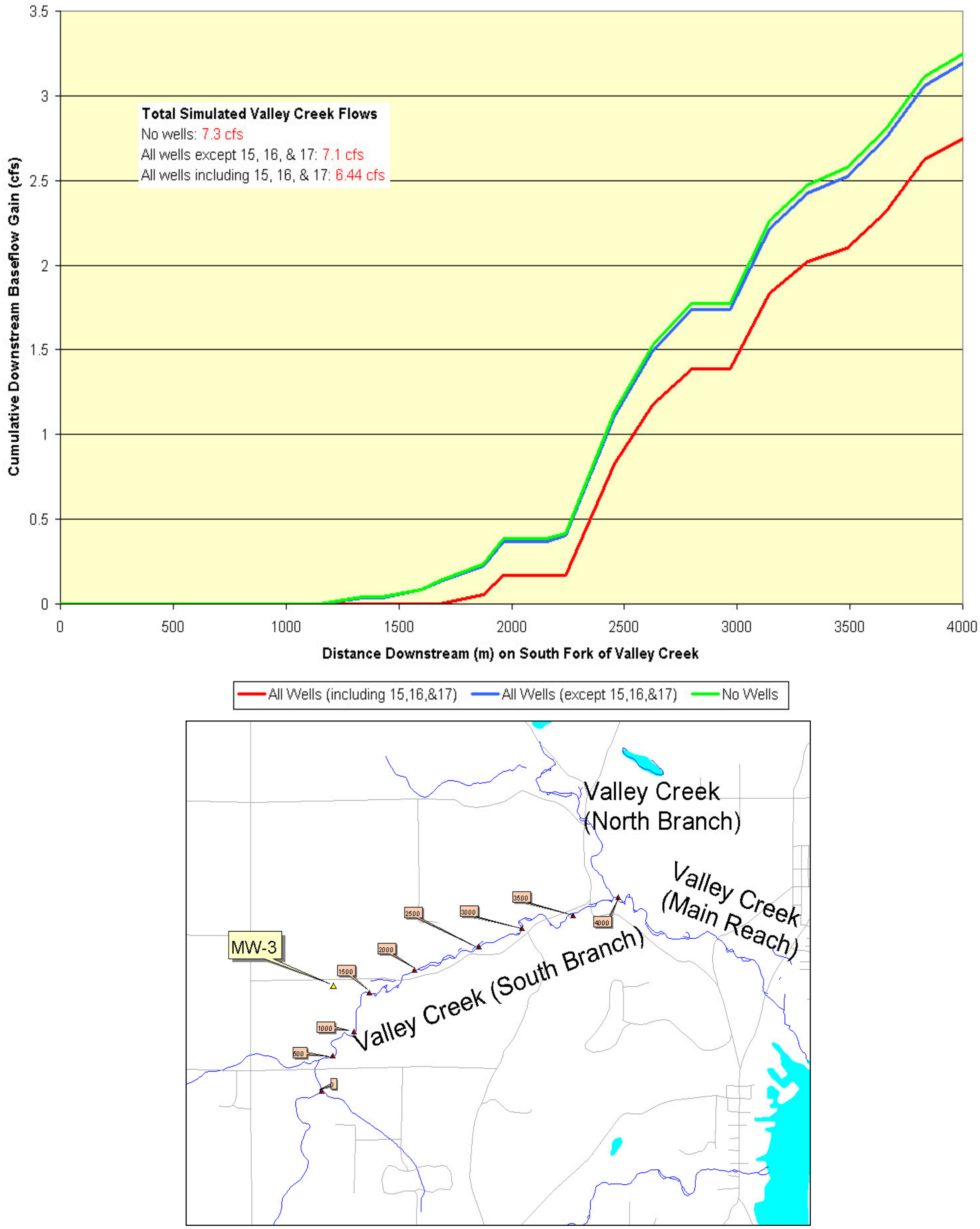

Figure 93

Predictions of Cumulative Base flow with Downstream Distance (meters) Along South Fork of Valley Creek – August 2018